

**IMPROVING *IN VIVO* FAST-SCAN CYCLIC
VOLTAMMETRIC DETECTION OF NEUROMODULATORS**

Richard Brandon Keithley

A dissertation submitted to the faculty of the University of North Carolina at Chapel Hill in
partial fulfillment of the requirements for the degree of Doctor of Philosophy in the
Department of Chemistry

Chapel Hill
2011

Approved by:

R. Mark Wightman

James W. Jorgenson

Royce W. Murray

Regina M. Carelli

Dorothy A. Erie

ABSTRACT

RICHARD BRANDON KEITHLEY: IMPROVING *IN VIVO* FAST-SCAN
CYCLIC VOLTAMMETRIC DETECTION OF NEUROMODULATORS
(Under the direction of R. Mark Wightman)

Fast-scan cyclic voltammetry is an electroanalytical technique used to probe neuromodulator signaling dynamics *in vivo*. The popularity of fast-scan cyclic voltammetry has grown in recent years because of its ability to address various neurobiology research interests in a simple, rapid, sensitive, manner *in vivo* in real time. However, there still remain challenges associated with the identification and detection of neuromodulators *in vivo*. Here, the application of principal component regression with residual analysis to *in vivo* fast-scan cyclic voltammetry data is presented for the first time in a straightforward, non-mathematical context. Changing the estimation of rank from the 99.5% cumulative variance method to Malinowski's *F*-test better separates relevant information from noise contained in the training set cyclic voltammograms. This allows the residual analysis procedure to function more accurately in determining whether the calibration model was applicable for the unknown data set being predicted. The presence of electrode drift is shown to dramatically alter concentration prediction when it is not included during the construction of the calibration model. Several tools including a residual color plot, the pseudoinverse of the principal component regression calibration matrix, and Cook's distance are shown to successfully improve the accuracy and robustness of training set construction and concentration prediction. In addition, the sensitivity of fast-scan cyclic voltammetry is increased by increasing the scan rate of the applied voltage waveform. Analog background subtraction allows some of the charging current to be neutralized, preventing saturation of the system. The *in vitro* and *in vivo*

sensitivities are significantly improved, approaching a sub-nanomolar limit of detection. Scanning to a potential of 1.3 V requires waveform modification to maintain the increased sensitivity, but the surface integrity of the carbon-fiber microelectrode is altered. Taken together, these improvements allow for a more sensitive detection scheme and a more robust and accurate quantitation methodology associated with the detection of neuromodulators *in vivo* with fast-scan cyclic voltammetry.

ACKNOWLEDGEMENTS

I have to start off by thanking my research advisor, Dr. R. Mark Wightman. You have put in a great deal of effort to help me develop my burgeoning scientific career. You never settled for anything less than perfection, which pushed me and made me strive for excellence. I hope that in the future we may be colleagues, pursuing exciting research prospects.

I thank several collaborators for their various contributions to the work presented here. Dr. Michael Heien provided helpful discussions and Dr. Leslie Sombers provided data for Chapters 2 and 3. I thank Dr. Manna Beyene, Dr. Fabio Cacciapaglia, Dr. Jeremy H. Day, Dr. Joshua L. Jones, Dr. Catarina Owesson-White, and Dr. Robert A. Wheeler for the use of their data for Chapter 3, as well as helpful conversations with Christopher Wiesen. Dr. Regina Carelli also supplied some of the data analyzed in Chapters 3 and 4. Pavel Takmakov, Elizabeth Bucher, Anna Belle, Dr. Catarina Owesson-White, and Dr. Jinwoo Park performed some of the experiments presented in Chapter 5 and provided helpful discussions. Pavel Takmakov, Dr. Jinwoo Park, Dr. Andre Hermans, and Dr. Matthew Zachek were also very helpful throughout my various investigations during my dissertation work, helping this separations chemist become more acquainted with electrochemistry. I also thank Collin McKinney for helpful electronics discussions/hardware repair, the Carolina Chemistry Electronics Facility, and funding from the National Institutes of Health, a National Defense Science & Engineering Graduate Fellowship, and the Society for Electroanalytical Chemistry. Finally, I thank all

other members of the Wightman lab because they deserve it after putting up with me for several years.

I also thank several faculty members for their guidance during my undergraduate education at Virginia Commonwealth University. I thank my mentor, Dr. Sarah Rutan, for helping me start asking questions and for not rolling her eyes when I asked them over and over again. She never lost faith in me and always pushed me forward. Plus, the printer outside the door was a welcome relief. Dr. Sally Hunnicutt helped me find my passion for teaching and guided me throughout my undergraduate career.

I thank my family for supporting me all these years and helping me get to this point. I didn't always call, I rarely visited, and I even dumped my cats with you. However, you stood by me, supported me (financially and emotionally), and always told me you were proud of me. To those looking down from Heaven, thank you for listening. To Ian, Chris, and Kaitlin, thank you for dragging me back from the edge and keeping me grounded.

TABLE OF CONTENTS

LIST OF TABLES.....	xi
LIST OF FIGURES.....	xii
LIST OF ABBREVIATIONS AND SYMBOLS.....	xiv
Chapter	
I. BUILDING A BETTER MOUSETRAP FOR FAST-SCAN CYCLIC VOLTAMMETRY	1
Introduction.....	1
Sensitivity and Limit of Detection Improvements	2
Pushing Beyond Rodent Dopamine	6
<i>In Vivo</i> Microelectrode Design Developments	10
Unscrambling Mixed Messages with Principal Component Regression.	11
Concluding Remarks	15
References	18
II. MULTIVARIATE CONCENTRATION DETERMINATION USING PRINCIPAL COMPONENT REGRESSION WITH RESIDUAL ANALYSIS.....	23
Abstract.....	23
Introduction.....	23

Multivariate Analysis in Analytical Chemistry	24
Construction of a multivariate model: principal component regression	26
PCR Model Validation.....	33
PCR Model Applicability: Residual Analysis.....	34
Q_α as a measure of significance	38
Interpretation of c_α	39
Q_t crossing Q_α :	41
Future Outlook / Conclusions.....	44
References	46
III. RANK ESTIMATION AND THE MULTIVARIATE ANALYSIS OF <i>IN VIVO</i> FAST-SCAN CYCLIC VOLTAMMETRIC DATA	49
Abstract	49
Introduction.....	50
Theory	53
Experimental.....	56
Fast-scan cyclic voltammetry and animal experimentation	56
Data analysis and principal component regression.....	57
Results and Discussion.....	59
Principal component selection & training set heterogeneity	59
Comparison of information contained in secondary PCs.....	65
Comparison of model validity.....	72

Comparison in concentration prediction.....	77
Conclusions.....	84
References.....	87
IV. ASSESSING PRINCIPAL COMPONENT REGRESSION WITH RESIDUAL ANALYSIS IN THE DETECTION OF NEUROMODULATORS.....	91
Abstract.....	91
Introduction.....	92
Theory.....	94
PCR and K generation.....	94
Leverage.....	95
Studentized residual.....	96
Cook's distance.....	97
Experimental.....	99
Electrochemical and animal experimentation.....	99
Data analysis.....	99
In vivo FSCV training sets.....	100
Results and Discussion.....	101
Proper accounting of electrode drift and failure of the residual analysis procedure.....	101
Transformation of the Q_{α} value.....	104
Interpretation of residual color plots for the identification of deterministic error.....	105
The use of K as a qualitative diagnostic tool.....	108

Identifying and removing training set outliers using Cook's distance.....	112
Conclusions.....	116
V. HIGHER SENSITIVITY DOPAMINE MEASUREMENTS WITH FASTER-SCAN CYCLIC VOLTAMMETRY.....	121
Abstract.....	121
Introduction.....	122
Experimental.....	125
Chemicals.....	125
Electrode fabrication.....	125
Data acquisition.....	126
Electrochemical experiments.....	127
Data analysis.....	128
Flow injection analysis.....	129
Etching studies.....	129
In vivo experiments in anesthetized rats.....	130
Use of ABS for faster scan rate experiments.....	130
Combined electrochemistry and electrophysiology.....	130
Results and Discussion.....	132
Scanning faster with the 1.0 V waveform.....	132
Scanning faster with the 1.3 V cyclic waveform.....	136
Modification of the 1.3 V cyclic waveform for maintaining increased sensitivity.....	141

Effect of increased charging current on neuronal firing	144
Surface integrity of carbon-fiber microelectrodes after waveform application	148
Conclusions	151
References	153

LIST OF TABLES

Table

3.1. Comparison of Rank Estimation Methods. Eigenvalue, reduced eigenvalue, calculated F -statistic, critical F -value at 5% significance, and PRESS value as a function of PC for an example FSCV training set spectral matrix.	60
3.2. Inter-researcher comparison of rank estimation between Malinowski's F -test and the 99.5% cumulative variance method.	63
3.3. Comparison of average Q_α values calculated using PCs retained with Malinowski's F -test and the 99.5% cumulative variance (C.V.) method.	76

LIST OF FIGURES

Figure

1.1. The application of the 1.3 V FSCV waveform alters carbon surface chemistry.....	5
1.2. PCR signal separation of complex in vivo FSCV data.....	14
1.3. Comparison of charge oscillations.....	16
2.1. Representation of UV-VIS data in an intensity space.....	28
2.2. PCR deconvolution of <i>in vivo</i> electrochemical data.....	32
2.3. Calculation of a Q value at a specific time point, <i>t</i>	37
2.4. The use of residual analysis as a diagnostic tool for significance in <i>in vivo</i> electrochemical data.....	43
3.1. Histograms of the estimated rank of Case I, II, and III training sets.....	64
3.2. Comparison of effective cyclic voltammograms in a representative Case I training set.....	66
3.3. RMS noise removed by the 99.5% cumulative variance method (99.5% C.V.) and Malinowski's <i>F</i> -test for all of the Case I training sets.....	69
3.4. Cyclic voltammetric representation of the secondary PCs from each method of factor selection for a representative Case II training set.....	71
3.5. Histograms of Q_{α} values of A) Case I and B) Case II training sets.....	74
3.6. Comparison of stimulated release predicted by PCR using primary PCs determined with both methods of factor selection for a representative Case I training set.....	79
3.7. Dopamine release predicted by PCR during an ICSS experiment using primary PCs determined with both methods of factor selection for a Case I training set.....	83

4.1. Neuromodulator prediction by PCR with and without electrode drift in the training set.....	102
4.2. Interpretation of a residual color plot when an unrepresentative training set is used for concentration prediction..	106
4.3. K representations of a proper and an improper training set.....	110
4.4. The use of Cook's distance to improve PCR calibration.....	114
5.1. ABS utilization for faster-scan cyclic voltammetry..	131
5.2. Performance characteristics of the 1.0 V waveform upon increasing scan rate.....	134
5.3. Performance characteristics of the 1.3 V cyclic waveform upon increasing scan rate.....	137
5.4. 1.3 V excursions versus time.....	140
5.5. In vitro performance of the 1.3 V sawhorse waveform..	142
5.6. In vivo performance of the 1.3 V sawhorse waveform in vivo in anesthetized rats..	145
5.7. The effect of waveform application on firing rate activity.....	147
5.8. Carbon fiber microelectrode etching as a function of the applied waveform.....	149

LIST OF ABBREVIATIONS AND SYMBOLS

*	Probability Less Than 0.05
**	Probability Less Than 0.01
***	Probability Less Than 0.001
α	Significance Level
A	Training Set Voltammetric Matrix
A/P	Anterior/Posterior
ABS	Analog Background Subtraction
ADC	Analog-to-Digital Converter
Ag/AgCl	Silver-Silver Chloride Reference Electrode
A_{jPC}	Discarded Noise of a Training Set
ANOVA	Analysis of Variance
A_{nPC}	Relevant Portion of Training Set Data
A_{proj}	Projection of Training Set Onto Relevant Principal Components
A_{projTS}	Relevant Scores of the Training Set Cyclic Voltammograms
A_{TS}	Training Set Cyclic Voltammogram Matrix
A.U.	Absorbance Units
A_{unk}	Unknown Cyclic Voltammograms Being Predicted
c	Columns in a Data Matrix
C.V.	Cumulative Variance
CH ₃ COOK	Potassium Acetate
C_{ts}	Training Set Concentration Matrix
C_{unk}	Unknown Neuromodulator Concentrations
c_{α}	Noise Threshold Z-Score
ΔE_p	Peak Separation

D/V	Dorsal/Ventral
DA	Dopamine
DAC	Digital-to-Analog Converter
D_i	Cook's Distance
diag	Diagonal Operation
e_i	Difference Between Estimated and Reference Concentration Values
ESEM	Environmental Scanning Electron Microscopy
F	Regression Coefficients Relating Unknown Concentrations to Relevant Scores
$F_{0.05}$	Critical F -Value at 5% Significance
FSCV	Fast-Scan Cyclic Voltammetry
F_{stat}	Calculated F -Statistic
γ	Cook's Distance Significance Level
g	Grams
h_i	Leverage of the i^{th} Sample
Hz	Hertz
i.p.	Intraperitoneal Injection
ICSS	Intracranial Self-Stimulation
IE	Current-to-Voltage Converter
i_{RMS}	Root Mean Square Current
i_{TH}	Significant Current Threshold
i_x	Current at the x^{th} potential
\hat{i}_x	Current Predicted From the Calibration Model at the x^{th} Potential
j	Number of Analytes
K	Matrix Containing Cyclic Voltammograms of Each Analyte in Units of Current Per Concentration
KCl	Potassium Chloride

k_{DA}	Dopamine Column of \mathbf{K}
kEV	Kiloelectronvolt
kg	Kilogram
kHz	KiloHertz
\mathbf{K}_j	Column of \mathbf{K}
k_{pH}	pH Column of \mathbf{K}
λ	Sum of Squares of the Data Projections From All Samples in the Training Set for Each Principal Component
λ_j	Eigenvalue of the j^{th} Principal Component
λ_j^0	Error Eigenvalue of the j^{th} Principal Component
LOD	Limit of Detection
μ	Mean
μA	Microamperes
μm	Micrometers
μM	Micromolar
μs	Microseconds
m	Number of Training Set Samples
M/L	Medial/Lateral
min	Minutes
mL	Milliliter
mM	Millimolar
ms	Millisecond
mV	Millivolts
n	Number of Retained Principal Components
n.s.	No Significant Difference
N_2	Nitrogen

nA	Nanoamperes
NaCl	Sodium Chloride
NaH ₂ PO ₄	Sodium Dihydrogen Phosphate
nM	Nanomolar
P	Probability
PBS	Phosphate Buffered Saline
PC	Principal Component
PCA	Principal Component Analysis
PCR	Principal Component Regression
PLS	Partial Least-Squares
PRESS	Predicted Residual Error Sum-of Squares
Q	Sum of the Squares of Residual Currents
Q _t	Sum of the Squares of Residual Currents at the time point <i>t</i>
Q _α	Tolerable Threshold for the Sum of the Squares of Residual Currents
r	Rows in a Data Matrix
R ²	Coefficient of Determination
REF	Reference Electrode
REV	Reduced Eigenvalue
RMS	Root-Mean-Square
σ	Standard Deviation
s	Seconds
SEC	Standard Error of the Calibration
SEM	Standard Error of the Mean
T	Matrix Transpose
t	Time
t _i	Studentized Residual of the <i>i</i> th Sample

V	Volts
Vc	Matrix of the Relevant Principal Components of the Training Set
V_n	Relevant Row Information of Training Set Voltammetric Matrix Calculated From Singular Value Decomposition
w	Total Number of Points in the Voltammetric Waveform
w/w	Weight by Weight
WE	Working Electrode
[X]	Concentration of Analyte X
[Y]	Concentration of Analyte Y
z	Z-Score

CHAPTER I

BUILDING A BETTER MOUSETRAP FOR FAST-SCAN CYCLIC VOLTAMMETRY

Introduction

To an analytical chemist, the brain provides both an extremely interesting and challenging measurement environment. *In vivo* measurements require rapid time response, excellent sensitivity, low limits of detection, high selectivity, all in an environment where biofouling is likely. By studying the brain, analytical chemists have the unique opportunity of improving *in vivo* measurement strategies while simultaneously learning fundamental information about brain signaling dynamics. The latter point may seem unusual to the traditional analytical chemist, but resolving long-standing questions in the field of neurobiology is exciting and often requires the unique skill set of an analytical chemist. The analyst can contribute to multiple fields of study including normal behavior, disease states, and drug-seeking behaviors, all of which require thorough chemical characterization to unravel.

Fast-scan cyclic voltammetry (FSCV) is an electroanalytical technique used to probe neuromodulator signaling dynamics *in vivo*. In this approach, the applied voltage is swept rapidly (> 100 V/s) and the shape of the resulting current response gives information regarding the electron transfer properties of the analyte (Baur et al., 1988). As such, the shapes of the cyclic voltammograms can serve as a unique identifier for the specific neuromodulator of interest, except for dopamine and norepinephrine which have nearly identical cyclic voltammograms (Baur et al., 1988; Park et al., 2009).

FSCV offers several advantages including sub-second temporal resolution, low nanomolar limits of detection, and the best selectivity of electrochemical methods for neuromodulator detection *in vivo* (Robinson and Wightman, 2007). A carbon-fiber microelectrode is typically used as the working electrode which gives two additional advantages: micrometer spatial resolution and minimal damage *in vivo* (Jaquins-Gerstl and Michael, 2009). One disadvantage to using FSCV is that a conventional commercial potentiostat is usually insufficient for *in vivo* recordings, so more sophisticated, expensive custom-made instrumentation is needed (Takmakov et al., 2011).

A true testament to any analytical chemistry technique is the number of non-analytical chemists that use it. FSCV is used today by psychologists, neuroscientists, pharmacologists, and others studying a variety of neurobiological applications. Measurement of the catecholamine dopamine has been of particular interest over the past several years. Dopamine is involved in various cognitive and motor processes (Cooper et al., 1996), with deficiencies in dopamine neurotransmission being associated with Parkinson's disease. Dopamine plays a critical role in the reward circuitry system of the brain and drugs of abuse such as cocaine are thought to hijack this system, contributing to drug addiction (Wightman and Robinson, 2002; Schultz, 2007).

Broadly, this work will highlight several recent advances in analytical chemistry regarding FSCV. Specifically, sensitivity improvements with proposed mechanisms, advancements in the measurement of analytes other than dopamine, and signal processing developments will be presented. Insights into neurotransmission gleaned from FSCV measurements are beyond the scope of this work and have recently been reviewed elsewhere (Robinson and Wightman, 2007; Huffman and Venton, 2009).

Sensitivity and Limit of Detection Improvements

Much of the recent work on improving sensitivity of *in vivo* FSCV measurements relies on modifying the surface of the carbon-fiber microelectrode. One approach developed by Swamy and Venton involved coating single wall carbon nanotubes (SWCNTs) onto carbon-fiber microelectrodes (Swamy and Venton, 2007). The SWCNTs increased signal-to-noise ratios of dopamine measurements up to 2.5-fold without decreasing response time, a common disadvantage with other methods such as electrochemical pretreatment. The SWCNT-coated carbon-fiber microelectrodes also showed resistance to the fouling oxidation byproducts of serotonin and allowed for co-detection of dopamine and serotonin *in vivo* after the administration of a serotonin precursor.

Electrochemical oxidation is known to enhance the sensitivity towards positively charged neuromodulators through the creation of adsorption sites, but the additional adsorption sites decreases the response time of the microelectrode and can increase noise (McCreery, 1991; Bath et al., 2000; Heien et al., 2003b). Carbon-fiber microelectrodes have recently been flame etched to improve signal to noise ratios towards dopamine. Flame etching lead to faster electron transfer kinetics, faster adsorption/desorption kinetics, and increased the signal to noise ratio for dopamine (Strand and Venton, 2008).

Rather than directly modifying the surface of carbon-fiber microelectrodes, the scan rate of FSCV measurements was increased to improve sensitivity (Keithley et al., 2011). Because dopamine adsorbs to the electrode surface, its current response is proportional to scan rate (Bath et al., 2000). Unfortunately background charging current is also proportional to scan rate so scanning faster will saturate the current-to-voltage converter or the analog-to-digital converter used in data collection, unless gain is decreased which increases quantization noise. Analog background subtraction (Hermans et al., 2008) was used to circumvent this problem. Charging current at 400

V/s was recorded and fed into the summing point of the current-to-voltage converter, thereby zeroing out some the measured response. Scan rate could then be increased without saturating the system to enhance the sensitivity for dopamine.

FSCV measurements are routinely made with a waveform with a potential limit of 1.0 V which has a rapid temporal response but poor sensitivity, or a potential limit of 1.3 V which has enhanced sensitivity but a poor temporal response (Heien et al., 2003b). Increasing the scan rate from 400 V/s to 2400 V/s with the 1.0 V excursion increased the signal-to-noise ratio *in vitro* for 1 μ M dopamine to $1.3 \pm 0.2 \times 10^3$ and a stable four-fold increase in peak current *in vivo* (Keithley et al., 2011). The 1.3 V waveform was adapted into a novel sawhorse design to maintain sensitivity over time with faster scan rate experiments. The 1.3 V sawhorse waveform at 2400 V/s increased the signal-to-noise ratio of 1 μ M dopamine *in vitro* to $3.3 \pm 0.3 \times 10^3$, lowering the limit of detection to 0.96 ± 0.08 nM.

A carbon electrode material based on the pyrolysis of novolac-containing photoresists has recently been used to uncover the underlying mechanism for enhanced sensitivity with the 1.3 V waveform (Takmakov et al., 2010b). Pyrolyzed photoresist films (PPF) have electrochemical properties very similar to glassy carbon, but have the capability of being microfabricated using photolithographic methods (Ranganathan et al., 2000). Takmakov and coworkers microfabricated a PPF electrode with a similar electroactive surface area of a carbon-fiber microelectrode onto a fused silica wafer (Figure 1.1A, top) (Takmakov et al., 2010b). Interestingly, after the application of the 1.3 V waveform for several hours, the electrode completely vanished (Figure 1.1A, bottom). When a carbon-fiber microelectrode was used, the electrode was visibly etched after the application of the 1.3 V waveform (Figure 1.1B). Both the PPF and carbon-fiber microelectrodes remained intact if the 1.0 V waveform was used.

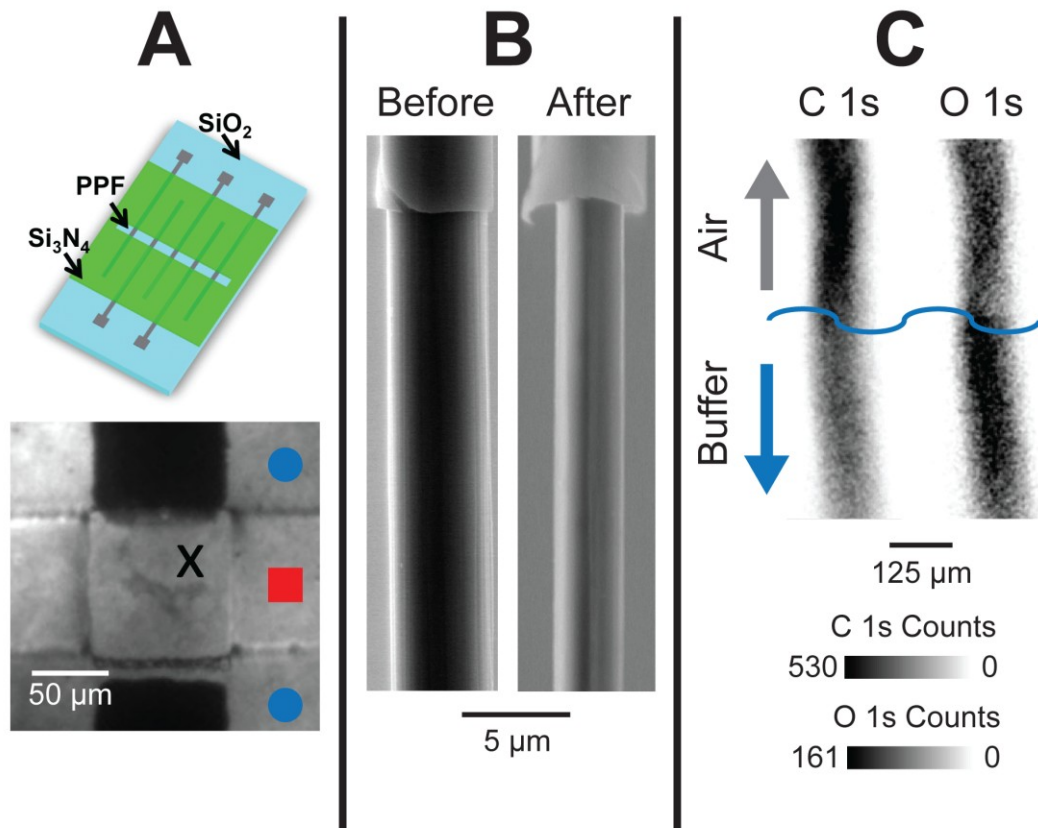


Figure 1.1. The application of the 1.3 V FSCV waveform alters carbon surface chemistry. A) Top: Cartoon of a microfabricated PPF electrode patterned on a fused silica wafer, insulated with silica nitride. Bottom: A scanning electron microscope image of the PPF electrode after the application of the 1.3 V waveform for 2.2 million cycles. The blue circles indicate silicon nitride insulated PPF not exposed to solution, the red square indicates the region of the PPF electrode that was exposed to solution, and the black X indicates an etched PPF electrode. Both top and bottom were adapted from Takmakov et al., 2010b. B) A carbon-fiber microelectrode before (left) and after (right) application of the 1.3 V cyclic waveform for 6.5 million cycles. C) XPS 1s carbon (left) and 1s oxygen (right) mapping of a PPF-coated tungsten wire that was partially immersed in physiological buffer after application of the 1.3 V waveform.

Scanning to potential limits above 1.0 V with FSCV is known to overoxidize carbon surfaces (Hafizi et al., 1990; Heien et al., 2003b). Indeed, x-ray photoelectron spectroscopy (XPS) mapping of carbon and oxygen on a PPF-coated tungsten microwire shows the application of the 1.3 V waveform increases the oxygen to carbon ratio on the electrode surface (Figure 1.1C). Unfortunately, the XPS signals can be faint because of the small area of the microelectrodes. Nevertheless, surface techniques such as XPS (Takmakov et al., 2010b), Raman spectroscopy (Roberts et al., 2010), and scanning electron and atomic force microscopies (Takmakov et al., 2010b; Keithley et al., 2011) are becoming routine to probe carbon microelectrode surface states associated with FSCV measurements.

Taken together, the literature suggests that dopamine sensitivity with carbon surfaces scanned to moderate anodic potential limits depends on an oxidative etching mechanism. The idea of a renewable electrode surface is similar to that of traditional polarography experiments using a mercury drop electrode and may provide useful at resisting biofouling *in vivo*. The exact functional groups providing enhanced sensitivity are unknown, but are likely a combination of carboxylic groups, quinine moieties, and hydroxyl groups (Roberts et al., 2010; Takmakov et al., 2010a).

Pushing Beyond Rodent Dopamine

Dopamine is readily detected with FSCV *in vivo* because of its favorable electron transfer properties and the significant amounts of dopamine released *in vivo* that enable high signal-to-noise ratios. Furthermore, the regions where dopamine rich nerve terminals are located are fairly large compared to other brain structures. Rats and mice are widely used for FSCV experiments, however dopamine has been recently measured in the anesthetized pig (Shon et al., 2010). The pig serves as a large animal model to study the therapeutic effects of deep brain stimulation in Parkinson's disease. It was

determined that maximal dopamine release occurred during stimulations typically given to patients afflicted with the disease.

The field of neuroeconomics blends neuroscientific observations, social sciences, and economic theories to try and understand the basis value judgments and human choice (Glimcher, 2011). Dopamine release has also been detected in the human striatum to investigate the role of dopamine in economic decision making (Sandberg et al., 2010). A subject was given the opportunity to invest money in a fictional stock market. It was shown that dopamine activity in this subject was a significant predictor of future market performance, indicating that dopamine may be an important player guiding human preference and choice.

Rice and Nicholson were the first to identify pH change using FSCV (Rice and Nicholson, 1989), but the origin of the characteristic peaks of its cyclic voltammogram were poorly characterized. Takmakov et al. identified several peaks consistent with *in vivo* pH change cyclic voltammograms: a C-peak at approximately -0.2 V on the oxidative sweep, a QH-peak at approximately 0.3 V on the oxidative sweep, and a Q-peak at approximately -0.3 V on the reductive sweep (Takmakov et al., 2010a). The C-peak is associated with non-faradaic charging of the electrode double layer and the QH- and Q-peaks are associated with hydroquinone electrochemistry at the electrode surface. The authors also identified a fourth peak associated with 3,4-dihydroxyacetic acid (DOPAC), a metabolite of dopamine that is present in the extracellular fluid. *In vivo* pH changes could also be induced without neuronal stimulation through inhalation of carbon dioxide. Most importantly, it was determined that the commonly used TRIS buffering system for calibration was unsuitable for proper generation of pH change cyclic voltammograms *in vitro*.

In vivo pH changes are routinely measured in rats after neuronal stimulation and are associated with blood flow and metabolism (Venton et al., 2003). pH changes have

been recently measured in the brains of non-human primates during reward delivery (Heien, 2005; Hermans, 2007). A cue preceding a predicted juice induced a basic pH change while a long term acidic shift was recorded after the juice reward delivery. These results correlated with those of functional magnetic resonance imaging, a technique conventionally used to measure neuronal activation *in vivo*.

Norepinephrine is a catecholamine involved in learning, stress and drug addiction, but its detection *in vivo* is difficult because the shape of its cyclic voltammogram is nearly identical to dopamine, physiological concentrations are low, and brain structures containing measureable levels of norepinephrine are only a few hundred microns in size (Park et al., 2009). Park et al. recently used FSCV to study norepinephrine signaling dynamics for the first time *in vivo* in the ventral bed nucleus of the stria terminalis, a major relay center for processing stressful and anxiety causing stimuli (Park et al., 2009). Because of the similar shape of dopamine and norepinephrine cyclic voltammograms, tissue content, anatomical, and pharmacological evidence was used to verify that norepinephrine rather than dopamine was detected. This study opens the door for using FSCV to study the connection between stress and drug addiction in freely-moving animals.

Serotonin is a neurotransmitter that regulates emotional processes and mood, with impairments of serotonin neurotransmission being implicated in depression and anxiety disorders (Jackson et al., 1995). Serotonin is electrochemically active, but its oxidation byproducts quickly foul the electrode surface. The FSCV waveform was previously altered to prevent the fouling from occurring which allowed for routine measurements in brain slices (Jackson et al., 1995). However, endogenous serotonin release had yet to be detected in the intact brain using FSCV without the administration of a large dose of a serotonin precursor.

Hashemi et al. identified that the presence of 5-hydroxyindoleacetic acid (5-HIAA), a metabolite of serotonin present in the extracellular space in concentrations up to 1000 times larger than serotonin, also caused fouling of the carbon-fiber microelectrode (Hashemi et al., 2009). 5-HIAA is washed out during normal brain slice preparations which would allow for its detection *in vitro*. Nafion® was electrodeposited onto the carbon-fiber microelectrode to prevent the negatively charged 5-HIAA from reaching and fouling the electrode surface. This modification allowed for the first measurement of endogenous serotonin release and uptake in the intact mammalian brain.

Adenosine is associated with metabolism, regulation of blood flow, and modulation of neurotransmitter release in the brain (Cunha, 2001). Swamy and Venton extended the anodic potential limit of the FSCV waveform to 1.5 V and characterized the electrochemical properties of adenosine (Swamy and Venton, 2006). Cechova and Venton then used this approach to simultaneously measure dopamine and adenosine efflux *in vivo* (Cechova and Venton, 2008). They also found that adenosine and oxygen efflux correlated after neuronal stimulation. Recent works have also been published using FSCV to characterize the release and transport of adenosine (Cechova et al., 2010; Pajski and Venton, 2010).

Hydrogen peroxide is a reactive oxygen species that can both be involved in cellular stress and play a role modulating neurotransmission *in vivo* (Halliwell, 2006; Kishida and Klann, 2007). Sanford et al. modified the FSCV waveform for hydrogen peroxide detection by extending the anodic potential limit to 1.4 V. Hydrogen peroxide was oxidized at 1.2 V on the reverse sweep because an overoxidized carbon surface was necessary to facilitate measurement. This work is extremely exciting because enzyme-modified electrodes typically detect hydrogen peroxide for the measurement of nonelectroactive biomolecules. Therefore, it may be possible to simultaneously detect

electroactive and non-electroactive neuromodulators voltammetrically rather than amperometrically which will greatly improve the selectivity. Furthermore, the greater selectivity of FSCV may reduce the need for electrode coatings, allowing for the fabrication of biosensors with a faster temporal response over conventional enzyme modified electrodes.

***In Vivo* Microelectrode Design Developments**

The modern era of microelectrode development for *in vivo* neuroanalytical measurements began with an enzyme-modified glutamate sensor developed by the Wilson group (Hu et al., 1994). Gerhardt introduced ceramic-based microelectrode devices for neuromodulator detection (Burmeister et al., 2000; Burmeister et al., 2002; Burmeister et al., 2004), which are stronger than traditional microfabricated silicon substrates and nonconducting. These electrodes have been used to amperometrically detect several analytes *in vivo* (Burmeister et al., 2004; Parikh et al., 2004; Parikh et al., 2007) using a self-referencing technique for the elimination of interferents (Burmeister and Gerhardt, 2001).

Recent progress has also been made in the development of microelectrodes for *in vivo* FSCV measurements. Carbon-fiber microelectrodes are traditionally insulated using pulled glass because of easy fabrication and low cost, but these sensors are fragile and prone to breakage during *in vivo* use. Fused silica has previously been shown to be a well insulating, flexible alternative to glass for carbon-fiber microelectrodes (Swiergiel et al., 1997; Gerhardt et al., 1999). An array of fused silica insulated carbon-fiber microelectrodes were used to monitor dopamine release at multiple locations simultaneously *in vivo*, but these electrodes were laser pulled at the tip and still fragile (Zachek et al., 2010b).

Clark and co-workers recently showed that fused silica insulated carbon-fiber microelectrodes can be implanted for chronic measurements of neuromodulator release *in vivo* because the polyimide insulation surrounding the fused silica resists the immune response (Clark et al., 2009). The electrodes were epoxied at the tip similar to the previous designs so they were more robust *in vivo*. The authors were able to monitor dopamine changes that occurred over several days as an animal acquired behavior, an unprecedented measurement on the sub-second time scale. While extremely powerful, a problem exists in that there is no way to validate the stability of the carbon-fiber microelectrode *in vivo* in real time. A decreased response could be indicative of decreased neuromodulator release/efflux or the degradation of the carbon-fiber microelectrode. The microelectrodes would then have to be excised from the skull and tested *in vitro* to identify the cause for any decrease in signal amplitude *in vivo*.

Microfabricated devices have also been used for FSCV measurements using PPF as the working electrode material. Dopamine and oxygen were simultaneously and separately detected *in vitro* with two different waveforms applied to two different microelectrodes on the same probe (Zachek et al., 2009). The original probe design was made smaller for *in vivo* use and dopamine was detected at multiple locations *in vivo*, highlighting differences in local neurotransmitter release upon the administration of pharmaceutical agents (Zachek et al., 2010a).

Unscrambling Mixed Messages with Principal Component Regression.

The increasing number of analytes detected with FSCV highlights its widespread utility for measuring neuromodulators *in vivo*. Unfortunately, the detection of multiple analytes with overlapping cyclic voltammogram presents a serious selectivity challenge. The recent introduction of microfabricated PPF array electrodes capable of performing FSCV will likely multiply to this problem.

Traditional approaches to calculate simultaneous dopamine and pH changes included visual matching of the pseudocolor representation of measured currents (Michael et al., 1998), statistical matching based on coefficients of determination (R^2) and mean-squared error values (Robinson et al., 2003; Cheer et al., 2004; Stuber et al., 2005), differential subtraction in the current versus time dimension (Phillips et al., 2003b; Phillips et al., 2003c; Cheer et al., 2004), and a sliding digital background algorithm (Stuber et al., 2005). The disadvantage of visual matching is that the analysis was highly subjective user bias could occur. Statistical matching and the sliding digital background approach avoid these criticisms, but are difficult to apply to multiple sequential cyclic voltammograms. Principal component regression (PCR) of *in vivo* FSCV data eliminates many of these restrictions and allows for improved concentration prediction (Heien et al., 2004b; Heien et al., 2005). PCR is a multivariate technique, meaning that signal quantitation is based on the amplitude and shape of the entire unknown cyclic voltammogram rather than peak current amplitude at a single potential. (Keithley et al., 2009; Keithley et al., 2010a).

PCR consists of four steps (Keithley et al., 2009; Keithley et al., 2010a). First, a set of representative reference *in vivo* cyclic voltammograms at known concentrations (termed a training set) is assembled. Second, principal component analysis is performed to separate the relevant principal components (PCs) that are necessary for accurate concentration prediction from principal components that describe only noise. Next, regression analysis is used to relate the distance of the training set cyclic voltammograms along the relevant PCs (called scores) to the reference concentration values. Finally, unknown concentration values are predicted by calculating the relevant scores of the unknown data and using the calibration relationship from the training set.

A residual analysis procedure was incorporated into the PCR algorithm to verify that the multivariate calibration model was applicable to the unknown data set being

predicted (Heien et al., 2005). PCR prediction of neuromodulator concentrations was improved by incorporating a statistical test during the separation of the relevant PCs from the noise PCs (Keithley et al., 2010b). This allowed for proper separation of relevant information from noise and improved the accuracy of the residual analysis procedure. The PCR with residual analysis procedure was further improved by the incorporation of other control procedures that increased the accuracy and robustness of concentration prediction for *in vivo* FSCV measurements (Keithley and Wightman).

Figure 1.2 shows the strength of PCR in the separation of multiple analytes during a typical *in vivo* FSCV measurement. A carbon-fiber microelectrode was lowered into the nucleus accumbens of a freely moving rat. The data shown in three-dimensional color representation at the center of Figure 1.2 was recorded three minutes after an intravenous dose of cocaine (0.3 mg/kg). Clearly, several analytes with distinct voltammetric signatures that overlap are recorded. PCR can separate this mixed neurochemical message into contributions from dopamine and pH change, even in the presence of substantial background electrode drift. All unknown currents not accounted for by the relevant PCs of the training set are contained in the residual. If any deterministic error is present in the residual, it can alert the user that the calibration model may not be appropriate to predict neuromodulator concentrations (Keithley and Wightman).

The analysis can be taken one step further to identify relevant fluctuations buried in the noise present in the predicted concentration trace (Hermans et al., 2008). The dopamine, pH change, and background drift cyclic voltammograms from Figure 1.2 were integrated to generate the charge for each analyte as a function of time. Since the contributions of each species at each time point are now all in the same units (rather than μM dopamine, pH change, and an arbitrary unit for background change after PCR

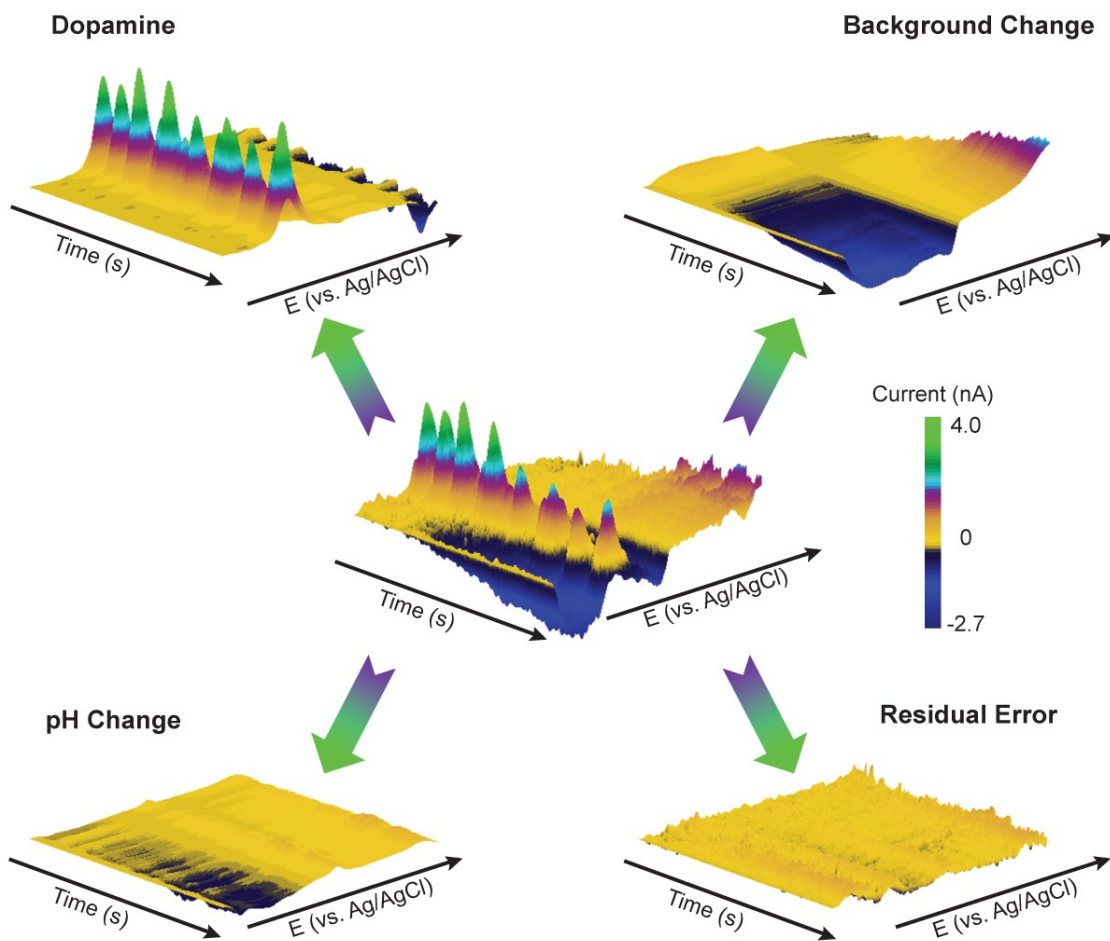


Figure 1.2. PCR signal separation of complex in vivo FSCV data. Three-dimensional representations of the traditional color plots associated with in vivo FSCV data are shown. After the intravenous infusion of cocaine (0.3 mg/kg), simultaneous dopamine and pH changes are detected, while the electrode continually drifts over the course of the 60 s measurement. PCR can split this total signal (center) into separate specific current contributions (corners). The voltage was swept from -0.4 V to 1.3 V to -0.4 V at 400 V/s.

prediction), oscillations in each analyte “channel” can be directly compared on the same scale.

Figure 1.3 shows the charge curves for each species as a function of time. The dopamine channel has large oscillations compared to pH change and background change. Because background change has no physiological relevance, the oscillations in this channel can be taken as a measure of noise (electronic and electrode) in the system (Hermans et al., 2008). The standard deviation of the oscillations in each channel was 1.1 pC for dopamine, 0.4 pC for pH change, and 0.4 pC for background drift. Comparing dopamine and pH change oscillations to background oscillations shows that after cocaine, dopamine levels significantly fluctuated while pH change did not. This behavior was expected because cocaine is known to cause transient concentration changes in dopamine (Heien et al., 2005). Therefore, analyzing background electrode drift can be useful in separating relevant information from noise.

Concluding Remarks

While the utility of *in vivo* electrochemistry has grown considerably over recent years, there remains considerable opportunity for analytical chemists to move the field forward. The works presented here highlight that there is still considerable research interest in increasing sensitivity for carbon-based *in vivo* FSCV microelectrodes. While every analytical chemist can benefit from enhanced sensitivity, FSCV measurements coupled to iontophoresis (Herr et al., 2010) and electrophysiology (Cheer et al., 2005) both suffer from decreased sensitivity. However, it is ideal that any method for enhanced sensitivity does not increase the temporal response of the carbon-based microelectrode.

Early work in the microfabrication of electrode arrays (Zachek et al., 2009; Zachek et al., 2010a) presents another direction of study. Microfabricated PPF

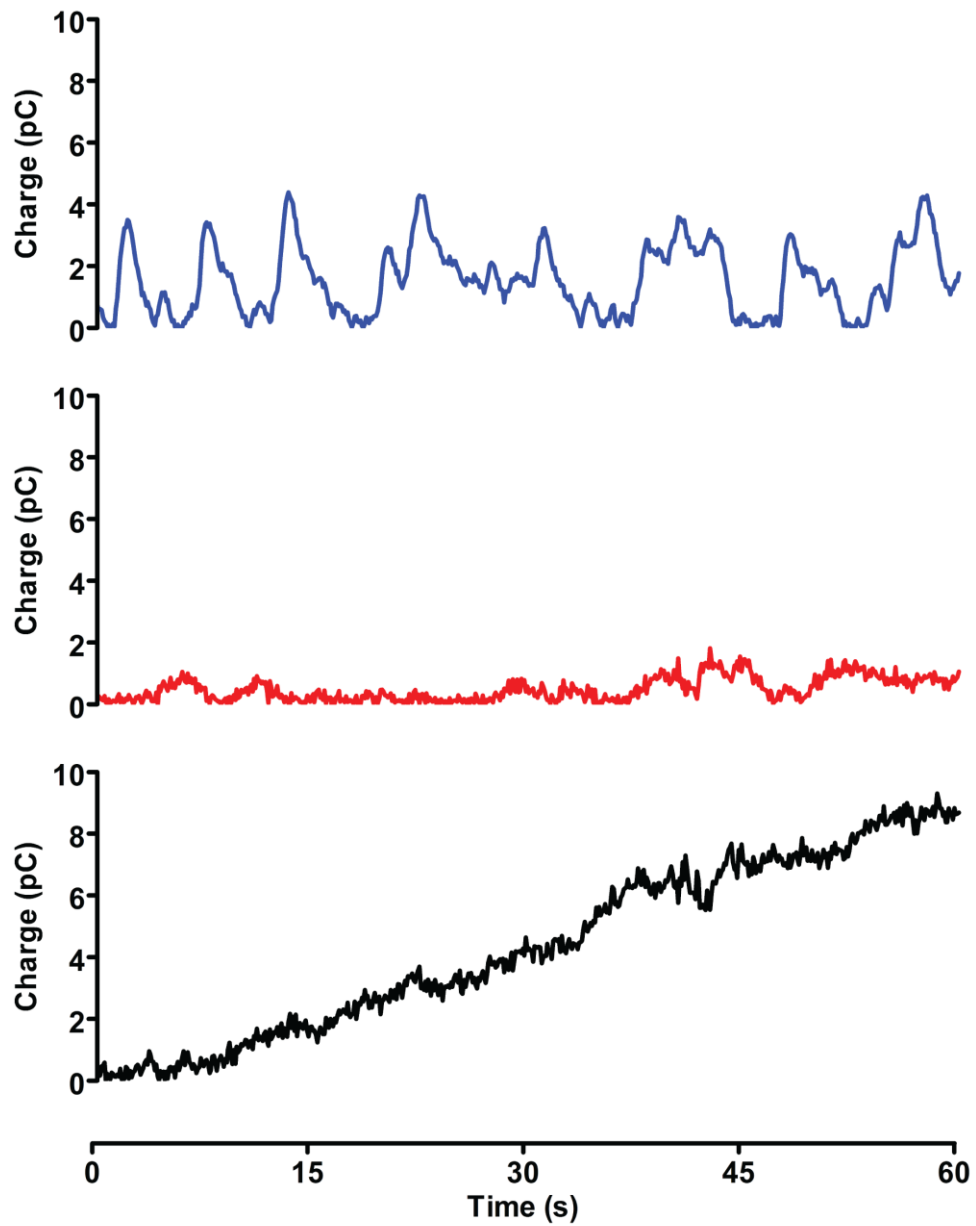


Figure 1.3. Comparison of charge oscillations. Dopamine (top), pH change (center), and background change (bottom) upon intravenous cocaine infusion. The charge oscillations were calculated using the data presented in Figure 1.2.

microelectrodes should allow for extreme precision in electrode design, ruggedness of the electrochemical sensor, spatial precision, and decreased microelectrode variability. One challenge that still remains is decreasing the size of the sensor to a size comparable to carbon-fiber microelectrodes for minimal damage *in vivo* (Jaquins-Gerstl and Michael, 2009). Recent developments in electrophysiological probe design allow for three-dimensional spatial detection (X, Y, and depth positioning, (Langhals and Kipke, 2009)) and construction of three-sided microelectrode arrays along the edge of a device (Seymour et al., 2011). Both of the approaches could be applied to improve FSCV measurements *in vivo*.

Data analysis strategies can also be improved. So far, the only chemometric method incorporated into the analysis of *in vivo* FSCV data is PCR. PCR is simple, yet unsophisticated. Other methods such as partial least-squares, multivariate curve resolution, and independent component analysis could improve concentration prediction.

If other methods are investigated, controls such as the residual analysis procedure for PCR must be included in the analysis so the user does not merely copy concentration data from computer like a general chemistry student from their calculator. Another caution to the analytical chemist is that a rat is not a beaker. *In vivo* electrochemical and biological variability is incredibly interesting and should not be minimized in favor of an easy calibration scheme. Finally, since researchers other than analytical chemists will use these data processing algorithms, any new data analysis strategies should be presented in the literature in a non-mathematical context.

References

- Bath BD, Michael DJ, Trafton BJ, Joseph JD, Runnels PL, Wightman RM (2000) Subsecond adsorption and desorption of dopamine at carbon-fiber microelectrodes. *Anal Chem* 72:5994-6002.
- Baur JE, Kristensen EW, May LJ, Wiedemann DJ, Wightman RM (1988) Fast-Scan Voltammetry of Biogenic-Amines. *Anal Chem* 60:1268-1272.
- Burmeister JJ, Gerhardt GA (2001) Self-referencing ceramic-based multisite microelectrodes for the detection and elimination of interferences from the measurement of L-glutamate and other analytes. *Anal Chem* 73:1037-1042.
- Burmeister JJ, Moxon K, Gerhardt GA (2000) Ceramic-based multisite microelectrodes for electrochemical recordings. *Anal Chem* 72:187-192.
- Burmeister JJ, Coates TD, Gerhardt GA (2004) Multisite microelectrode arrays for measurements of multiple neurochemicals. *Conf Proc IEEE Eng Med Biol Soc* 7:5348-5351.
- Burmeister JJ, Pomerleau F, Palmer M, Day BK, Huettl P, Gerhardt GA (2002) Improved ceramic-based multisite microelectrode for rapid measurements of -glutamate in the CNS. *J Neurosci Meth* 119:163-171.
- Cechova S, Venton BJ (2008) Transient adenosine efflux in the rat caudate-putamen. *Journal of Neurochemistry* 105:1253-1263.
- Cechova S, Elsobky AM, Venton BJ (2010) A1 receptors self-regulate adenosine release in the striatum: evidence of autoreceptor characteristics. *Neuroscience* 171:1006-1015.
- Cheer JF, Wassum KM, Heien MLAV, Phillips PEM, Wightman RM (2004) Cannabinoids Enhance Subsecond Dopamine Release in the Nucleus Accumbens of Awake Rats. *J Neurosci* 24:4393-4400.
- Cheer JF, Heien MLAV, Garris PA, Carelli RM, Wightman RM (2005) Simultaneous dopamine and single-unit recordings reveal accumbens GABAergic responses: Implications for intracranial self-stimulation. *Proc Natl Acad Sci U S A* 102:19150-19155.
- Clark JJ, Sandberg SG, Wanat MJ, Gan JO, Horne EA, Hart AS, Akers CA, Parker JG, Willuhn I, Martinez V, Evans SB, Stella N, Phillips PEM (2009) Chronic microsensors for longitudinal, subsecond dopamine detection in behaving animals. *Nat Meth* 7:126-129.
- Cooper JR, Bloom FE, Roth RH (1996) *The biochemical basis of neuropharmacology*. New York: Oxford University Press.
- Cunha RA (2001) Adenosine as a neuromodulator and as a homeostatic regulator in the nervous system: different roles, different sources and different receptors. *Neurochemistry International* 38:107-125.

- Gerhardt GA, Ksir C, Pivik C, Dickinson SD, Sabeti J, Zahniser NR (1999) Methodology for coupling local application of dopamine and other chemicals with rapid *in vivo* electrochemical recordings in freely-moving rats. *J Neurosci Meth* 87:67-76.
- Glimcher PW (2011) Foundations of neuroeconomic analysis. Oxford ; New York: Oxford University Press.
- Hafizi S, Kruk ZL, Stamford JA (1990) Fast cyclic voltammetry: improved sensitivity to dopamine with extended oxidation scan limits. *J Neurosci Meth* 33:41-49.
- Halliwel B (2006) Oxidative stress and neurodegeneration: where are we now? *Journal of Neurochemistry* 97:1634-1658.
- Hashemi P, Dankoski EC, Petrovic J, Keithley RB, Wightman RM (2009) Voltammetric Detection of 5-Hydroxytryptamine Release in the Rat Brain. *Anal Chem* 81:9462-9471.
- Heien M, Khan AS, Ariansen JL, Cheer JF, Phillips PEM, Wassum KM, Wightman RM (2005) Real-time measurement of dopamine fluctuations after cocaine in the brain of behaving rats. *Proc Natl Acad Sci U S A* 102:10023-10028.
- Heien ML (2005) Probing dopamine release and function with carbon-fiber microelectrodes. In: Doctoral Dissertation (Wightman RM, ed). Chapel Hill, N.C.: University of North Carolina at Chapel Hill.
- Heien ML, Johnson MA, Wightman RM (2004) Resolving neurotransmitters detected by fast-scan cyclic voltammetry. *Anal Chem* 76:5697-5704.
- Heien ML, Phillips PE, Stuber GD, Seipel AT, Wightman RM (2003) Overoxidation of carbon-fiber microelectrodes enhances dopamine adsorption and increases sensitivity. *Analyst* 128:1413-1419.
- Hermans A (2007) Fabrication and applications of dopamine-sensitive electrodes. In: Doctoral Dissertation (Wightman RM, ed). Chapel Hill, N.C.: University of North Carolina at Chapel Hill.
- Hermans A, Keithley RB, Kita JM, Sombers LA, Wightman RM (2008) Dopamine detection with fast-scan cyclic voltammetry used with analog background subtraction. *Anal Chem* 80:4040-4048.
- Herr NR, Belle AM, Daniel KB, Carelli RM, Wightman RM (2010) Probing Presynaptic Regulation of Extracellular Dopamine with Iontophoresis. *ACS Chem Neurosci* 1:627-638.
- Hu Y, Mitchell KM, Albahadily FN, Michaelis EK, Wilson GS (1994) Direct measurement of glutamate release in the brain using a dual enzyme-based electrochemical sensor. *Brain Res* 659:117-125.
- Huffman ML, Venton BJ (2009) Carbon-fiber microelectrodes for *in vivo* applications. *Analyst* 134:18-24.

- Jackson BP, Dietz SM, Wightman RM (1995) Fast-Scan Cyclic Voltammetry of 5-Hydroxytryptamine. *Anal Chem* 67:1115-1120.
- Jaquins-Gerstl A, Michael AC (2009) Comparison of the brain penetration injury associated with microdialysis and voltammetry. *J Neurosci Meth* 183:127-135.
- Keithley RB, Wightman RM Assessing principal component regression with residual analysis in the detection of neuromodulators. In Preparation.
- Keithley RB, Wightman RM, Heien ML (2009) Multivariate concentration determination using principal component regression with residual analysis. *TrAC Trends Anal Chem* 28:1127-1136.
- Keithley RB, Wightman RM, Heien ML (2010a) Erratum to Multivariate concentration determination using principal component regression with residual analysis. *TrAC Trends Anal Chem* 29:110-110.
- Keithley RB, Carelli RM, Wightman RM (2010b) Rank Estimation and the Multivariate Analysis of *in vivo* Fast-Scan Cyclic Voltammetric Data. *Anal Chem* 82:5541-5551.
- Keithley RB, Takmakov P, Bucher ES, Belle AM, Owesson-White CA, Park J, Wightman RM (2011) Higher Sensitivity Dopamine Measurements with Faster-Scan Cyclic Voltammetry. *Anal Chem* Submitted.
- Kishida KT, Klann E (2007) Sources and targets of reactive oxygen species in synaptic plasticity and memory. *Antioxid Redox Signal* 9:233-244.
- Langhals NB, Kipke DR (2009) Validation of a novel three-dimensional electrode array within auditory cortex. In: *Engineering in Medicine and Biology Society, 2009. EMBC 2009. Annual International Conference of the IEEE*, pp 2066-2069.
- McCreery RL (1991) Carbon Electrodes: Structural Effects on Electron Transfer Kinetics. In: *Electroanalytical Chemistry: A Series of Advances* (Bard AJ, ed), pp 221-374. New York, NY: Marcel Dekker.
- Michael D, Travis ER, Wightman RM (1998) Color images for fast-scan CV. *Anal Chem* 70:586a-592a.
- Pajski ML, Venton BJ (2010) Adenosine Release Evoked by Short Electrical Stimulations in Striatal Brain Slices is Primarily Activity Dependent. *ACS Chem Neurosci* 1:775-787.
- Parikh V, Kozak R, Martinez V, Sarter M (2007) Prefrontal Acetylcholine Release Controls Cue Detection on Multiple Timescales. *Neuron* 56:141-154.
- Parikh V, Pomerleau F, Huettl P, Gerhardt GA, Sarter M, Bruno JP (2004) Rapid assessment of *in vivo* cholinergic transmission by amperometric detection of changes in extracellular choline levels. *European Journal of Neuroscience* 20:1545-1554.

- Park J, Kile BM, Wightman RM (2009) *In vivo* voltammetric monitoring of norepinephrine release in the rat ventral bed nucleus of the stria terminalis and anteroventral thalamic nucleus. *Eur J Neurosci* 30:2121-2133.
- Phillips PEM, Stuber GD, Heien MLAV, Wightman RM, Carelli RM (2003a) Subsecond dopamine release promotes cocaine seeking. *Nature* 422:614-618.
- Phillips PEM, Stuber GD, Heien MLAV, Wightman RM, Carelli RM (2003b) Subsecond dopamine release promotes cocaine seeking, Erratum. *Nature* 423:461-461.
- Ranganathan S, McCreery R, Majji SM, Madou M (2000) Photoresist-derived carbon for microelectromechanical systems and electrochemical applications. *Journal of the Electrochemical Society* 147:277-282.
- Rice ME, Nicholson C (1989) Measurement of nanomolar dopamine diffusion using low-noise perfluorinated ionomer-coated carbon fiber microelectrodes and high-speed cyclic voltammetry. *Anal Chem* 61:1805-1810.
- Roberts JG, Moody BP, McCarty GS, Sombers LA (2010) Specific Oxygen-Containing Functional Groups on the Carbon Surface Underlie an Enhanced Sensitivity to Dopamine at Electrochemically Pretreated Carbon Fiber Microelectrodes. *Langmuir* 26:9116-9122.
- Robinson DL, Wightman RM (2007) Rapid Dopamine Release in Freely Moving Rats. In: *Electrochemical Methods for Neuroscience* (Michael AC, Borland LM, eds), pp 17-34. Boca Raton, FL, USA: CRC Press.
- Robinson DL, Venton BJ, Heien ML, Wightman RM (2003) Detecting subsecond dopamine release with fast-scan cyclic voltammetry *in vivo*. *Clin Chem* 49:1763-1773.
- Sandberg SG, Kishida K, Lohrenz T, Comair Y, Montague PR, Phillips PE (2010) Sub-second dopamine detection in human striatum. In: *Monitoring Molecules in Neuroscience, 13th International Conference on In vivo Methods*, pp 188-191. Brussels, Belgium.
- Schultz W (2007) Multiple dopamine functions at different time courses. *Annual Review of Neuroscience* 30:259-288.
- Seymour J, Langhals N, Anderson D, Kipke D (2011) Novel multi-sided, microelectrode arrays for implantable neural applications. *Biomedical Microdevices*:In Press.
- Shon Y-M, Lee KH, Goerss SJ, Kim IY, Kimble C, Van Gompel JJ, Bennet K, Blaha CD, Chang S-Y (2010) High frequency stimulation of the subthalamic nucleus evokes striatal dopamine release in a large animal model of human DBS neurosurgery. *Neuroscience Letters* 475:136-140.
- Strand AM, Venton BJ (2008) Flame etching enhances the sensitivity of carbon-fiber microelectrodes. *Anal Chem* 80:3708-3715.

- Stuber GD, Roitman MF, Phillips PEM, Carelli RM, Wightman RM (2005) Rapid dopamine signaling in the nucleus accumbens during contingent and noncontingent cocaine administration. *Neuropsychopharmacol* 30:853-863.
- Swamy BEK, Venton BJ (2006) Subsecond Detection of Physiological Adenosine Concentrations Using Fast-Scan Cyclic Voltammetry. *Anal Chem* 79:744-750.
- Swamy BEK, Venton BJ (2007) Carbon nanotube-modified microelectrodes for simultaneous detection of dopamine and serotonin *in vivo*. *Analyst* 132:876-884.
- Swiergiel AH, Palamarchouk VS, Dunn AJ (1997) A new design of carbon fiber microelectrode for *in vivo* voltammetry using fused silica. *J Neurosci Meth* 73:29-33.
- Takmakov P, McKinney CJ, Carelli RM, Wightman RM (2011) Instrumentation for Fast-Scan Cyclic Voltammetry Combined with Electrophysiology for Behavioral Experiments in Freely Moving Animals. *Review of Scientific Instruments* Submitted.
- Takmakov P, Zachek MK, Keithley RB, Bucher ES, McCarty GS, Wightman RM (2010a) Characterization of Local pH Changes in Brain Using Fast-Scan Cyclic Voltammetry with Carbon Microelectrodes. *Anal Chem* 82:9892-9900.
- Takmakov P, Zachek MK, Keithley RB, Walsh PL, Donley C, McCarty GS, Wightman RM (2010b) Carbon Microelectrodes with a Renewable Surface. *Anal Chem* 82:2020-2028.
- Venton BJ, Michael DJ, Wightman RM (2003) Correlation of local changes in extracellular oxygen and pH that accompany dopaminergic terminal activity in the rat caudate-putamen. *Journal of Neurochemistry* 84:373-381.
- Wightman RM, Robinson DL (2002) Transient changes in mesolimbic dopamine and their association with 'reward'. *Journal of Neurochemistry* 82:721-735.
- Zachek MK, Takmakov P, Moody B, Wightman RM, McCarty GS (2009) Simultaneous Decoupled Detection of Dopamine and Oxygen Using Pyrolyzed Carbon Microarrays and Fast-Scan Cyclic Voltammetry. *Anal Chem* 81:6258-6265.
- Zachek MK, Takmakov P, Park J, Wightman RM, McCarty GS (2010a) Simultaneous monitoring of dopamine concentration at spatially different brain locations *in vivo*. *Biosens Bioelectron* 25:1179-1185.
- Zachek MK, Park J, Takmakov P, Wightman RM, McCarty GS (2010b) Microfabricated FSCV-compatible microelectrode array for real-time monitoring of heterogeneous dopamine release. *Analyst* 135:1556-1563.

CHAPTER II

MULTIVARIATE CONCENTRATION DETERMINATION USING PRINCIPAL COMPONENT REGRESSION WITH RESIDUAL ANALYSIS

Abstract

Data analysis is an essential tenet of analytical chemistry, extending the possible information obtained from the measurement of chemical phenomena. Chemometric methods have grown considerably in recent years, but are still considered by some too complicated hindering wide use. The purpose of this review is to inform a general scientific audience about a multivariate chemometric method, principal component regression, in a simple manner from the point of view of an analytical chemist, to demonstrate the need for proper quality control measures in multivariate analysis, and to advocate the use of residuals as a proper method of quality control.

Introduction

Advances in electronics and computing over the past 30 years have revolutionized the analytical laboratory. Technological developments have allowed instruments to become smaller, faster, and cheaper while continuing to increase accuracy, precision, and availability. Data analysis methods have also benefitted from advances in technical computing; commercially available mathematical programming packages allow scientists to perform complex calculations with a few simple keystrokes. Furthermore, software sold with many commercial instruments contains automatic data processing algorithms (e.g. Fourier transform analysis, data filtering, peak recognition).

The advances in computing allow researchers to obtain more and more chemically relevant information from their data; however this is not always achieved using simple data processing techniques.

Svante Wold first coined the term kemometri (chemometrics in English) in 1972 by combining the words *kemo* for chemistry and *metri* for measure (R. Kiralj, 2006). Presently, the journal *Chemometrics and Intelligent Laboratory Systems* defines chemometrics as “the chemical discipline that uses mathematical and statistical methods to design or select optimal procedures and experiments, and to provide maximum chemical information by analyzing chemical data” (Elsevier, 2009). The field of chemometrics has also benefitted from technological advances in the past 30 years, causing the number of researchers using chemometric methods to grow (Brown and Bear, 1993; Bro, 2003; Lavine and Workman, 2008). Unfortunately, however, chemometrics has not been as rapidly integrated into the analytical laboratory as other advances.

The slow adaptation of these methods may be attributed to several factors. Technical articles on the subject are often written by chemometricians for chemometricians; it can be difficult for the general scientist to approach this field and comprehend the material presented. Even introductory texts and review articles often require working knowledge of linear algebra and matrix manipulations. Chemometric methods have developed such that they are readily available to any scientist and in this article we hope to show the importance of chemometrics to the benchtop analytical chemist in concentration determination using a technique known as principal component regression.

Multivariate Analysis in Analytical Chemistry

Traditional concentration determinations are usually *univariate*, isolating one variable such as peak current at one potential in an electrochemical measurement or the wavelength of maximum absorbance in a spectroscopic measurement. While intuitive and simple, this approach to data analysis is limited and wasteful. As an example, consider a UV-VIS spectrum of a particular analyte containing 500 data points. With only one data point being used for concentration determination (absorbance at one wavelength), after identification 99.8% of the data will be discarded. Data collection can limit the throughput of an analytical methodology; it is not efficient to collect data that will not be used. In addition, a univariate measurement is extremely sensitive to interferences. It is often times impossible to differentiate an analyte-specific signal from an interferent when looking only at one point of a data spectrum.

Multivariate calibration methods involve the use of the multiple variables such as the response at a range of potentials or wavelengths, or even over the entire range collected to calculate concentrations. This offers several advantages, often reducing noise and removing interferences (Bro, 2003). It can be easier to identify and remove noise when looking at the entire data set, rather than one point. In addition, interferences can be taken into account, provided their measurement profile differs sufficiently from the analyte of interest (Heien et al., 2004a). Multivariate methods are generally better than univariate methods. They increase the amount of possible information that can be obtained without losing any information; multivariate models can always be simplified to a univariate model (Bro, 2003). The advantages of multivariate methods come at a cost of computational power and complexity, but these drawbacks are easily handled with common mathematical software packages such as Matlab.

Analytical techniques are often misused because their limitations are not always clearly understood. Multivariate analysis methods are no different and have the potential to be misused more than instrumental techniques because all of the computations are

performed behind the computer screen. Chemometricians have derived a series of rules, statistical tests, and other criteria in order for users to judge and validate the accuracy of the information obtained with multivariate methods (International, 2000). It is important for any new user of multivariate methods to remember that the computer will always give an output but it is up to the scientist to make sure that both precautions are taken and the answers obtained make chemical sense.

Construction of a multivariate model: principal component regression

Principal component regression (PCR) is a basic, but very powerful multivariate calibration method. A brief overview of PCR will be presented here, but for a more detailed explanation readers are referred elsewhere (Jackson, 2004). In addition, Kramer offers an excellent review of the topic in a manner that the benchtop analytical chemist can understand and use and we highly recommend it to anyone interested in using the technique (Kramer, 1998b). PCR is a combination of principal component analysis (PCA) and least-squares regression.

When discussing multivariate analysis techniques, including PCR, three terms are often used: variance, vector, and projection. Variance is another word for information of a data set. Sources of variance within a data set include the changes in the chemical make-up of analyzed samples (concentrations and/or composition), changes in environmental parameters (e.g. temperature, pressure, etc.), and changes in instrument performance such (e.g. a drifting baseline). The term vector is used to describe a line segment in a coordinate system with a specific direction (e.g. an axis) and the term projection is used to describe the distance of a point along a vector.

We will illustrate how PCR is performed using simulated data taken from a hypothetical UV-VIS experiment. This example is an oversimplification, but explains the technique of PCR in a manner that can be easily understood without overbearing mathematical descriptions.

The solid line in Figure 2.1A shows an example UV-VIS absorption trace of component X at a specific concentration, [X]. The information in the absorption spectrum of component X can be plotted in a different manner (Figure 2.1B). Figure 2.1B shows a plot of the intensities at 425 nm and 475 nm. Component X has intensities of 0.1 A.U. and 0 A.U. at 425 nm and 475 nm, respectively and can be represented as the point (0.1, 0) in the two-dimensional coordinate system shown in Figure 2.1B. According to Beer's law, if analyte X is doubled ([2X]), tripled ([3X]), and quadrupled ([4X]), the absorbance spectrum will increase by 2, 3, and 4-fold, respectively, as shown in the dashed lines in Figure 2.1A. These absorption spectra can also be plotted the same way as the first spectrum in a two-dimensional manner as shown in Figure 2.1B (purple squares). Similarly, component Y, which has a different absorption spectrum (Figure 2.1C) and at concentrations [Y], [2Y], [3Y], and [4Y] can be plotted in a two-dimensional manner as shown in Figure 2.1D (green diamonds) as multiples of the point (0, 0.1).

As shown in Figures 2.1B and 2.1D, lines can be drawn through the two-dimensional representations of the absorption spectra of components X and Y. Each of these lines describes important information about the measured absorption spectra. The horizontal line in Figure 2.1B describes how intensities change based on [X] and the vertical line in Figure 2.1D describes how intensities change based on [Y]. In this simplified case, moving in a horizontal direction in these graphs describes only how [X] is changing and says nothing about how [Y] is changing. Conversely, moving in a vertical direction in these graphs describes only how [Y] is changing and says nothing about how [X] is changing. Mathematically speaking these lines are orthogonal, meaning that each describes information that another does not. These lines, which each describe different information about the original data drawn in an alternative coordinate system, can be thought of as principal components. Stated another way, principal

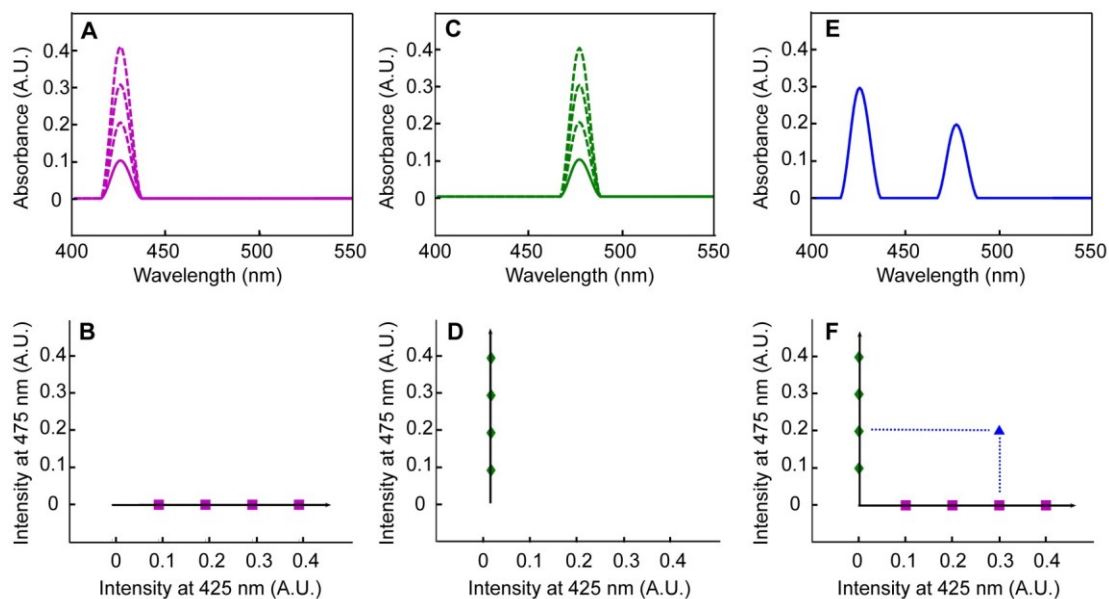


Figure 2.1. Representation of UV-VIS data in an intensity space. A) UV-VIS spectra of component X in concentrations [X] (solid line) to [2X], [3X], and [4X] (dashed lines). B) Spectra in A) plotted in an intensity coordinate system with intensity at 425 nm on the x-axis, intensity at 475 nm on the y-axis, and intensity at 525 nm on the z-axis (going in and out of the page, omitted for clarity). C) UV-VIS spectra of component Y in concentrations [Y] (solid line) to [2Y], [3Y], and [4Y] (dotted lines). D) Spectra in C) plotted in an intensity coordinate system. E) UV-VIS spectra of an unknown mixture of X and Y. F) Spectrum in E) plotted in an intensity coordinate system with the dotted lines representing projections onto each principal component.

components can be thought of as vectors in an abstract coordinate system that describe sources of variance of a data set. Chemometricians and mathematicians advocate the use of a slightly different definition of a principal component, but our definition is common and is used in many introductory texts (Kramer, 1998b; Jolliffe, 2004a; Ralston et al., 2004).

The projection of the points onto the principal components shown in Figures 2.1B and 2.1D is related to concentration just like a traditional univariate calibration curve. Figure 2.1E shows an example of an absorption spectrum from an unknown mixture of components X and Y. It can be represented as the point (0.3, 0.2) in the two-dimensional space depicted in Figure 2.1F. This unknown sample has a projection along the horizontal principal component of 0.3 and a projection along the vertical principal component of 0.2, correspond to concentrations of [3X] and [2Y]. Comparing the unknown spectrum in Figure 2.1E with the standards in Figure 2.1B and 2.1D confirm this result. Mathematically, the projection onto a principal component is related to concentration by performing a simple least-squares regression.

In a univariate calibration, known concentrations of standards are assembled. Peak responses are plotted as a function of concentration and a regression is performed relating a measured value to concentration. Finally, the measured response is projected back onto the calibration line in order to determine a concentration. PCR is a multivariate calibration method that works in a similar manner using up to all the data points in a spectrum instead of just one. First, a series of known spectra and concentrations known as a training set is assembled. Second, principal components are calculated that describe relevant portions of the assembled calibration spectra using PCA. Third, a regression is performed that relates concentrations to distances along principal components. Finally, concentrations are predicted by projecting an unknown

sample onto the principal component and relating its distance back to concentration (Kramer, 1998a).

The number of principal components calculated equals the number of spectra in the training set that are input into the algorithm, but principal components themselves are not always directly interpretable. The above example showed that one principal component described only component X and one principal component described only component Y, but principal components are abstract and should not be thought of as belonging solely to one component or as pure analyte spectra (Brown and Green, 2009). Sometimes, however, mathematical manipulations can be performed on the principal components in order to give the user something that relates back to a specific source of variance in the experiment (Jolliffe, 2004b).

PCR offers several advantages to an analytical chemist. First, one can separate and retain principal components that describe relevant information and discard principal components that contain noise, thereby eliminating sources of random error. Principal components that describe relevant information should have larger projections because they describe more of the collected dataset than those that describe noise, which should be a small percentage of the overall measured signal. There are numerous ways to decide how many principal components to keep, but all rely on the same basic assumption that principal components that describe relevant information will describe more of the collected data than principal components that describe only noise (Malinowski, 1990; Jackson, 1991b; Jolliffe, 2004c). Second, the size of a data matrix is drastically reduced (Heien et al., 2004a). An entire spectrum can be replaced by its distance (or projection) along a few principal components. For example, a data set comprised of 1,000 data point cyclic voltammogram measured at 10 Hz for 60 seconds contains 600,000 data points. If only three principal components are needed to fully describe all the relevant information of the collected data set, the number of data points

can be reduced by from 600,000 (1,000 points x 10 Hz x 60 s) to 1,800 (3 x 10 Hz x 60 s), or 0.3% of the size of the original data set. This example illustrates how PCA can reduce the dimensionality, or size, of a data set by orders of magnitude and still keep the relevant information.

Samples used in multivariate training sets must meet several requirements (Kramer, 1998d; International, 2000). First, training set samples must contain all expected components because concentrations obtained may not be accurate if the unknown sample contains spectral information not present in the training set. Second, training set samples must uniformly span the expected concentrations of each of the components to insure that unknown concentrations fall within the calibration range. Third, training set samples must span the conditions of interest in order to properly account for environmental parameters and sample matrix. Fourth, samples used in training sets must be mutually independent. Samples created by serial dilutions are examples of samples that are not mutually independent because relative concentrations of the different components and relative errors in the concentration values are do not vary. Finally, there needs to be sufficient number of samples in the training set to build an accurate model. For infrared data, ASTM International recommends at least 24 samples for a model that contains up to 3 relevant principal components and 6 samples per relevant principal component for a model with more than 3 relevant principal components. Unfortunately, this means that a user will only know if enough samples were included in the training set after a model is constructed.

PCR has been used in order to predict concentrations of *in vivo* electroactive species using fast-scan cyclic voltammetry (Heien et al., 2004a; Heien et al., 2005; Hermans et al., 2008). Figure 2.2 shows how PCR can be used to separate the neuromodulators dopamine and pH during stimulated release. A carbon fiber microelectrode is placed in a region of the brain containing dopaminergic neuron

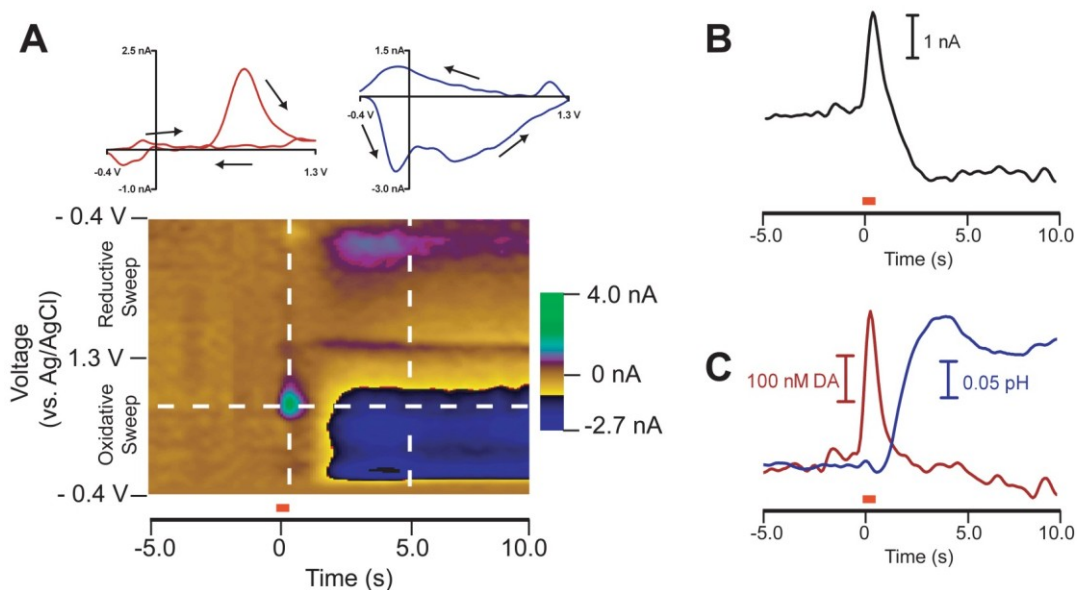


Figure 2.2. PCR deconvolution of *in vivo* electrochemical data. A) Color plot representation of cyclic voltammograms taken in the brain of a freely moving rat after a stimulation given at 0 s (60 Hz, 24 pulses, 300 μ A depicted by the red bar). Each vertical slice represents a cyclic voltammogram collected at a specific time point and each horizontal slice represents a current versus time trace at a specific potential. The horizontal dashed line represents the oxidation potential of dopamine, 0.6 V. Insets are cyclic voltammograms of dopamine (red, taken at the dashed line at 0 sec) and pH (blue, taken at the dashed line at 5 sec) with arrows drawn indicating the direction of the voltammetric sweep. B) Current versus time trace at the oxidation potential of dopamine with the red bar marking the onset of the stimulation. C) Dopamine (DA) and pH concentrations predicted using PCR.

terminals while a stimulating electrode is placed in a region containing dopaminergic cell bodies. Figure 2.2A displays *in vivo* cyclic voltammograms in the form of a color plot, with each vertical slice a cyclic voltammogram at a specific time point, each horizontal slice a current versus time trace at a specific potential, and current in false color. The cyclic voltammograms taken around 0 s are characteristic of the neurotransmitter dopamine while those taken between 2 and 10 s are characteristic of a pH change (Figure 2.2A inset). The increase in dopamine concentration occurs due to a local stimulation given to the cell bodies of dopaminergic neurons that causes release in the terminal region. The observed pH response is due to changes in blood flow and metabolism accompanying terminal activity which cause a decrease in carbon dioxide, a component of the extracellular buffering system of the brain (Venton et al., 2003). The current versus time trace taken at the oxidation potential of dopamine in Figure 2.2B shows a convoluted response between dopamine and pH so a univariate calibration would be insufficient to determine dopamine concentration as a function of time. Using a training set of *in vivo* cyclic voltammograms of dopamine and pH at varying intensities, PCR can separate these two components and generate concentration traces for each analyte as shown in Figure 2.2C.

PCR Model Validation

When fitting any calibration model to a data set, univariate or multivariate, an analytical chemist should ask two questions: 1. How accurate is my calibration model at predicting concentrations? and 2. How applicable is my calibration model an unknown data set? When using multivariate calibrations, the accuracy of a model is addressed with a process called validation. A set of test samples distinct from the calibration set with known concentrations are used to determine the accuracy of the calibration at predicting unknown concentrations. The predicted residual error sum-of-squares

(PRESS) is the squared difference between the actual and predicted concentrations for all validation samples and serves as a figure of merit for the multivariate model (Kramer, 1998c). PRESS gives the experimenter an idea of how well the model can predict new concentrations and how much error can be expected in the concentrations obtained from the analysis of unknowns. The extra work to validate a model before running an experiment is necessary; it is better to test the accuracy of a model first rather than using it blindly on unknowns and hoping for accuracy (Kramer, 1998c).

Unfortunately, validation samples are not always available due to cost, time constraints, or other experimentation conditions. In these cases the training set can be used as a test set in a process called cross validation. When using cross validation with PCR, the regression is performed using all the samples of the training set except one. The concentration of this training set sample is predicted using the regression model and a PRESS value is calculated. The excluded sample is reintroduced into the training set and another training set sample is excluded and its concentration and PRESS value is estimated and added to the previous PRESS value. The process is repeated until all of the training set samples have been estimated and a final PRESS value is calculated (Kramer, 1998c).

A PRESS value calculated in this way can also be used as a measure of the proper number of principal components of a data set to retain. As more principal components are retained, the PCR model will predict concentrations more accurately and PRESS values will decrease. However, there will come a point where increasing the number of principal components retained does not significantly improve the accuracy of the prediction and those principal components should be discarded (Jackson, 1991b; Kramer, 1998a; Jolliffe, 2004c).

PCR Model Applicability: Residual Analysis

The accuracy and applicability of a model are two distinct questions (*vide supra*) (Daszykowski and Walczak, 2006). Some users of PCR do not address applicability of their calibration model and thus assume that the calibration model is always applicable to an unknown data set. Stated another way, one assumes that the relevant principal components of a data set describe all relevant information in the unknown data set. Instrumental errors such as drift, experimental system errors such as pressure and temperature, and impurities or interferences can invalidate this assumption if they contribute significantly to the measured signal (Nomikos and Macgregor, 1995; Bro, 2003).

There are situations in which a scientist may not always know the complete composition of the unknown data set a priori and will not be able to predict if there are any unknown components that will significantly affect the measured response. As an example, *in vivo* electrochemists use fast-scan cyclic voltammetry to measure electroactive species in the brain of freely moving rats. Training set cyclic voltammograms often incorporate only dopamine and pH but measure in brain regions containing many electroactive species (Justice Jr., 1987). If dopamine and pH are the only significant current contributions to the overall measurement, concentration data should be accurate. However, if other electroactive species are present in concentrations large enough to contribute a significant amount of current, the training set cyclic voltammograms would be insufficient to model all of the collected data and concentration data obtained from PCR would be questionable.

Jackson and Mudholkar proposed a method in order to evaluate the goodness of fit of training set data to an unknown data set in PCR using residuals (Jackson and Mudholkar, 1979; Jackson, 1991c). In general, a residual is defined as the difference between an experimental observation and a predicted value from a model. Residual analysis has several advantages including quality control monitoring, interferent

identification, and outlier detection. An advantage with working with multivariate data is that it can sometimes be possible to visualize the data spectrum of an interferent, something that is impossible with a univariate measurement.

In PCR residuals are a measure of the unknown signal (e.g. current) that is not accounted for by the retained principal components of the training set. This includes noise and any signal arising from the response of any interfering analytes. Ideally, the training set contains all the relevant information of an unknown data set and the residuals should contain only noise. We will continue to use *in vivo* electrochemical data as an example throughout this section, but the principles apply to all other fields of analytical chemistry.

The quantity Q is defined as the sum of the squares of the residual values at each variable in each sample of the data set. Using *in vivo* electrochemistry as an example, one Q value is calculated for each cyclic voltammogram in the unknown data set by summing the squares of the current at each potential scanned that was not accounted for by the retained principal components of the training set used as shown in Figure 2.3. Mathematically, the Q value of a cyclic voltammogram at time t, Q_t , can be represented by

$$Q_t = \sum_{x=1}^w (i_x^2 - \hat{i}_x^2) \quad (\text{eq 2.1})$$

where i_x is the current at x point number of the wth point cyclic voltammogram and \hat{i}_x is the current predicted from the PCR model containing only the relevant principal components at x point number of the wth point cyclic voltammogram. These Q_t values are tabulated for each sample and plotted consecutively for unknown data set to make a Q plot, with a y-axis is in units of nA^2 for this example.

$$Q_t = \int \left(\text{Cyclic Voltammogram} \times \text{Cyclic Voltammogram} \right)$$

The diagram shows the mathematical representation of the Q value calculation. On the left, the symbol Q_t is followed by an equals sign and a large integral sign. To the right of the integral sign, two cyclic voltammograms are shown, separated by a multiplication sign (X). Each voltammogram plot has a horizontal axis labeled 'Voltage (vs. Ag/AgCl)' with tick marks at -0.4, 0, and 1.3. A vertical scale bar above each plot is labeled '0.1 nA'. The two plots are identical, representing the same cyclic voltammogram being squared and summed.

Figure 2.3. Calculation of a Q value at a specific time point, t . The cyclic voltammetric representation of residual current is squared and summed at time t in order to obtain a Q_t value.

Q_α as a measure of significance

The threshold for the sum of the squares of the residuals (Q_α) is a threshold that establishes whether a satisfactory description of the experimental data by the retained principal components is achieved. The discarded principal components should only contain noise and thus provide a measure of a noise level. If the Q_t values exceed Q_α then there is measured signal that exceeds the noise anticipated by the principal components discarded. The value of Q_α includes a significance level that can be set by the user for how much noise can be tolerated.

Q_α is calculated using the following equations (Jackson and Mudholkar, 1979)

$$Q_{\alpha} = \Theta_1 \left[\frac{c_{\alpha} \sqrt{2\Theta_2 h_0^2}}{\Theta_1} + 1 + \frac{\Theta_2 h_0 (h_0 - 1)}{\Theta_1^2} \right]^{\frac{1}{h_0}} \quad (\text{eq 2.2})$$

$$\Theta_i = \sum_{j=n+1}^m \lambda_j^i \text{ for } i=1, 2, \text{ or } 3 \quad (\text{eq 2.3})$$

$$h_0 = 1 - \frac{2\Theta_1 \Theta_3}{3\Theta_2^2} \quad (\text{eq 2.4})$$

where c_{α} is the z-score that determines the (1- α)% of noise that will be tolerated, n is the number of principal components retained to describe all significant signal contributions of the training set (i.e. if the training set contained 10 cyclic voltammograms n could vary between 1 and 10 depending on the number retained), m is the total number of principal components calculated (10 in the example described above because the number of principal components calculated equals the number of cyclic voltammograms in the training set), and λ is the sum of the squares of the data projections from all the samples in the training set for each principal component. The remaining terms (Θ_1 , Θ_2 , and Θ_3 , and thus h_0) are simply calculated from the λ values of the discarded noise components ($(k + 1) \rightarrow m$). From this description, the calculation of Q_α is based on only two pieces of

information: a noise level threshold (c_α) and the information contained in the discarded principal components of the training set ($\lambda_{(n+1) \rightarrow m}$). Here noise is defined as any signal that has a low probability of containing relevant information (Bezegh and Janata, 1987). When the principal components of the training set were discarded they were assumed to be irrelevant and thus serve as an estimated noise level.

Q_α is a threshold for significance of the Q_t values. Q_α is an upper limit on the amount of noise or random error that will be tolerated from collected data, based on the amount of error contained in the discarded principal components of the training set. A cyclic voltammogram with a Q_t value above this threshold will be considered to contain significant information not accounted for by the retained principal components and concentration values obtained with PCR would be questionable.

A chief advantage to using PCA is to help separate the significant deterministic information from non-deterministic error. Deterministic variation is a non-random change in a signal—for example, the signature shape of the cyclic voltammogram that lets one determine its chemical identity. Non-deterministic noise or error is random and should thus follow a normal distribution. If Q_t exceeds Q_α then the level of the noise is greater than expected and may contain deterministic information that is not accounted for by the retained principal components.

Interpretation of c_α

The c_α term in equation 2 is the z-score corresponding to the $(1-\alpha)\%$ of noise that will be tolerated. Q_t values are the sum of differences of squares and are not normally distributed. However, Jensen and Solomon (Jensen and Solomon, 1972) have shown that the quantity $(Q/\Theta_1)^{h_0}$ can be approximated by a normal distribution with a mean and standard deviation, respectively, equal to

$$\mu = 1 + \frac{\Theta_2 h_0 (h_0 - 1)}{\Theta_1^2} \quad (\text{eq 2.5})$$

$$\sigma = \frac{\sqrt{2\Theta_2 h_0^2}}{\Theta_1} \quad (\text{eq 2.6})$$

From elementary statistics, a z-score for a normal distribution is calculated as the difference between an observed value and the mean, divided by the standard deviation.

This would make the z-score for the $(Q/\Theta_1)^{h_0}$ distribution

$$z = \frac{\Theta_1 \left[(Q/\Theta_1)^{h_0} - 1 - \frac{\Theta_2 h_0 (h_0 - 1)}{\Theta_1^2} \right]}{\sqrt{2\Theta_2 h_0^2}} \quad (\text{eq 2.7})$$

Substituting c_α for z and Q_α for Q in equation 7 and rearranging to solve for Q_α gives equation 2.

Approximately 95% of random, non-deterministic error will fall below a c_α of 1.645 (Jackson, 1991c). An unknown sample will be significantly different from the training set if its Q_t exceeds Q_α . Its signal contribution is larger than where a certain percentage of the signal contributions due solely to random error would be. Using our example with a c_α of 1.645, a Q_t value will only be significant (cross Q_α) if its current contributions are larger than 95% of current contributions due to random noise. Q_α is a measure of significance, not confidence. If Q_t exceeds Q_α , Q_t has a significant value and the use of the retained principal components is insufficient to describe the experimental data. It is incorrect to say that one is $(1-\alpha)\%$ confident concentration data obtained from principal component regression is correct if the residuals do not cross Q_α . Accuracy of concentrations is addressed using validation, but if Q_t crosses Q_α , the validation cannot be trusted because significant interferences are present.

As c_α increases, Q_α increases. As an example, increasing from 95% to 99% increases c_α from 1.645 to 2.326. This increase would mean that a residual (Q_t) would only be significant if it has a current contribution larger than 99% of current contributions due to random noise. Q_α has to increase because an extra 4% of larger random error

current contributions will have to be accounted for. Mathematically, equation 2 shows increasing c_α increases Q_α (h_0 is less than 1). Also, decreasing c_α decreases Q_α and the smaller the Q_t value will have to be in order to be deemed to contain significant information.

Q_t crossing Q_α :

One of three possibilities is occurring if Q_t crosses Q_α . First, there is an $\alpha\%$ chance that random noise would cross Q_α , but since α is small, this reason is not very probable. Second, too many principal components were kept and tolerance for noise is essentially zero. Each consecutive principal component is calculated by determining the maximum amount of variance present not accounted for by previous principal components. The first PC describes the largest source of variance in the training set; the second PC describes the largest source of variance not described by the first principal component, etc. Increasing the number of retained principal components deems more and more of a data set significant, leaving less to be counted as noise. Thus, if the amount of noise decreases, the threshold for what is significant must also decrease. Mathematically speaking, equation 3 decreases as k increases. This possibility is also not likely if the proper number of principal components is retained. The third and most important reason that Q_t crosses Q_α is because significant deterministic variation is present in the residual. If Q_t crosses Q_α , significant information is present in the residual because the principal components retained in the training set do not accurately model all of the significant current contributions in experimental data set.

Q_α is a trigger of significance and is not related to the accuracy of the predicted concentrations. Q_α is a threshold to determine if significant information is present in the residual. If Q_t does not cross Q_α , it means that all significant signals in the collected data set have been accounted for, where significance is defined as having a Q_t value larger than $(1-\alpha)\%$ of Q_t values that would be calculated by chance from random noise.

Figure 2.4 shows how residuals and Q_t values can be visualized for the *in vivo* electrochemical data set used previously. Figure 2.4B shows a color plot representation of the residual currents when both dopamine and pH are included in the training set. There are no features in the color plot, suggesting that the training set accurately describes all relevant sources of information present in the unknown data set. Furthermore, the Q plot in Figure 2.4C also shows no significant current contributions at the 95% significance level. If the training set used contains both dopamine and pH, its principal components should describe all the relevant information in the measured color plot leaving only noise.

However, if we construct a model with a training set which only includes dopamine, its principal components should fail to describe all relevant information in the measured color plot. The residual color plot in Figure 2.4D shows features in the pH region and its Q plot in Figure 2.4E crosses Q_α at the 95% significance level, meaning that the dopamine principal components fail to describe all significant current contributions in the cyclic voltammograms taken between 2 s and 10 s and concentration values should not be trusted. The residual cyclic voltammograms do not look identical to pH, but they have some pH-like features. Residuals cannot always be directly interpreted as an interferent spectrum as shown in Figure 2.4, but the Q residual plot will inform the experimenter of any samples in the unknown data set that possibly contain an interferent (Jouan-Rimbaud et al., 1999).

It is not always true that a training set with 4 relevant principal components will have a larger Q_α than a different training set with 3 relevant principal components. In fact, this is an erroneous assumption because the Q_α threshold for two different training sets cannot be compared in this way. This statement is true *only* if one is referring to the same training set when the PCA decomposition is calculated. The principal components in the two training sets shown in Figure 2.4 are calculated differently because the two

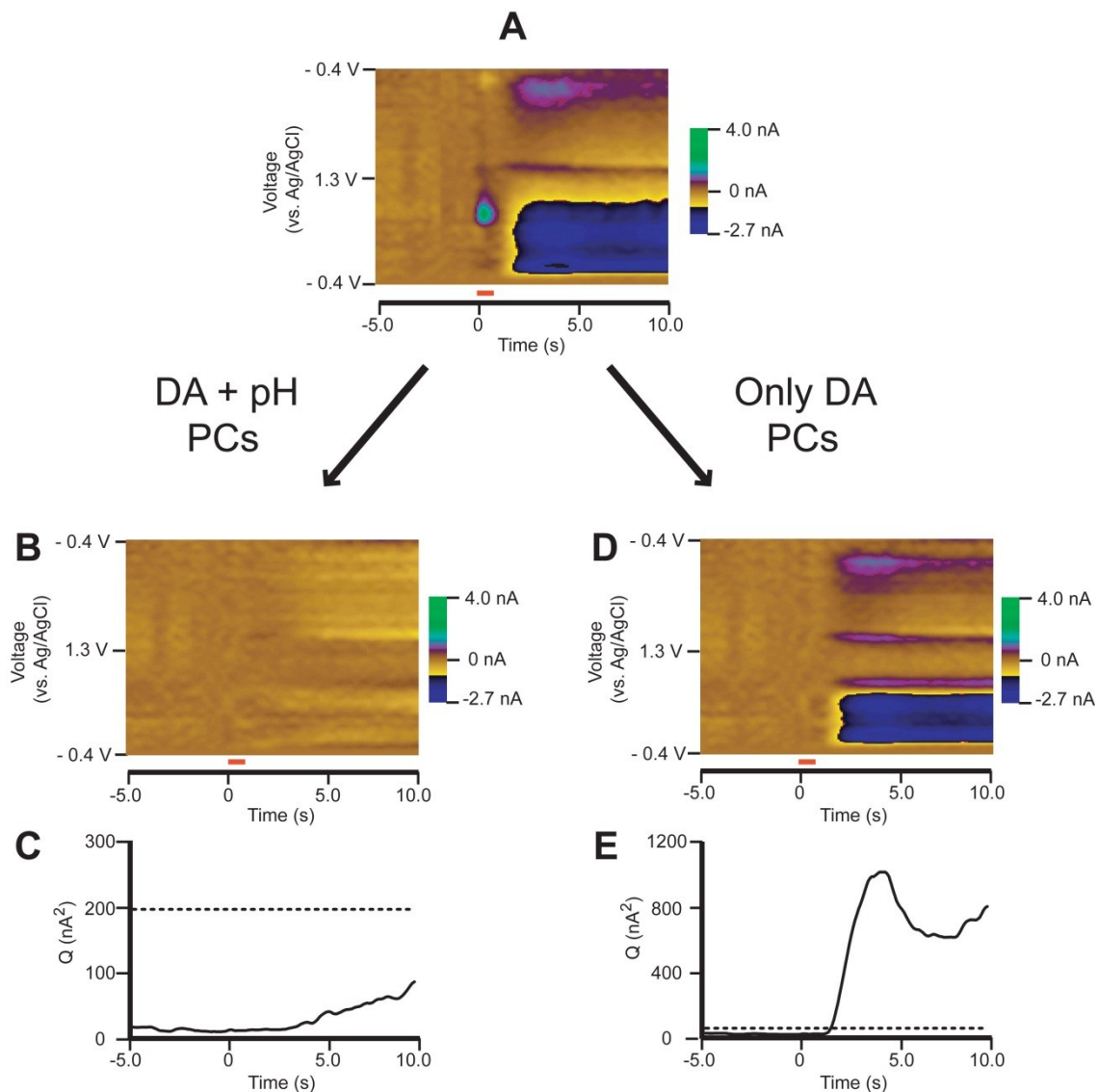


Figure 2.4. The use of residual analysis as a diagnostic tool for significance in *in vivo* electrochemical data. A) Color plot taken from Figure 2. B) Residual color plot when both dopamine (DA) and pH were used in the PCR training set. Malinowski's F-Test was used in order to determine the proper number of principal components to keep ($k = 2$) [9,16]. C) Q trace of the residuals from B) with the dashed line marking Q_{α} at 95% significance. All Q values are below Q_{α} indicating the principal components of the training set accurately describe all relevant sources of information. D) Residual color plot when only DA was used in the PCR training set. Malinowski's F-Test was used in order to determine the proper number of principal components to keep ($k = 1$). E) Q_t trace of the residuals from D) with the dashed line marking Q_{α} at 95% significance. Q_t values crossed Q_{α} in the pH region of the color plot indicating significant information present in the residual.

training sets have different sources of variation (one training set contains dopamine and pH the other training set contains only dopamine). Further, the pH cyclic voltammograms used in the training set are noisier than the dopamine cyclic voltammograms so the training set with only dopamine cyclic voltammograms contains less noise so the noise threshold and thus Q_α is smaller.

Any multivariate model used for quality control purposes should fulfill four requirements (Jackson, 1991d). First, it should provide a yes or no answer as to if the model used accurately describes all relevant measured responses of an unknown data set. The rate of false positives, concluding the model does not accurately model all relevant measured responses of an unknown data set when it actually does, should also be specified. Any relationships that exist between experimental variables must be taken into account. Finally, there should be a way to identify *why* the model does not accurately describe an unknown data set. All of these points, especially the latter, are very interesting to the analytical chemist and residual analysis is an excellent tool that meets all of these requirements.

Future Outlook / Conclusions

PCR is a powerful data analysis tool used in analytical chemistry (Heien et al., 2005; De Beer et al., 2006; Fang et al., 2006; Hermans et al., 2008), however another technique called partial least-squares (Geladi and Kowalski, 1986) (PLS) has become the de facto standard in multivariate calibration in recent years due to a technical advantage and availability of commercial software programs (Faber and Rajko, 2007; Lavine and Workman, 2008). PCR calculates each principal component of data matrix to maximize the amount of variance described without using concentration information so there is no guarantee that the calculated principal components are important for concentration prediction (Thomas and Haaland, 1990). PLS calculates principal

components using concentration information, enabling better prediction while sacrificing some spectral fit. For example, if some of the training set spectra contained a substantial linear baseline shift, PCA decomposition of the data matrix would be significantly altered while PLS should disregard the baseline shift since it has little to do with concentration of an analyte. PCR and PLS have been extensively compared theoretically and practically. However, despite their theoretical difference, both methods offer similar predictive abilities with only a slight advantage to PLS in some cases (Wentzell and Montoto, 2003).

Multivariate techniques offer several advantages over univariate calibration methods. Noise is more easily removed and interferences can be identified. PCR can drastically reduce the dimensionality of a data set while still retaining all of the pertinent information. Residual analysis assures users that the calibration data take into account all relevant components of measured data and can identify specific samples that contain significant amounts of an interfering signal.

References

- Bezegh A, Janata J (1987) Information from Noise. *Anal Chem* 59:A494-&.
- Bro R (2003) Multivariate calibration - What is in chemometrics for the analytical chemist? *Anal Chim Acta* 500:185-194.
- Brown CD, Green RL (2009) Critical Factors Limiting the Interpretation of Regression Vectors in Multivariate Calibration. *TrAC, Trends Anal Chem* 28:506-514.
- Brown SD, Bear RS (1993) Chemometric Techniques in Electrochemistry - a Critical-Review. *Crit Rev Anal Chem* 24:99-131.
- Daszykowski M, Walczak B (2006) Use and abuse of chemometrics in chromatography. *TrAC, Trends Anal Chem* 25:1081-1096.
- De Beer TRM, Baeyens WRG, Ouyang J, Vervaet C, Remon JP (2006) Raman spectroscopy as a process analytical technology tool for the understanding and the quantitative in-line monitoring of the homogenization process of a pharmaceutical suspension. *Analyst* 131:1137-1144.
- Elsevier (2009) In: *Chemometrics and Intelligent Laboratory Systems*.
- Faber NM, Rajko R (2007) How to avoid over-fitting in multivariate calibration - The conventional validation approach and an alternative. *Anal Chim Acta* 295:98-106.
- Fang F, Chu SG, Hong CS (2006) Air-water Henry's law constants for PCB congeners: Experimental determination and modeling of structure-property relationship. *Anal Chem* 78:5412-5418.
- Geladi P, Kowalski BR (1986) Partial Least-Squares Regression - a Tutorial. *Anal Chim Acta* 185:1-17.
- Heien M, Johnson MA, Wightman RM (2004) Resolving neurotransmitters detected by fast-scan cyclic voltammetry. *Anal Chem* 76:5697-5704.
- Heien M, Khan AS, Ariansen JL, Cheer JF, Phillips PEM, Wassum KM, Wightman RM (2005) Real-time measurement of dopamine fluctuations after cocaine in the brain of behaving rats. *Proc Natl Acad Sci U S A* 102:10023-10028.
- Hermans A, Keithley RB, Kita JM, Sombers LA, Wightman RM (2008) Dopamine detection with fast-scan cyclic voltammetry used with analog background subtraction. *Anal Chem* 80:4040-4048.
- International A (2000) ASTM Standard E1655, "Standard Practices for Infrared Multivariate Quantitative Analysis,". West Conshohocken, PA: ASTM International.
- Jackson JE (1991a) In: *A User's Guide To Principal Components*, pp 41-51. New York, NY: John Wiley & Sons, Inc.

- Jackson JE (1991b) In: A User's Guide to Principal Components, pp 34-38. New York, NY: John Wiley & Sons, Inc.
- Jackson JE (1991c) In: A User's Guide to Principal Components, p 21. New York, NY: John Wiley & Sons, Inc.
- Jackson JE (2004) Principal Component Analysis. New York: Springer Science.
- Jackson JE, Mudholkar GS (1979) Control Procedures for Residuals Associated with Principal Component Analysis. *Technometrics* 21:341-349.
- Jensen DR, Solomon H (1972) Gaussian Approximation to Distribution of a Definite Quadratic Form. *Journal of the American Statistical Association* 67:898-902.
- Jolliffe IT (2004a) In: Principal Component Analysis, 2nd Edition, p 6. New York, NY: Springer Science.
- Jolliffe IT (2004b) In: Principal Component Analysis, p 269. New York, NY: Springer Science.
- Jolliffe IT (2004c) In: Principal Component Analysis, pp 111-131. New York, NY: Springer Science.
- Jouan-Rimbaud D, Bouveresse E, Massart DL, de Noord OE (1999) Detection of prediction outliers and inliers in multivariate calibration. *Anal Chim Acta* 388:283-301.
- Justice Jr. JB (1987) *Voltammetry in the Neurosciences: Principles, Methods, and Applications*. Clifton, NJ: Humana Press.
- Kramer R (1998a) *Chemometric Techniques for Quantitative Analysis*. New York, NY: Marcel Dekker, Inc.
- Kramer R (1998b) In: *Chemometric Techniques for Quantitative Analysis*, pp 99-130. New York, NY: Marcel Dekker, Inc.
- Kramer R (1998c) In: *Chemometric Techniques for Quantitative Analysis*, pp 13-15. New York, NY: Marcel Dekker, Inc.
- Kramer R (1998d) In: *Chemometric Techniques for Quantitative Analysis*, pp 17-26, 107-108. New York, NY: Marcel Dekker, Inc.
- Lavine B, Workman J (2008) *Chemometrics*. *Anal Chem* 80:4519-4531.
- Malinowski ER (1990) Erratum to Statistical F-tests for abstract factor analysis and target testing. *J Chemom* 4:102.
- Nomikos P, Macgregor JF (1995) Multivariate SPC Charts for Monitoring Batch Processes. *Technometrics* 37:41-59.
- R. Kiralj MMCF (2006) The past, present, and future of chemometrics worldwide: some etymological, linguistic, and bibliometric investigations. *J Chemom* 20:247-272.

- Ralston P, DePuy G, Graham JH (2004) Graphical enhancement to support PCA-based process monitoring and fault diagnosis. *ISA T* 43:639-653.
- Thomas EV, Haaland DM (1990) Comparison of Multivariate Calibration Methods for Quantitative Spectral-Analysis. *Anal Chem* 62:1091-1099.
- Venton BJ, Michael DJ, Wightman RM (2003) Correlation of local changes in extracellular oxygen and pH that accompany dopaminergic terminal activity in the rat caudate-putamen. *Journal of Neurochemistry* 84:373-381.
- Wentzell PD, Montoto LV (2003) Comparison of principal components regression and partial least squares regression through generic simulations of complex mixtures. *Chemom Intell Lab Syst* 65:257-279.

CHAPTER III

RANK ESTIMATION AND THE MULTIVARIATE ANALYSIS OF *IN VIVO* FAST-SCAN CYCLIC VOLTAMMETRIC DATA

Abstract

Principal component regression has been used in the past to separate current contributions from different neuromodulators measured with *in vivo* fast-scan cyclic voltammetry. Traditionally, a percent cumulative variance approach has been used to determine the rank of the training set voltammetric matrix during model development, however this approach suffers from several disadvantages including the use of arbitrary percentages and the requirement of extreme precision of training sets. Here we propose that Malinowski's *F*-test, a method based on a statistical analysis of the variance contained within the training set, can be used to improve factor selection for the analysis of *in vivo* fast-scan cyclic voltammetric data. These two methods of rank estimation were compared at all steps in the calibration protocol including the number of principal components retained, overall noise levels, model validation as determined using a residual analysis procedure, and predicted concentration information. By analyzing 119 training sets from two different laboratories amassed over several years, we were able to gain insight into the heterogeneity of *in vivo* fast-scan cyclic voltammetric data and study how differences in factor selection propagate throughout the entire principal component regression analysis procedure. Visualizing cyclic voltammetric representations of the data contained in the retained and discarded principal components showed that using Malinowski's *F*-test for rank estimation of *in vivo* training sets allowed for noise to be

more accurately removed. Malinowski's *F*-test also improved the robustness of our criterion for judging multivariate model validity, even though signal-to-noise ratios of the data varied. In addition, pH change was the majority noise carrier of *in vivo* training sets while dopamine prediction was more sensitive to noise.

Introduction

Chemometrics has become more prevalent in recent years because of advances in technical computing. Specifically, multivariate calibration represents the fastest growing subdivision of the field (Lavine and Workman, 2008). Multivariate calibration is superior to univariate calibration because multivariate calibration can simultaneously improve selectivity, reduce noise, and handle interferences during concentration determination (Bro, 2003). These reasons have led to the use of multivariate calibration techniques for the analysis of *in vivo* data (Hansson et al., 1995; Heise, 1996; Bjallmark et al., 2010).

Principal component regression (PCR) is a multivariate calibration methodology that combines principal component analysis (PCA) with inverse least-squares regression (Kramer, 1998a). In this technique, a data set consisting of measured spectra and the corresponding concentrations known as a training set is first assembled. The measured spectra in the training set is broken up into principal components (PCs) which are abstract representations of the information (termed variance) present. Some of the PCs in the data set describe relevant variance and are essential for proper model development and concentration prediction. PCs of this type are termed primary PCs. The rest of the PCs, termed secondary or error PCs, describe only noise and can be discarded (Malinowski, 1977). A model is constructed using the relevant primary PCs and a regression matrix is calculated using the concentration data from the training set. Finally, concentration data of an unknown data set is predicted by projecting the

unknown data set onto the retained PCs and relating the distance back into concentration using the regression matrix.

Fast-scan cyclic voltammetry (FSCV) is an electroanalytical technique that uses scan rates above 100 V/s to monitor neuromodulator release in biological systems, including freely-moving rats capable of performing behavioral tasks (Phillips et al., 2003a). FSCV offers many advantages including excellent sensitivity, sub-second time resolution, micrometer spatial resolution, and minimal damage from the carbon-fiber microelectrode. Unfortunately, the moderate selectivity obtained using FSCV can complicate the analysis of in vivo data (Heien et al., 2004b). Incorporating PCR into the analysis of in vivo FSCV spectral data allowed for a more widely acceptable, robust, unbiased multivariate approach to determine the concentration of multiple neuromodulators while simultaneously removing noise.

PCR has been used in conjunction with FSCV to investigate neuromodulator release in cells (Heien et al., 2004b), brain slices (Heien et al., 2004b), and in freely-moving rats (Heien et al., 2005; Wightman et al., 2007a). PCR has also been used to account for electrode drift, enabling continual FSCV measurements to be made for up to 30 minutes (Hermans et al., 2008). A residual analysis procedure developed by Jackson and Mudholkar (Jackson and Mudholkar, 1979) was incorporated to make sure that the primary PCs of the training set describe all relevant sources of variance present in the unknown data set being predicted. Any developed PCR model that fails to meet this requirement is discarded and not used for concentration prediction (Keithley et al., 2009; Keithley et al., 2010a).

Determining the proper rank (number of primary PCs to retain) of multivariate data is a difficult problem in chemometrics. Although many chemometric texts include a brief overview of some of the more popular methods (Jackson, 1991b; Malinowski, 1991; Kramer, 1998a; Jolliffe, 2004c), a general consensus about which method should be

used remains undetermined. Broadly, these approaches can be divided into two categories: methods that require estimation of the error level and methods that require no a priori information on experimental error. Furthermore, some techniques have a statistical basis and significance tests can be developed to determine the proper number of PCs to retain in the PCR model.

In our original work we used the method of cumulative variance to decide the rank of the voltammetric matrix of the training set (Heien et al., 2004b). In this method, sufficient PCs are retained to describe a specified percentage of the overall variance. A value of 99.5% of the cumulative variance was arbitrarily chosen for factor selection. While the percent cumulative variance method is both extremely simple to comprehend and calculate, this approach has several drawbacks. First, it assumes that all training sets are sufficiently precise to satisfy a specified value of the error present; in our case noise would represent 0.5% of the variance in every training set voltammetric matrix. Differences in experimental variables such as users, equipment, biological variability, and laboratories will most certainly violate this rule (Malinowski, 1999). Second, there is not a specific percentage of the variance corresponding to noise that works for all users in all cases so the percentage choice will always have to be arbitrary and inconsistent. Methods exist to determine a distribution of the percentage cumulative variance so more formal procedures could be used (Jolliffe, 2004c). Finally, because of the extreme precision required for widespread usage and the lack of a constant value that works in all cases, the use of the cumulative variance method is not advocated (Jackson, 1991b; Malinowski, 1991). Therefore, there is a need for the use of a different method of factor selection in the PCR analysis of FSCV data.

There are several requirements in choosing a method of factor selection for the analysis of FSCV data. First, the method should be accepted in chemometrics literature. Second, the method requires robustness sufficient to provide consistent results across

laboratories. Third, the method should not require any a priori estimation of error levels. Fourth, a statistical measure should be employed in rank determination to remove any subjectivity and interpretation to make the results more comparable between laboratories. Finally, the method should be simple to understand and calculate.

We have previously used Malinowski's F-test for factor selection with much success (Hermans et al., 2008). A thorough evaluation and comparison with the 99.5% cumulative variance method, however, has not been presented. In this work, the two methods of factor selection are compared in several ways beyond estimating rank. Noise removal, model validity, and concentration prediction constructed using the primary PCs retained with each approach are discussed.

Theory

Malinowski introduced the concept of a reduced eigenvalue (REV) of a data matrix

$$\text{REV}_j = \frac{\lambda_j}{(r-j+1)(c-j+1)} \quad (\text{eq 3.1})$$

where λ_j is the eigenvalue corresponding to j^{th} PC, r is the number of rows in the data matrix, and c is the number of columns in the data matrix (Malinowski, 1987). He proposed that REV of secondary PCs should be statistically equal and REV of primary PCs would be larger because of contributions due to significant information present in the data matrix. An F -test was developed using REV to statistically differentiate between primary and secondary PCs, thereby determining the rank of a data matrix (Malinowski, 1988, 1990). The F -statistic used to test whether the n^{th} PC is a primary or secondary PC is calculated as

$$F(1, s - n) = \frac{\sum_{j=n+1}^s (r - j + 1)(c - j + 1)}{(r - n + 1)(c - n + 1)} \frac{\lambda_n}{\sum_{j=n+1}^s \lambda_j^0} \quad (\text{eq 3.2})$$

where s is equal to r or c , whichever is smaller, and λ_j^0 corresponds to the error eigenvalue of the j^{th} PC. Each PC is orthogonal, capturing variance previous PCs did not, thereby satisfying the requirement of independence necessary for an F -test (Malinowski, 1988, 1990). These calculations are easy to perform and Matlab command lines are available (Gemperline, 2006).

Malinowski's F -test is conducted as follows. First, the smallest eigenvalue is assumed to represent only noise and is assigned to the null pool. The next smallest eigenvalue is tested for significance using equation 2. If the calculated F -statistic is larger than the tabulated F -statistic at a specific value of α (i.e. 0.05, 0.1, etc.), the null hypothesis is rejected because the n^{th} PC had a variance statistically larger than the error and the rank of the data matrix is determined. If the calculated F -statistic is smaller than the tabulated F -statistic, the tested eigenvalue is also assigned to the null pool. The test is repeated with the next smallest eigenvalue compared to the pool of eigenvalues until the null hypothesis is rejected. At each iteration of Malinowski's F -test, there is an $\alpha\%$ chance that the n^{th} PC describes error rather than significant information present in the spectral matrix of the training set. Malinowski determined that an α value of 5% tended to underestimate the rank and an α value of 10% tended to overestimate the rank (Malinowski, 1988, 1990).

Malinowski originally suggested that REVs would only be constant for uniformly distributed error and normally distributed error could contain one REV that may be significantly larger than the other error REVs, thereby causing Malinowski's F -test to erroneously overestimate rank (Malinowski, 1977). This result was unsubstantiated,

however, because uniform, normal, or random sign simulated noise distributions gave identical REVs (Faber et al., 1994). Malinowski's *F*-test also performed well in the presence of Gaussian error and moderately well in the presence of multiplicative noise (Malinowski, 2004). In addition, Malinowski's *F*-test takes advantage of the central limit theorem, giving a theoretical basis for the insignificance of the underlying distribution of the noise present in the original data spectrum (Malinowski, 1987; Malinowski, 2004). Through simulations of random matrices error REVs were determined not to follow a normal distribution when *r* and *c* deviated substantially from one another (Faber et al., 1994) which violate the assumption necessary for an *F*-test, but Malinowski's *F*-test has been used successfully to estimate the rank of these "skinny" matrices in the literature (Malinowski, 2004; Wasim and Brereton, 2004).

One of the assumptions of Malinowski's *F*-test is that the noise present in the training set spectral matrix is homoscedastic (has a constant *statistical* variance) and is uncorrelated between variables (Faber and Kowalski, 1997b; Malinowski, 1999). If multiple sources of error are present with significantly different amplitudes or if the data are autocorrelated, Malinowski's *F*-test will erroneously overestimate rank (Malinowski, 1999; Vivo-Truyols et al., 2007). In addition, if the primary PCs contain variance similar to secondary PCs, Malinowski's *F*-test is expected to assign those primary PCs to the null pool, thereby underestimating the rank (Wasim and Brereton, 2004).

One of the criticisms against Malinowski's *F*-test is that an incorrect number of degrees of freedom are used in the calculation of the *F*-statistic (Faber and Kowalski, 1997a). The Faber-Kowalski *F*-test uses much larger degrees of freedom calculated from the analysis of simulations of random matrices, thus increasing the power of the statistical test and having a much sharper significance level ($\alpha \leq 1\%$). This method is computationally intensive; however, the authors have supplied command lines for mathematical software programs (Faber, 1999). However, this adaptation of

Malinowski's *F*-test has been criticized for being hypersensitive to the requirement of a normal error distribution which many chemical measurements fail to meet (Malinowski, 1999; Wasim and Brereton, 2004).

In sum, there are several assumptions and limitations that we recognize for the use of Malinowski's *F*-test. First, we assume the noise to be homoscedastic among the cyclic voltammograms contained in each training set voltammetric matrix. If heteroscedastic noise is present, we recognize noise will be retained in model construction. Second, any PCs that describe variance similar to that of noise will be discarded, even if it is possible that relevant information is buried within noise. We define significant variance as having an amplitude statistically larger than noise variance so any PC that fails to meet this requirement will be discarded. Third, an α value of 5% will be used for Malinowski's *F*-test because of the size of the training set voltammetric matrix and we wish to be more confident in the identification of primary PCs.

Experimental

Fast-scan cyclic voltammetry and animal experimentation

Carbon-fiber microelectrodes were prepared as described previously using T-650 carbon fibers cut to an exposed length of 25-100 μm (Kawagoe et al., 1993). The voltage of the carbon-fiber microelectrode was held at -0.4 V, increased to 1.3 V, and decreased back to -0.4 V at 400 V/s. This triangular excursion was repeated at 10 Hz. All potentials are reported versus a Ag/AgCl reference electrode. Data acquisition was performed as previously described using locally constructed hardware and software (Michael et al., 1999). All cyclic voltammograms were low-pass filtered at 2 kHz. The stimulated release and intracranial self stimulation data was also smoothed using a one-pass moving average.

All animal experiments were performed on freely-moving male Sprague Dawley rats weighing approximately 300 g in accordance with the University of North Carolina Animal Care and Use Committee. Surgeries were carried out as described elsewhere (Heien et al., 2005; Day et al., 2007; Owesson-White et al., 2008). The coordinates used for stimulating and working electrodes varied according to the desired experiment because training sets from multiple users and laboratories were pooled. Generally, the training sets focused on measuring in the dorsal and ventral striatum, with the nucleus accumbens being a region of specific interest. The location in the brain that the cyclic voltammograms in the training set were taken from was irrelevant for the analyses. All training sets used were taken from freely-moving rat experiments so the cyclic voltammograms used in prediction were the best approximation to those recorded in the unknown data sets (Heien et al., 2005). *In vitro* cyclic voltammograms were not included in the training sets because inconsistencies in the shapes of the cyclic voltammograms, peak potentials, and noise levels.

Data analysis and principal component regression

All chemometric and statistical analyses were carried out in MATLAB (Mathworks, Natick, MA), GraphPad Prism (GraphPad Software Incorporated, La Jolla, CA), Excel (Microsoft Corporation, Redmond, WA) and LabVIEW (National Instruments, Austin, TX). All values are reported as averages \pm standard error of the mean (SEM).

Each *in vivo* training set constructed met specific requirements (Kramer, 1998d; ASTM International, 2000). First, cyclic voltammograms of all expected analytes were included, generated by electrically stimulating the animal. Second, no more than one cyclic voltammogram for each species was taken per stimulated release event, satisfying the requirement of mutual independence. Third, the training set mimicked the experimental conditions as closely as possible. The same electrode, electronics, and other equipment were used to collect both the training set and the unknown data set.

The various cyclic voltammograms in the training set were consistent in shape and representative in noise level to the unknown data set. Cyclic voltammograms of the unknown data set were not used to build the training set. Finally, the training set spanned the concentration range contained in the unknown data set being predicted. Cyclic voltammograms of varying intensity were generated by changing the stimulation parameters (i.e. current, number of pulses, and frequency). Concentrations were estimated using flow injection analysis (Kristensen et al., 1986b) after the experiment was completed (Owesson-White et al., 2008).

In total, 119 training sets were assembled from five users in two different laboratories over the course of several years. These training sets have been used for concentration prediction from a variety of experiments including various behavioral experiments and stimulated release studies. Each training set consisted of five dopamine and five pH change cyclic voltammograms. Any training sets that contained more than five cyclic voltammograms per analyte were truncated to make all training sets consistent in size. However, a uniform distribution of concentration values within the training set was maintained.

PCA was performed using singular value decomposition (Hendler and Shrager, 1994). PCR using residual analysis was performed as described previously (Keithley et al., 2009; Keithley et al., 2010a). Cyclic voltammetric representations of the training set consisting of only the primary PCs were calculated as follows. First, the primary PCs of the training set determined by either the 99.5% cumulative variance method or Malinowski's *F*-test were organized in a matrix, \mathbf{Vc} . The projection of the training set onto the primary PCs, \mathbf{A}_{proj} was calculated,

$$\mathbf{A}_{\text{proj}} = \mathbf{Vc}^T \mathbf{A} \quad (\text{eq 3.3})$$

where the superscript T represents the transpose of the matrix and \mathbf{A} contains the training set voltammetric matrix. Finally, the training set consisting of only the primary

PCs, \mathbf{A}_{nPC} , was reconstructed by multiplying the retained PCs by the projection of the training set onto the primary PCs (Jackson and Mudholkar, 1979)

$$\mathbf{A}_{nPC} = \mathbf{VcA}_{proj} \quad (\text{eq 3.4})$$

To determine the noise discarded in the secondary PCs of a training set, \mathbf{A}_{jPC} , \mathbf{A}_{nPC} was subtracted from the original training set voltammetric matrix \mathbf{A} .

The signal-to-noise ratios of the dopamine cyclic voltammograms were calculated by dividing oxidative peak current by the standard deviation of a flat portion of the cyclic voltammogram, specifically from 0.95 V to 0.25 V on the reductive sweep. Root-mean-square (RMS) noise was calculated from \mathbf{A}_{jPC} . The RMS current, i_{RMS} , was calculated for each cyclic voltammogram in the training set using the following equation

$$i_{RMS} = \sqrt{\frac{\sum_{x=1}^w (i_x)^2}{w}} \quad (\text{eq 3.5})$$

where i_x is the current at the x^{th} point of the voltammetric waveform containing w total points taken from the \mathbf{A}_{jPC} matrix. An average i_{RMS} value for each analyte using each method of factor selection was calculated for each training set.

Results and Discussion

Principal component selection & training set heterogeneity

Table 3.1 compares how Malinowski's F -test and the 99.5% cumulative variance method determine the rank of a data matrix. Eigenvalues are given for each PC along with the corresponding cumulative variance percentage as rank increases. From this data, the 99.5% cumulative variance method would estimate the rank of this training set voltammetric matrix to be four. REVs are also given for each PC. For PCs four through ten the REVs are comparable, as evidenced by the small F -statistics. PC ten does not have an F -statistic because its REV is placed in the null pool. Starting from the bottom

Table 3.1. Comparison of Rank Estimation Methods. Eigenvalue, reduced eigenvalue, calculated F -statistic, critical F -value at 5% significance, and PRESS value as a function of PC for an example FSCV training set spectral matrix.

PC	λ	% Cum. Var.	REV	F_{Stat}	$F_{0.05}$	PRESS
1	4875.4	85.33	0.4875	26.08	5.12	25.4
2	551.2	94.98	0.0613	7.66	5.32	17.7
3	238.6	99.15	0.0299	17.23	5.59	11.0
4	26.9	99.63	0.0039	3.76	5.99	9.6
5	11.5	99.83	0.0019	2.91	6.61	8.0
6	5.0	99.91	0.0010	2.04	7.71	6.3
7	2.3	99.95	0.0006	1.29	10.13	3.1
8	1.7	99.98	0.0006	1.91	18.51	2.1
9	0.5	99.99	0.0003	0.74	161.45	~ 0
10	0.4	100	0.0004	--	--	--

of the table working upwards, the F -statistic becomes larger than the 5% critical F -values (National Institute of Standards and Technology) for a rank of three, indicating that three PCs are statistically relevant in model construction for this training set.

Leave one out cross validation is also a popular method of rank determination in which the training set concentration matrix is incorporated (Malinowski, 1991; Beebe and Seasholtz, 1998; Kramer, 1998c). Predicted residual error sum-of-squares (PRESS) values are calculated as a function of rank and give the user an idea of the error between the actual concentrations and those predicted using the retained PCs (Kramer, 1998c). A minimum or stabilization of PRESS values is indicative of the proper rank of the training set. This test is subjective, but more formal statistical tests are available (Haaland and Thomas, 1988; Osten, 1988; Beebe and Seasholtz, 1998). Malinowski's F -test and cross validation have been compared in the past, yielding mixed results (Wasim and Brereton, 2004; Hasegawa, 2006; Wahbi et al., 2009; Virkler and Lednev, 2010). Here, cross validation was not able to estimate rank for all data sets because the rank of many training sets (as in Table 3.1) was ambiguous using this approach.

When comparing the 99.5% cumulative variance method and Malinowski's F -test in the number of PCs to retain in the model used for concentration prediction, three outcomes are possible. First, if the number of PCs to retain in the model is fewer for Malinowski's F -test compared to the 99.5% cumulative variance method (referred to as Case I) then the overall noise level is greater than 0.5% of the cumulative variance and models developed using the 99.5% cumulative variance rule are retaining noise during concentration prediction. Keeping noise should not significantly impact concentration data as long as any noise retained does not significantly alter the factor space generated during PCA deconvolution of a training set. Second, if the number of PCs to retain in the model is greater for Malinowski's F -test compared to the 99.5% cumulative variance method (referred to as Case II) then the overall noise level is less than 0.5% of the

cumulative variance and models developed using the 99.5% cumulative variance rule are discarding significant information in the training set when calculating concentration data. Finally, if the number of PCs to retain in the model is the same for both Malinowski's *F*-test and the 99.5% cumulative variance method (referred to as Case III) then the overall noise level is 0.5% of the cumulative variance.

Table 3.2 compares the 99.5% cumulative variance method to Malinowski's *F*-test in the number of PCs to retain in 119 training sets from five different users in two different laboratories. Table 3.2 shows both the heterogeneity of training sets between researchers and failure of the 99.5% cumulative variance method in determining the number of principal components to retain. The vast majority (65.5%) of the evaluated training sets were classified as Case I, a much smaller percentage (10.0%) were classified as Case II, and the rest (24.4%) were classified as Case III.

Table 3.2 shows how inadequate using a fixed number percentage of the cumulative variance for PC retention was at removing noise from training sets as stated in chemometric texts (Malinowski, 1991; Jolliffe, 2004c). The 99.5% cumulative variance rule worked well only for user 1 and moderately overall. In fact, if these training sets were analyzed with the 99.5% cumulative variance rule 65.5% of the PCR models constructed would retain noise during PCR prediction and 10% of PCR models constructed would discard significant information used for concentration prediction.

Figure 3.1 shows the number of PCs retained from the training sets in Table 3.2 using both the 99.5% cumulative variance method and Malinowski's *F*-test. Figure 3.1A compares both methods for all of the Case I training sets. While the 99.5% cumulative variance method retained a wider distribution of PCs, Malinowski's *F*-test retained no more than 3 PCs, with two PCs being the mode of the distribution. On average, Malinowski's *F*-test retained two fewer PCs than the 99.5% cumulative variance method for Case I training sets. Figure 3.1B compares both methods for all of the Case II

Table 3.2. Inter-researcher comparison of rank estimation between Malinowski's *F*-test and the 99.5% cumulative variance method.

	User 1 N = 13	User 2 N = 16	User 3 N = 20	User 4 N = 14	User 5 N = 56	Totals N = 119
Case I	2	8	16	8	44	78 (65.5%)
Case II	2	3	0	5	2	12 (10.0%)
Case III	9	5	4	1	10	29 (24.4%)

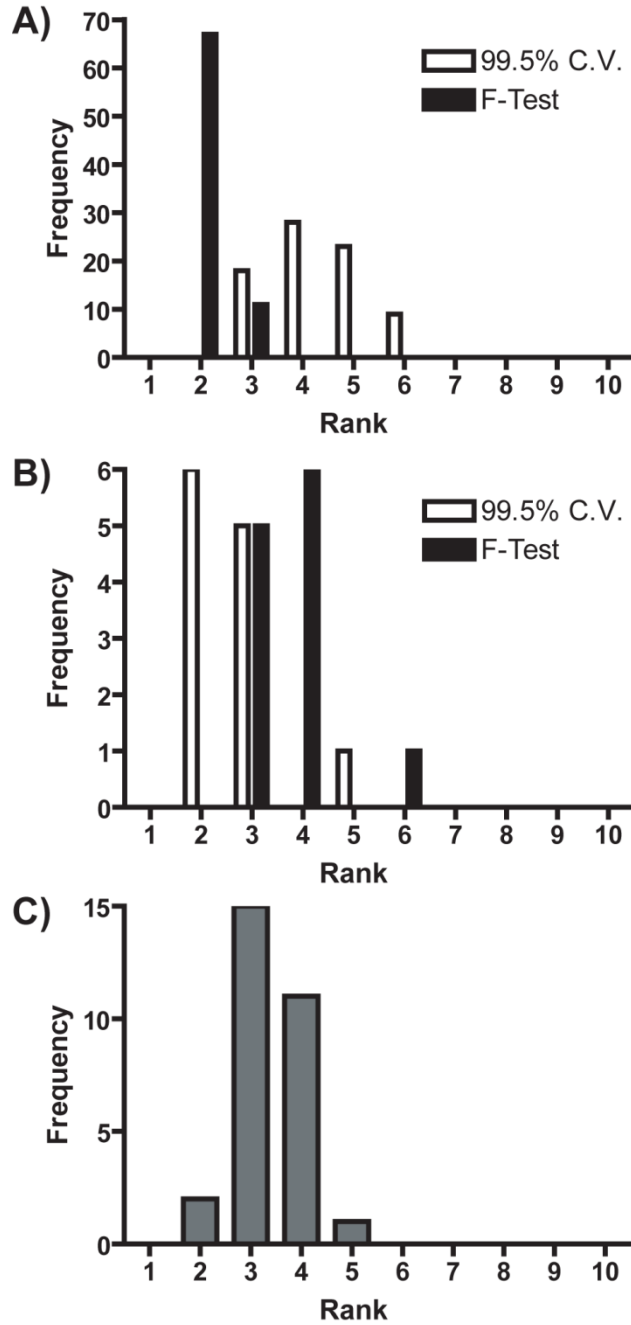


Figure 3.1. Histograms of the estimated rank of A) Case I and B) Case II training sets. White and black represent rank determined by the 99.5% cumulative variance method and Malinowski's *F*-test, respectively. C) Histogram of the estimated rank of Case III training sets.

training sets. The distribution of the number of primary PCs retained by Malinowski's F -test was shifted higher by approximately one PC on average. Finally, Figure 3.1C shows the distribution of retained PCs for all of the Case III training sets. For these training sets the average number of primary PCs was three.

There were only two analytes in all of these training sets, but one PC does not always necessarily correspond to one analyte (Brown and Green, 2009). It is possible that any training set voltammetric matrix with a rank higher than two could be due to differences in signal-to-noise ratio, the presence of heteroscedastic noise, or to inconsistencies present in the various cyclic voltammograms of the training set that were larger than noise. In addition, pH change cyclic voltammograms do not have a consistent "correct" shape (Heien et al., 2004a; Heien et al., 2005; Cheer et al., 2006). This discrepancy makes the process of separating significant information from noise difficult for the pH change cyclic voltammograms of the training set. It is also possible that more than two primary PCs were needed to span significant current contributions to the analytes of interest.

Comparison of information contained in secondary PCs

In PCR, some of the principal components are discarded in an effort to remove noise from the training set before concentration prediction. Visualizing how the training set cyclic voltammograms change as rank is estimated differently should give qualitative information on how noise is removed. This process will also show researchers "effective" cyclic voltammograms of the training set used by PCR for concentration prediction. In addition, visualizing the secondary PCs will determine if any significant information was discarded during factor selection.

Figure 3.2 shows a representative training set comparing how both methods of factor selection remove noise for a Case I training set. Since there were ten cyclic voltammograms in the training set, ten PCs were calculated. For this training set, the

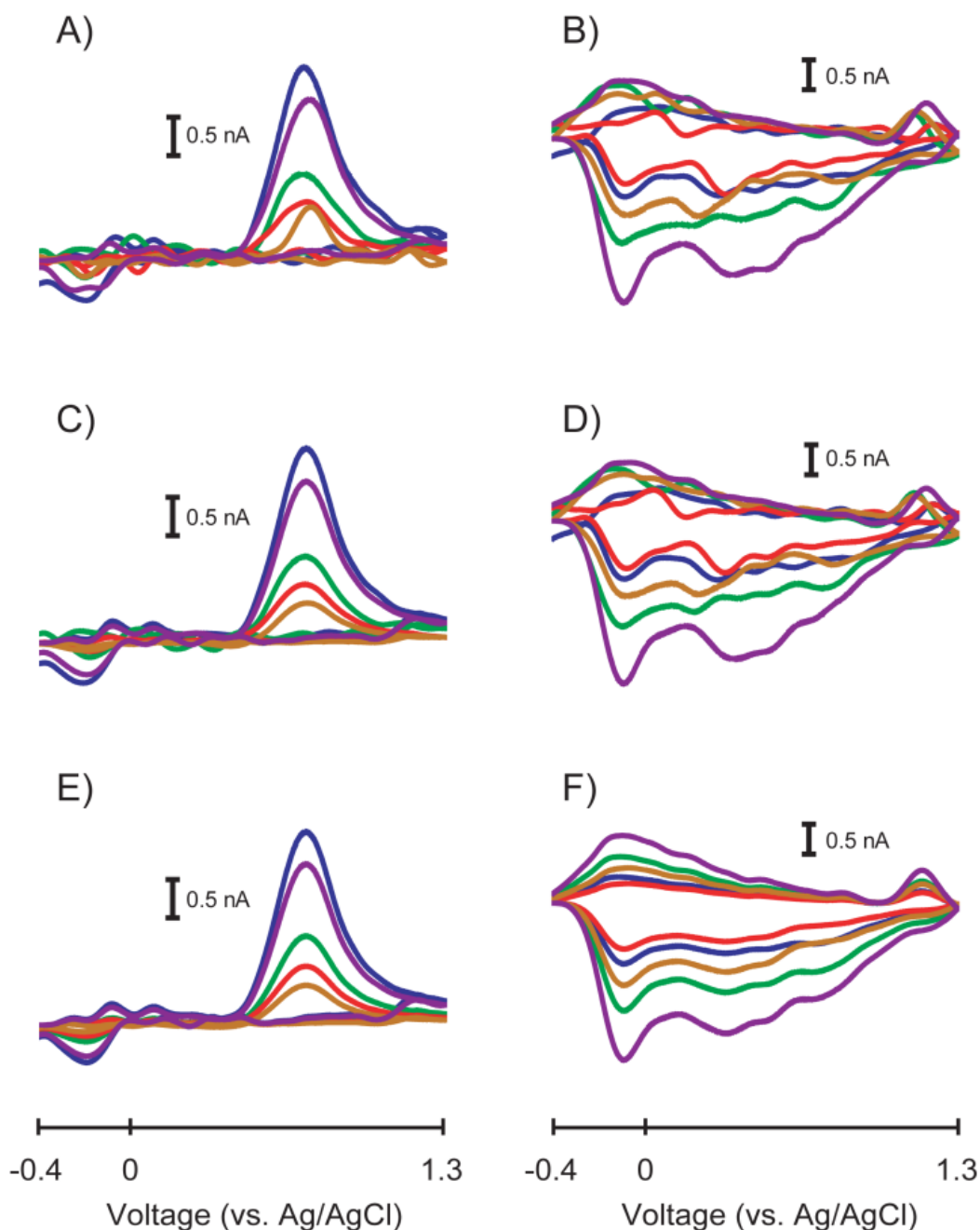


Figure 3.2. Comparison of effective cyclic voltammograms in a representative Case I training set. A) Original dopamine cyclic voltammograms containing all PCs before factor selection. B) Original pH change cyclic voltammograms containing all PCs before factor selection. C) Dopamine cyclic voltammograms from A) constructed using only the PCs retained by the 99.5% cumulative variance method ($n = 5$ PCs). D) pH change cyclic voltammograms from B) constructed using only the PCs retained by the 99.5% cumulative variance method ($n = 5$ PCs). E) Dopamine cyclic voltammograms from A) constructed using only the PCs retained by Malinowski's F -test ($n = 2$ PCs). F) pH change cyclic voltammograms from B) constructed using only the PCs retained by Malinowski's F -test ($n = 2$ PCs).

99.5% cumulative variance method retained five PCs in the model while Malinowski's *F*-test retained two PCs. Figures 3.2A and 3.2B show the original dopamine and pH change cyclic voltammograms, respectively, in the training set. The noise in the dopamine cyclic voltammograms caused the peak shapes and peak potentials to vary. In addition, there is substantially more noise present in the pH change cyclic voltammograms. By discarding five PCs, the 99.5% cumulative variance method only slightly improved the condition of the cyclic voltammograms as shown in Figures 3.2C and 3.2D. Some of the noise in the dopamine cyclic voltammograms was removed and their peak shapes and peak potentials became more consistent. Unfortunately, the pH change cyclic voltammograms showed only a small decrease in noise as evidenced in the similarity between Figures 3.2B and 3.2D. Substantial noise remained in the pH change cyclic voltammograms as evidenced by extraneous peaks and inconsistent shapes.

By discarding eight PCs, Malinowski's *F*-test was able to remove more noise in the dopamine and pH change cyclic voltammograms as shown in Figures 3.2E and 3.2F, respectively. The dopamine cyclic voltammograms were less noisy than those computed using the 99.5% cumulative variance method, specifically at the beginning and end of the cyclic voltammetric sweeps and in the green cyclic voltammogram overall. Some small peaks at -0.1 V and 0.1 V were retained in some of the dopamine cyclic voltammograms. The amplitudes of these peaks were comparable to the noise level in the original dopamine cyclic voltammograms, but since these peaks were conserved in several of the cyclic voltammograms, PCA was able to separate them as a relevant portion of the dopamine cyclic voltammograms. The small peak at the switching potential in some of the dopamine cyclic voltammograms was probably retained for a similar reason. The pH change cyclic voltammograms calculated with Malinowski's *F*-test showed a dramatic decrease in the overall noise level. As with the dopamine cyclic

voltammograms, the shape of the pH change cyclic voltammograms was conserved as the amplitude of the cyclic voltammograms varied.

Figure 3.2 showed qualitatively how Malinowski's *F*-test could remove more noise than the 99.5% cumulative variance method for Case I training sets, which were the majority of training sets analyzed. It is important to quantify the amount of noise each method removes from Case I training sets rather than relying only on qualitative evaluations. Figure 3.3 displays the amount of RMS noise removed from dopamine and pH change cyclic voltammograms using both methods of factor selection for all Case I training sets. Overall, Malinowski's *F*-test was able to remove significantly more noise than the 99.5% cumulative variance method from dopamine cyclic voltammograms ($P < 0.0001$, Wilcoxon Signed Rank Test) and from the pH change cyclic voltammograms ($P < 0.0001$, Wilcoxon Signed Rank Test) proving that the 99.5% cumulative variance method was unsuitable for noise removal in these training sets.

The noise removed by the 99.5% cumulative variance method was not significantly different between dopamine and pH change ($P = 0.3057$, Mann-Whitney Test). In addition, significantly more noise was present in the pH change cyclic voltammograms compared to the dopamine cyclic voltammograms ($P = 0.0033$, Mann-Whitney Test) when Malinowski's *F*-test was used for rank estimation. A possible reason for this increased noise could be due to the origin of the pH change cyclic voltammograms used for the *in vivo* training sets. Background currents that occur when surface functional groups on the electrode are protonated and deprotonated contribute to the shape of the pH change cyclic voltammogram (Runnels et al., 1999). It is therefore plausible that the pH change cyclic voltammograms are highly dependent on the local environment of the electrode *in vivo*. Subtle changes in extracellular species could impact the shape of cyclic voltammograms. Changes in the shape of the cyclic voltammograms comparable to noise would be discarded increasing the overall noise

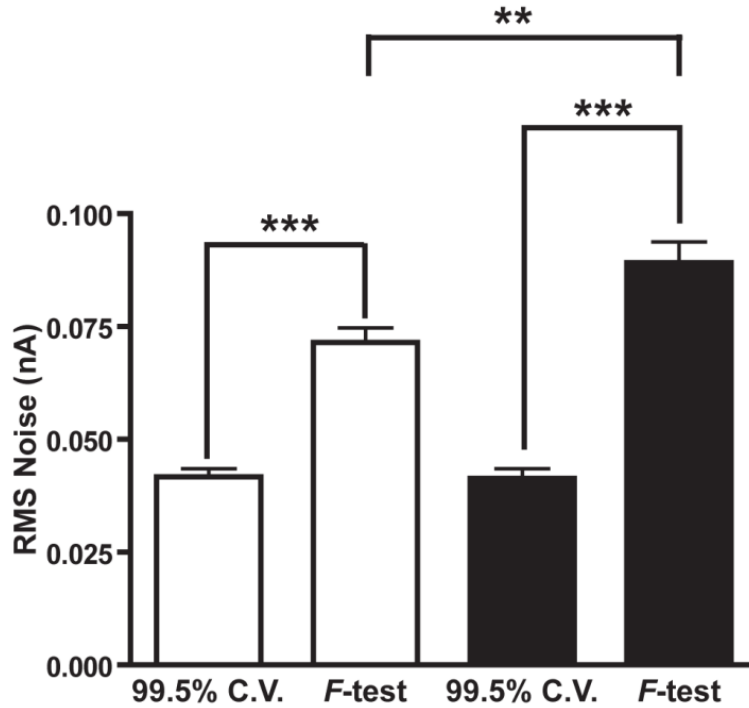


Figure 3.3. RMS noise removed by the 99.5% cumulative variance method (99.5% C.V.) and Malinowski's *F*-test for all of the Case I training sets. Error bars represent SEM. White bars represent noise from dopamine secondary PCs and black bars represent noise from pH change secondary PCs. Two stars and three stars represent $P < 0.01$ and $P < 0.001$ significance, respectively.

level. In addition, the pH change cyclic voltammograms are obtained approximately 2-5 seconds after an electrical stimulation is given to the animal, during which time locomotor activity is increased which can increase electrical noise. Either way, since the signal-to-noise ratio of the cyclic voltammograms used in Figure 3.3 was low (16 - 61), these differences were not significantly larger than the noise present in the training set cyclic voltammograms and were thus discarded by Malinowski's *F*-test.

Potentially significant information could be discarded by the 99.5% cumulative variance method for Case II training sets because statistically more PCs should be retained. Figure 3.4 more clearly illustrates what each method considers error for a representative Case II training set. The 99.5% cumulative variance method estimated rank to be two and Malinowski's *F*-test estimated rank to be four for this training set. Figure 3.4A contains cyclic voltammetric representations of PCs three through ten that were discarded with the 99.5% cumulative variance method for each dopamine sample in the Case II training set. Similarly, Figure 3.4B contains cyclic voltammetric representations of PCs three through ten for each pH change sample in the training set. Figure 3.4C and 4D contain cyclic voltammetric representations of PCs five through ten that were discarded with Malinowski's *F*-test for dopamine and pH changes, respectively. Figures 3.4E and 3.4F contain cyclic voltammetric representations of PCs three and four for both dopamine and pH changes, respectively, in the original training set.

Interestingly, a conserved distinct shape emerged in the difference between the secondary PCs discarded between the two methods for the dopamine cyclic voltammograms. Error with such a pattern suggest that PCs three and four represent deterministic variance which was why Malinowski's *F*-test retained these PCs. The shapes of the cyclic voltammograms in Figures 3.4E and 3.4F show that heteroscedastic noise was not present which could have caused Malinowski's *F*-test to overestimate

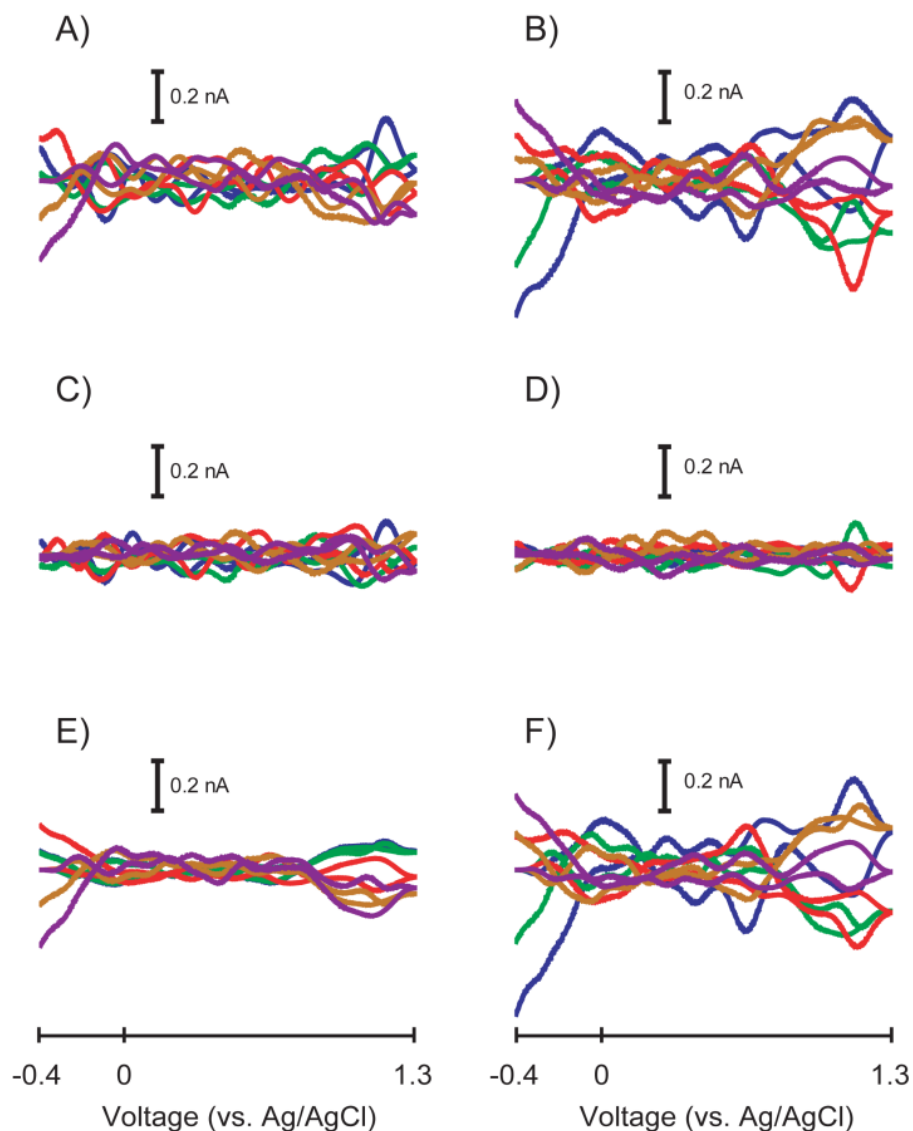


Figure 3.4. Cyclic voltammetric representation of the secondary PCs from each method of factor selection for a representative Case II training set. A) Secondary PCs of the dopamine cyclic voltammograms determined by the 99.5% cumulative variance method (PCs 3-10). B) Secondary PCs of the pH change cyclic voltammograms determined by the 99.5% cumulative variance method (PCs 3-10). C) Secondary PCs of the dopamine cyclic voltammograms determined by Malinowski's *F*-test (PCs 5-10). D) Secondary PCs of the pH change cyclic voltammograms determined by Malinowski's *F*-test (PCs 5-10). E) The difference of secondary PCs between methods for the dopamine cyclic voltammograms (PCs 3-4). F) The difference of secondary PCs between methods for the pH change cyclic voltammograms (PCs 3-4).

rank. Since the signal-to-noise ratio of the original cyclic voltammograms of this representative Case II training set was high (114 - 307), PCs three and four discarded by the 99.5% cumulative variance rule contained variance that was significantly larger than the variance of the noise present. While discarding these PCs may have helped create more consistently shaped cyclic voltammograms and these PCs may not be necessary for concentration prediction, it is our assertion that it is better and more conservative to retain all statistically significant information present in training sets.

Figures 3.4E and 3.4F showed that more than two primary PCs were necessary to describe currents measured at the switching potential and at the end of the voltammetric sweep when signal-to-noise ratios of the cyclic voltammograms in a training set are high. This data, taken with the data presented in Figures 3.1 and 3.3 suggest that the number of primary PCs required for *in vivo* FSCV voltammetric data varies with signal-to-noise ratio. The signal-to-noise ratios of the dopamine cyclic voltammograms for Case I, Case II, and Case III training sets were significantly different ($P < 0.0001$, Kruskal-Wallis Test) with averages of 74 ± 3 ($N = 390$), 200 ± 17 ($N = 60$), and 147 ± 12 ($N = 145$), respectively, giving evidence for this hypothesis.

Training sets with smaller signal-to-noise ratios will have more room to discard inconsistencies in the cyclic voltammograms with amplitudes similar to that of noise. As signal-to-noise ratio increases, inconsistencies in the shapes of the cyclic voltammograms of the training set become more significant compared to the noise present. In addition, PCs describing only a small amount of the overall variance of the training set become more significant.

Comparison of model validity

The most important aspect to our *in vivo* calibration protocol is PCR model validation. We use a residual analysis method developed by Jackson and Mudholkar to determine if the multivariate model is valid and predicted concentration values can be

trusted (Jackson and Mudholkar, 1979; Keithley et al., 2009; Keithley et al., 2010a).

This method uses the data contained in the discarded PCs from the training set to determine a threshold for tolerable error (Q_α). Q_α represents a threshold where 1- α % of the sum of squared residuals due to noise would fall below. By convention, we use an α value of 5% for the residual analysis procedure (Keithley et al., 2009; Keithley et al., 2010a). The sum of the squared residual error present in each cyclic voltammogram at time t of the unknown data file being predicted is calculated as the quantity Q_t , plotted as a function of time, and compared to Q_α . The quantity Q_t is calculated as

$$Q_t = \sum_{x=1}^w (i_x - \hat{i}_x)^2 \quad (\text{eq 3.6})$$

where i_x is the current at the x^{th} point of the cyclic voltammogram, \hat{i}_x is the current predicted using only the relevant PCs of the PCR model, and w is the number of points in the cyclic voltammogram. As long as the Q_t plot falls below Q_α , the retained PCs accurately describe all significant sources of variance present. However, if the Q_t plot crosses Q_α , the retained PCs of the model do not accurately describe all relevant sources of variance in the unknown data set and the model cannot be used for concentration prediction.

Incorrect estimation of the proper noise level would cause an incorrect value of Q_α to be calculated which would impair proper judgment of PCR model validity. Figure 3.5 shows Q_α distributions for Case I, II, and III training sets shown in Figure 3.1. Figure 3.5A shows a histogram of Q_α values calculated for all Case I training sets. First, the Q_α values calculated using the PCs retained with Malinowski's F -test have a considerably larger distribution, indicating that the amount of error contained in training sets is variable. This variability could be due to low signal-to-noise ratios or to differences in users, electrodes, equipment, or other experimental variables. Second, the Q_α values calculated using the 99.5% cumulative variance method were shifted to lower threshold

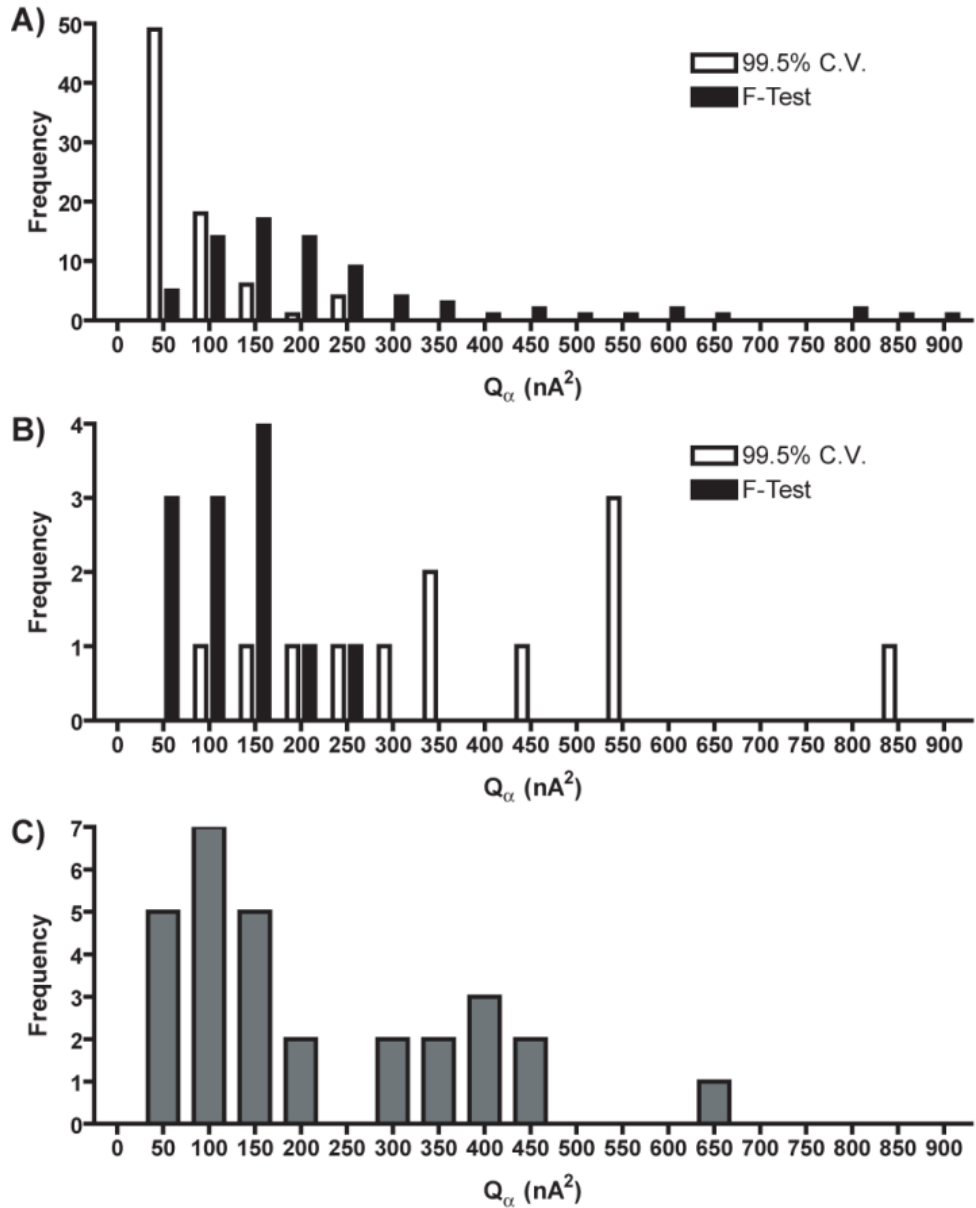


Figure 3.5. Histograms of Q_α values of A) Case I and B) Case II training sets. White and black represent the rank determined by the 99.5% cumulative variance method and Malinowski's F -test, respectively. C) Histogram of Q_α values of Case III training sets.

values because more PCs were retained than necessary. Retaining more primary PCs would decrease the amount of variance contained in the secondary PCs. This difference would render a value of Q_α that would be artificially lower than it rightfully should be, which may lead to possibly rejecting an otherwise valid PCR model.

Figure 3.5B shows a histogram of Q_α values for all Case II training sets. The Q_α values calculated using the PCs retained with Malinowski's F -test were lower than those calculated using the PCs retained with the 99.5% cumulative variance method. The distribution of Q_α values calculated using the PCs retained with Malinowski's F -test was also smaller. Retaining too few primary PCs with the 99.5% cumulative variance method would leave more variance in the secondary PCs which would render a value of Q_α that would be artificially higher than it should be, possibly leading to the use of an invalid PCR model for concentration prediction. Figure 3.5C shows a bimodal distribution of Q_α values existed for all of the Case III training sets.

Table 3.3 gives average Q_α and values for the data presented in Figure 3.5. The average Q_α value calculated using the PCs retained with Malinowski's F -test was approximately four times larger than the average Q_α value calculated using the PCs retained with the 99.5% cumulative variance method for Case I training sets. For Case II training sets the average Q_α value calculated using the PCs retained with Malinowski's F -test was approximately 3.5-fold lower than the average Q_α value calculated using the PCs retained with the 99.5% cumulative variance method. The average Q_α values from Case III training sets were comparable to the values calculated using the PCs retained with Malinowski's F -test from Case I training sets.

The data in Table 3.3 suggest that it was possible that the validity of PCR models was improperly assessed. Since Case I training sets were the majority of training sets used, in most instances researchers were being overly cautious, possibly discarding valid PCR models. The analysis of the much smaller number of Case II training sets

Table 3.3. Comparison of average Q_α values calculated using PCs retained with Malinowski's F -test and the 99.5% cumulative variance (C.V.) method.

	F -test Q_α (nA^2)	99.5% C.V. Q_α (nA^2)
Case I (N = 78)	220 \pm 22	58 \pm 6
Case II (N = 12)	102 \pm 17	364 \pm 59
	Q_α (nA^2)	
Case III (N = 29)	186 \pm 30	

suggests it was possible that invalid PCR models were used for concentration prediction. However, we do not doubt the validity of our previous results for several reasons. First, Table 3.2 shows that no more than five of such training sets originated from a specific researcher over several years so any discrepancies were probably averaged out. Second, cyclic voltammograms contained in Case II training sets had such a large signal-to-noise ratio, any errors in concentration prediction using a proper PCR model should be small. Third, it is very unlikely that all of the Case II training sets produced invalid PCR models in the analysis of all experiments. Nevertheless, a statistical-based rank estimation approach that properly distinguishes between information and noise, such as Malinowski's F -test, should be used with the residual analysis procedure to properly assess multivariate model validity. Because a distribution, rather than one specific value, existed for Q_a suggests that a universal training set does not exist for the analysis of *in vivo* FSCV data.

Comparison in concentration prediction

Ideally, it would be best to assess accuracy of both methods of factor selection in concentration prediction using *in vitro* training sets, however there are several important features of our *in vitro* training sets which can limit their applicability to *in vivo* training sets. First, the shapes of the cyclic voltammograms are more consistent *in vitro* than *in vivo*. Second, the shapes of the cyclic voltammograms *in vitro* are not always consistent with the shapes of the cyclic voltammograms *in vivo*. Third, the signal-to-noise ratios of the cyclic voltammograms *in vitro* are different than those *in vivo* and signal-to-noise ratios are important in determining the type of training set being analyzed (Case I, Case II, or Case III). To guarantee Case I training sets one could artificially add noise through simulations, but the applicability of such data sets could be in question.

In vitro training sets have an independent measure of concentration (i.e. the concentrations we believe we are creating during solution preparation) so accuracy of

the prediction can always be determined. However, *in vivo* training sets have their concentrations determined by dividing measured peak height by sensitivity without an independent measure of concentration. Unfortunately, because the “true” concentration of species *in vivo* is unknown, we cannot determine whether the extra PCs retained by the 99.5% cumulative variance method were necessary for accurate concentration prediction *in vivo*. Instead, all that can be inferred is if the extra PCs retained significantly affect the concentration data determined by PCR. We then have to decide which method of factor selection allows us to build the better model, remove noise, and generate the best estimate for *in vivo* concentration data.

Since the number of Case II training sets is small and no difference in concentration values would be seen for Case III training sets, this section will focus solely on Case I training sets. In every instance that the 99.5% cumulative variance method retains more PCs in the model compared to Malinowski’s *F*-test, noise will be used in concentration prediction. In theory, concentration information should not be appreciably different between both methods as long as the signal-to-noise ratio of the cyclic voltammograms in the training set is large.

Figure 3.6 compares the 99.5% cumulative variance method and Malinowski’s *F*-test in the calculation of both dopamine concentration data and pH changes *in vivo*. Figure 3.6A shows a color plot (Michael et al., 1998) containing stimulated dopamine release, basic pH shifts, and naturally occurring dopamine transients in a freely-moving rat. The white dotted line represents the oxidation potential of dopamine. A current versus time trace at this potential is shown in Figure 3.6B. As previously reported, a current versus time trace is insufficient in measuring dopamine fluctuations because pH change information is also contained at this potential which convolutes the response (Keithley et al., 2009; Keithley et al., 2010a). Figures 3.6C and 3.6D show dopamine concentration and pH change information, respectively, predicted using both the 99.5%

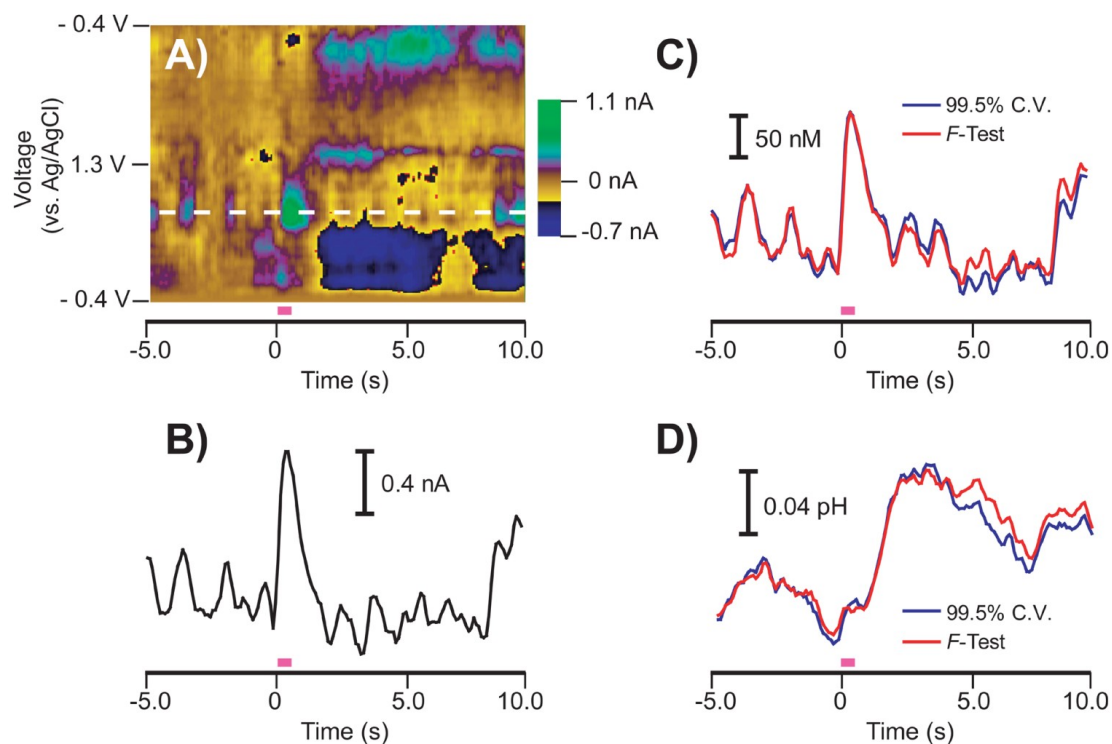


Figure 3.6. Comparison of stimulated release predicted by PCR using primary PCs determined with both methods of factor selection for a representative Case I training set. A) Color plot representation of *in vivo* cyclic voltammograms collected in a freely-moving rat. The pink bar indicates a stimulation given to the animal to evoke dopamine release and pH changes (60 Hz, 24 pulses, 125 μ A). The white dashed line indicates the oxidation potential of dopamine. B) Current versus time trace at the oxidation potential of dopamine showing a convoluted response with pH changes. C) Dopamine concentration predicted by PCR using the primary PCs determined by the 99.5% cumulative variance method (blue) and Malinowski's *F*-test (red). D) pH change predicted by PCR using the primary PCs determined by the 99.5% cumulative variance method (blue) and Malinowski's *F*-test (red).

cumulative variance method and Malinowski's *F*-test. The 99.5% cumulative variance method retained six PCs while Malinowski's *F*-test retained two PCs. Malinowski's *F*-test was able to predict virtually identical changes in dopamine and pH levels as the 99.5% cumulative variance method, including dopamine transients at and below 50 nM. Since concentration data was unaffected, these results support the assertion made by Malinowski's *F*-test that the extra four PCs retained by the 99.5% cumulative variance method span only noise.

Figure 3.6 shows a representative stimulated release example, but more quantitative evidence from a larger data set was needed in the comparison of concentration values. First, changes in dopamine and pH levels were predicted using each method of factor selection using multiple stimulated release events. These stimulated release events were taken from multiple animals from user 5 in Table 3.2. Accordingly, these multiple stimulated release events used multiple Case I training sets for concentration prediction. Next, coefficients of determination (R^2) values were calculated comparing the results obtained with the 99.5% cumulative variance method to those predicted using Malinowski's *F*-test from each stimulated release event for both dopamine and pH changes.

Average R^2 values were 0.963 ± 0.010 for dopamine and 0.992 ± 0.003 for pH change ($N = 7$ training sets predicting dopamine and pH changes in 18 stimulated release data files). One of two possibilities exists for the average R^2 value of approximately unity for the pH change data. First, the extra PCs retained by the 99.5% cumulative variance method could be inherently unimportant during concentration prediction. Second, since noise should not have large peaks that substantially deviate from baseline, the broad-shaped pH change information obtained from PCR could be less sensitive to added noise. This second possibility suggests that dopamine cyclic voltammograms, which do not deviate from the baseline for approximately 3/4 of the

length of the voltammetric sweep, would be more sensitive to noise, especially if their signal-to-noise ratio is low.

Supporting this theory, five of the eighteen stimulated release files had R^2 values for dopamine concentrations below 0.95 while all R^2 values for pH change concentrations were above this value. In the five cases where R^2 values were below 0.95, the extra noise PCs retained with the 99.5% cumulative variance method led to different dopamine concentration information. One possibility is that noise PCs were retained by the 99.5% cumulative variance method and were included in the factor space during model generation, leading to the calculation of a different regression matrix. In addition, during concentration prediction of the unknown stimulated release data, cyclic voltammograms that contained noise could have had projections onto noise PCs and noise could have been interpreted by PCR as dopamine changes. Training sets with low signal-to-noise ratios would be the most susceptible.

Another possibility for the lower R^2 values for dopamine is that Malinowski's F -test discarded significant information necessary for concentration prediction. Qualitative evaluations of the PCs discarded by Malinowski's F -test (similar to Figure 3.4) showed no consistent or significant shape distinct from noise, suggesting that the inclusion of noise using the 99.5% cumulative variance method could significantly change concentration information in some instances. Taken together with the data in Figure 3.3, pH change cyclic voltammograms contained a larger amount of noise, but dopamine concentration data was more sensitive to noise for Case I training sets.

We define the limit of detection (LOD) for a significant event as a concentration change larger than five times the standard deviation of the noise in the concentration versus time trace. To provide evidence for the fact that the noise contained in the training set does not impact our LOD, noise levels were estimated by taking the standard deviations of the pre-stimulation dopamine and pH change baselines predicted using

both the 99.5% cumulative variance method and Malinowski's *F*-test for the data used in the calculation of R^2 values (N = 7 training sets and 18 stimulated release data files). While Figure 3.3 showed that Malinowski's *F*-test discarded significantly more noise from the training set cyclic voltammograms, the choice of factor selection did not significantly impact noise levels for either dopamine or pH changes in the concentration versus time dimension (data not shown).

We also wanted to provide evidence of how Malinowski's *F*-test was able to predict dopamine concentration information during a behavioral experiment. Intracranial self-stimulation (ICSS) is a behavioral model that mimics reward-seeking behavior in animals and we have extensively studied this experimental paradigm previously (Cheer et al., 2007; Owesson-White et al., 2008). We have shown that extracellular dopamine increases following both the presentation of a cue associated with lever presentation and immediately after the stimulation is given (Owesson-White et al., 2008).

Figure 3.7 shows how the 99.5% cumulative variance method and Malinowski's *F*-test predicted concentrations during an ICSS experiment where the time between trials was allowed to vary (Owesson-White et al., 2008). Each trace represents an average \pm SEM of thirty-nine trials. Malinowski's *F*-test and the 99.5% cumulative variance method estimated the rank to be two and four, respectively. The concentration values predicted by Malinowski's *F*-test were identical within error to those predicted by the 99.5% cumulative variance method, including the approximately 30 nM cue-evoked release. Since the training set for this experiment was classified as a Case I training set and the results were identical for both methods, the extra PCs retained by the cumulative variance method were, in fact, noise.

A calibration set must contain all expected components or the concentration values predicted with PCR may be significantly different (Kramer, 1998d). The black trace in Figure 3.7 shows this effect when pH change was removed from the training set.

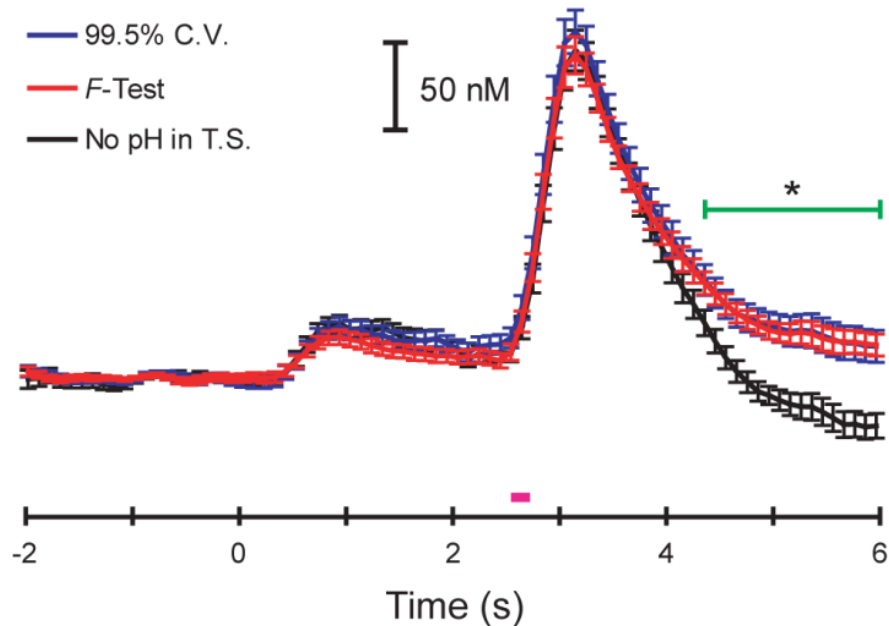


Figure 3.7. Dopamine release predicted by PCR during an ICSS experiment using primary PCs determined with both methods of factor selection for a Case I training set. Time 0 s represents cue presentation and the pink bar represents the stimulation. The blue and red traces are average (error bars representing SEM) dopamine concentrations predicted using the primary PCs from the 99.5% cumulative variance method (rank = 4) and Malinowski's *F*-test (rank = 2), respectively. The black trace is an average dopamine concentration predicted using Malinowski's *F*-test without pH in the training set. The green bar represents a significant difference in concentrations predicted when pH was excluded from the training set (one-way ANOVA, $p < 0.05$).

There was no significant difference in dopamine concentrations during either the cue or stimulation. However, dopamine concentrations were significantly underestimated ($P < 0.05$, one-way ANOVA) after the stimulation, when basic pH changes occur because basic pH change cyclic voltammograms resemble “anti-dopamine” in a dopamine factor space.

Our residual analysis protocol should notify the user that a specified training set does not contain all significant sources of variation in the unknown data set, however it is not perfect. One limitation to residual analysis is that if a large amount of noise is present in the cyclic voltammograms of the training set, Q_α would be very large and may be unable to inform a user that a training set is invalid. This was the case for the black trace in Figure 3.7. All of the Q_t values fell below Q_α during concentration prediction indicating a proper model was constructed. During these instances seemingly insignificant sources of variance present in the unknown data set can cause an error in the prediction of concentration changes. Therefore all expected components, no matter how small in amplitude, should be included in the training set to eliminate this type of error from occurring during the validation step. Furthermore, visualizing a residual color plot should aid in determining if other analytes are present, even though residuals are not always directly interpretable (Keithley et al., 2009; Keithley et al., 2010a).

Conclusions

Here we have shown that Malinowski’s F -test offered a more accurate, statistical-based approach for the removal of noise from an *in vivo* FSCV training set. The literature suggested it was possible that the dimensions of our training sets may limit the usage of Malinowski’s F -test (Faber et al., 1994), but this result was unsubstantiated in this work. Visualizing the discarded PCs in terms of the original data offers an easily

interpretable alternative to looking at complicated loading plots or abstract vector transformations of PCs in conventional PCA.

Malinowski's *F*-test improved the overall consistency in the shapes of the effective analyte cyclic voltammograms within a particular training set. Malinowski's *F*-test was able to remove noise even though its underlying distribution was unknown and the data was already filtered and smoothed before rank estimation. The 99.5% cumulative variance method deteriorated the quality of training sets with large signal-to-noise ratios by discarding potentially important voltammetric information. Interestingly, pH change contributed the majority of error of training sets while dopamine concentrations were more sensitive to error present. Neuromodulator concentration values were not significantly affected for either stimulated release files or an ICCS experiment in most instances using Malinowski's *F*-test for factor selection, except when the error PCs retained by the 99.5% cumulative variance method influenced the factor space such that noise from the unknown data set was interpreted as dopamine. Training sets with low signal-to-noise ratios were more susceptible to this type of error.

The specific value of rank for a particular training set was irrelevant because it varied with signal-to-noise ratio, no matter whether the 99.5% cumulative variance method or Malinowski's *F*-test was used for factor selection. Even though the number of PCs retained varied depending on the Case, the distributions of the Q_α values calculated using Malinowski's *F*-test from all three Cases were similar. The average Q_α value for Case II training sets was significantly lower than the other two Cases, but this could be due to a low number of training sets in the distribution.

The similar overall distributions of Q_α values give new insights into Malinowski's *F*-test and the residual analysis validation protocol. Even though the signal-to-noise ratios of the training set cyclic voltammograms varied, on average Malinowski's *F*-test was able to remove the similar amounts of noise from all training sets. The residual

analysis validation protocol is an excellent measure of quality control and its usage can be improved with using Malinowski's F -test as a method of rank estimation, even if training sets are heterogeneous. As long as signal-to-noise ratios of training set spectra are moderate (>10 , (Malinowski, 2004)) Malinowski's F -test is robust enough to analyze *in vivo* data from multiple laboratories with varying signal-to-noise ratios and obtain a comparable standard for validation of multivariate calibration models.

References

- ASTM International (2000) Standard Practices for Infrared Multivariate Quantitative Analysis, Doc. E 1655-00 in ASTM Annual Book of Standards, vol. 03.06. Standard Practices for Infrared Multivariate Quantitative Analysis, Doc E 1655-00 in ASTM Annual Book of Standards, Vol 0306.
- Beebe KR, Seasholtz MB (1998) Chemometrics : A Practical Guide. In: Chemometrics : A Practical Guide, pp 287-290. New York: Wiley.
- Bjallmark A, Lind B, Peolsson M, Shahgaldi K, Brodin LA, Nowak J (2010) Ultrasonographic strain imaging is superior to conventional non-invasive measures of vascular stiffness in the detection of age-dependent differences in the mechanical properties of the common carotid artery. *J Eur J Echocardiogr.*
- Bro R (2003) Multivariate calibration - What is in chemometrics for the analytical chemist? *Anal Chim Acta* 500:185-194.
- Brown CD, Green RL (2009) Critical Factors Limiting the Interpretation of Regression Vectors in Multivariate Calibration. *TrAC, Trends Anal Chem* 28:506-514.
- Cheer JF, Wassum KM, Wightman RM (2006) Cannabinoid modulation of electrically evoked pH and oxygen transients in the nucleus accumbens of awake rats. *J Neurochem* 97:1145-1154.
- Cheer JF, Aragona BJ, Heien MLAV, Seipel AT, Carelli RM, Wightman RM (2007) Coordinated accumbal dopamine release and neural activity drive goal-directed behavior. *Neuron* 54:237-244.
- Day JJ, Roitman MF, Wightman RM, Carelli RM (2007) Associative learning mediates dynamic shifts in dopamine signaling in the nucleus accumbens. *Nat Neurosci* 10:1020-1028.
- Faber K, Kowalski BR (1997a) Modification of Malinowski's F-test for abstract factor analysis applied to the Quail Roost II data sets. *J Chemom* 11:53-72.
- Faber K, Kowalski BR (1997b) Critical evaluation of two F-tests for selecting the number of factors in abstract factor analysis. *Anal Chim Acta* 337:57-71.
- Faber NKM (1999) Modification of Malinowski's F-test for pseudo rank estimation revisited. *Comput Chem* 23:565-570.
- Faber NM, Buydens LMC, Kateman G (1994) Aspects of Pseudorank Estimation Methods Based on the Eigenvalues of Principal Component Analysis of Random Matrices. *Chemometr Intell Lab* 25:203-226.
- Gemperline P (2006) Practical Guide to Chemometrics. In: Practical Guide to Chemometrics, pp 93-96. Boca Raton, FL: CRC Press.

- Haaland DM, Thomas EV (1988) Partial Least-Squares Methods for Spectral Analyses .1. Relation to Other Quantitative Calibration Methods and the Extraction of Qualitative Information. *Anal Chem* 60:1193-1202.
- Hansson LO, Waters N, Holm S, Sonesson C (1995) On the Quantitative Structure-Activity-Relationships of Meta-Substituted (S)-Phenylpiperidines, a Class of Preferential Dopamine D-2 Autoreceptor Ligands - Modeling of Dopamine Synthesis and Release In-Vivo by Means of Partial Least-Squares Regression. *J Med Chem* 38:3121-3131.
- Hasegawa T (2006) Spectral simulation study on the influence of the principal component analysis step on principal component regression. *Appl Spectros* 60:95-98.
- Heien M, Johnson MA, Wightman RM (2004a) Resolving neurotransmitters detected by fast-scan cyclic voltammetry. *Anal Chem* 76:5697-5704.
- Heien M, Khan AS, Ariansen JL, Cheer JF, Phillips PEM, Wassum KM, Wightman RM (2005) Real-time measurement of dopamine fluctuations after cocaine in the brain of behaving rats. *Proc Natl Acad Sci U S A* 102:10023-10028.
- Heien ML, Johnson MA, Wightman RM (2004b) Resolving neurotransmitters detected by fast-scan cyclic voltammetry. *Anal Chem* 76:5697-5704.
- Heise HM (1996) Non-invasive monitoring of metabolites using near infrared spectroscopy: State of the art. *Horm Metab Res* 28:527-534.
- Hendler RW, Shrager RI (1994) Deconvolutions Based on Singular-Value Decomposition and the Pseudoinverse - a Guide for Beginners. *J Biochem Bioph Meth* 28:1-33.
- Hermans A, Keithley RB, Kita JM, Sombors LA, Wightman RM (2008) Dopamine detection with fast-scan cyclic voltammetry used with analog background subtraction. *Anal Chem* 80:4040-4048.
- Jackson JE (1991) In: *A User's Guide To Principal Components*, pp 41-51. New York, NY: John Wiley & Sons, Inc.
- Jackson JE, Mudholkar GS (1979) Control Procedures for Residuals Associated with Principal Component Analysis. *Technometrics* 21:341-349.
- Jolliffe IT (2004) In: *Principal Component Analysis*, pp 111-131. New York, NY: Springer Science.
- Kawagoe KT, Zimmerman JB, Wightman RM (1993) Principles of voltammetry and microelectrode surface states. *J Neurosci Meth* 48:225-240.
- Keithley RB, Wightman RM, Heien ML (2009) Multivariate concentration determination using principal component regression with residual analysis. *TrAC Trends Anal Chem* 28:1127-1136.

- Keithley RB, Wightman RM, Heien ML (2010) Erratum to Multivariate concentration determination using principal component regression with residual analysis. *TrAC Trends Anal Chem* 29:110-110.
- Kramer R (1998a) In: *Chemometric Techniques for Quantitative Analysis*, pp 99-130. New York, NY: Marcel Dekker, Inc.
- Kramer R (1998b) In: *Chemometric Techniques for Quantitative Analysis*, pp 13-15. New York, NY: Marcel Dekker, Inc.
- Kramer R (1998c) In: *Chemometric Techniques for Quantitative Analysis*, pp 17-26, 107-108. New York, NY: Marcel Dekker, Inc.
- Kristensen EW, Wilson RL, Wightman RM (1986) Dispersion in flow injection analysis measured with microvoltammetric electrodes. *Anal Chem* 58:986-988.
- Lavine B, Workman J (2008) *Chemometrics*. *Anal Chem* 80:4519-4531.
- Malinowski ER (1977) Theory of error in factor analysis. *Anal Chem* 49:606-612.
- Malinowski ER (1987) Theory of the distribution of error eigenvalues resulting from principal component analysis with applications to spectroscopic data. *J Chemom* 1:33-40.
- Malinowski ER (1988) Statistical F-tests for abstract factor analysis and target testing. *J Chemom* 3:49-60.
- Malinowski ER (1990) Erratum to Statistical F-tests for abstract factor analysis and target testing. *J Chemom* 4:102.
- Malinowski ER (1991) *Factor Analysis in Chemistry*. In: *Factor Analysis in Chemistry*, pp 98-121. New York: Wiley.
- Malinowski ER (1999) Abstract factor analysis of data with multiple sources of error and a modified Faber-Kowalski F-test. *J Chemom* 13:69-81.
- Malinowski ER (2004) Adaptation of the Vogt-Mizaikoff F-test to determine the number of principal factors responsible for a data matrix and comparison with other popular methods. *J Chemom* 18:387-392.
- Michael D, Travis ER, Wightman RM (1998) Color images for fast-scan CV. *Anal Chem* 70:586a-592a.
- Michael DJ, Joseph JD, Kilpatrick MR, Travis ER, Wightman RM (1999) Improving Data Acquisition for Fast-Scan Cyclic Voltammetry. *Anal Chem* 71:3941-3947.
- National Institute of Standards and Technology 1.3.5.4. One-Factor ANOVA. In: <http://www.itl.nist.gov/div898/handbook/eda/section3/eda354.htm>
- Osten DW (1988) Selection of optimal regression models via cross-validation. *J Chemom* 2:39-48.

- Owesson-White CA, Cheer JF, Beyene M, Carelli RM, Wightman RM (2008) Dynamic changes in accumbens dopamine correlate with learning during intracranial self-stimulation. *Proc Natl Acad Sci U S A* 105:11957-11962.
- Phillips PE, Robinson DL, Stuber GD, Carelli RM, Wightman RM (2003) Real-time measurements of phasic changes in extracellular dopamine concentration in freely moving rats by fast-scan cyclic voltammetry. *Methods Mol Med* 79:443-464.
- Runnels PL, Joseph JD, Logman MJ, Wightman RM (1999) Effect of pH and Surface Functionalities on the Cyclic Voltammetric Responses of Carbon-Fiber Microelectrodes. *Anal Chem* 71:2782-2789.
- Virkler K, Lednev IK (2010) Raman spectroscopic signature of blood and its potential application to forensic body fluid identification. *Anal Bioanal Chem* 396:525-534.
- Vivo-Truyols G, Torres-Lapasio JR, Garcia-Alvarez-Coque MC, Schoenmakers PJ (2007) Towards unsupervised analysis of second-order chromatographic data: automated selection of number of components in multivariate curve-resolution methods. *J Chromatogr A* 1158:258-272.
- Wahbi AAM, Mabrouk MM, Moneeb MS, Kamal AH (2009) Simultaneous Determination of the Two Non-Steroidal Anti-Inflammatory Drugs; Diflunisal and Naproxen in their Tablets by Chemometric Spectrophotometry and Hplc. *Pak J Pharm Sci* 22:8-17.
- Wasim M, Brereton RG (2004) Determination of the number of significant components in liquid chromatography nuclear magnetic resonance spectroscopy. *Chemometr Intell Lab* 72:133-151.
- Wightman RM, Heien MLAV, Wassum KM, Sombers LA, Aragona BJ, Khan AS, Ariansen JL, Cheer JF, Phillips PEM, Carelli RM (2007) Dopamine release is heterogeneous within microenvironments of the rat nucleus accumbens. *Eur J Neurosci* 26:2046-2054.

CHAPTER IV

ASSESSING PRINCIPAL COMPONENT REGRESSION WITH RESIDUAL ANALYSIS IN THE DETECTION OF NEUROMODULATORS

Abstract

Principal component regression with residual analysis is routinely used to predict neuromodulator concentrations from *in vivo* fast-scan cyclic voltammetry measurements. This combined approach suffers from a lack of a proper validation protocol and includes no procedure to assess the overall quality of the calibration standards, both of which can lead to erroneous concentration prediction. Here, we evaluate several methods that can be used to dramatically improve multivariate concentration determination. First, separate analyses of smaller increments of a single continuous measurement could not be concatenated without substantial error in the predicted neuromodulator concentrations due to electrode drift, even though the residual analysis procedure suggested the concentrations were predicted properly. This work also presents the first direct interpretation of a residual color plot and demonstrated how it can be used to identify the specific potentials that contribute to the error quantified in the residual analysis procedure. A cyclic voltammetric representation of the calculated regression vector is shown to be a valuable tool in determining whether or not the calculated multivariate model is chemically appropriate. Finally, the use of Cook's distance successfully identified outliers contained within *in vivo* fast-scan cyclic voltammetry training sets. Taken together, these tools allow for the construction of more robust,

precise, and accurate multivariate calibration models and significantly improve the validity of predicted neuromodulator concentration data.

Introduction

Fast-scan cyclic voltammetry (FSCV) is an electroanalytical technique used to measure real time neuromodulator signaling dynamics *in vivo* of electroactive biomolecules including catecholamines (Heien et al., 2003b). FSCV used with carbon-fiber microelectrodes offers several advantages including sub-second temporal resolution, excellent sensitivity, micrometer spatial resolution, and minimal damage *in vivo* (Robinson and Wightman, 2007; Jaquins-Gerstl and Michael, 2009). FSCV is also one of the most selective electrochemical approaches because FSCV is a multivariate technique. The shape of the characteristic cyclic voltammogram for most neuromodulators is unique and can be used as a fingerprint identifier for the species being measured (Phillips and Wightman, 2003; Heien et al., 2004b).

Principal component regression (PCR) is a chemometric technique that combines principal component analysis with inverse least-squares regression (Kramer, 1998b; Keithley et al., 2009; Keithley et al., 2010a). In PCR, a training set containing reference spectra at known concentrations is assembled. Abstract representations of the training set spectra called principal components (PCs) are calculated. PCs that describe relevant information necessary for concentration prediction are retained and PCs that describe noise are discarded. The projection of the training set spectra onto the relevant PCs (called scores) are calibrated to the reference concentration values through regression analysis. Finally, concentration values of unknown spectra are predicted by calculating their relevant scores and using the calibration determined from the training set. Incorporation of PCR into the analysis of *in vivo* FSCV measurements dramatically improved neuromodulator concentration determination of analytes with

overlapping cyclic voltammograms in single cells, in brain slices, and in awake behaving rats (Heien et al., 2004b; Heien et al., 2005; Wightman et al., 2007b; Keithley et al., 2009; Keithley et al., 2010b; Keithley et al., 2010a).

The applicability of all calibration models to the unknown data sets being predicted should be properly characterized before concentration prediction of unknown samples (Daszykowski and Walczak, 2006). A residual analysis procedure developed by Jackson and Mudholkar (Jackson and Mudholkar, 1979) has been incorporated into the PCR analysis of *in vivo* FSCV data to address this concern (Heien et al., 2005; Keithley et al., 2009; Keithley et al., 2010a). If the extraneous variance in the unknown measurement (denoted as Q) is greater than a calculated tolerance level (denoted as Q_α) the multivariate calibration is insufficient to predict neuromodulator concentration values in the unknown measurement. However, this procedure is not perfect and has been shown to fail (Keithley et al., 2010b).

The accuracy of multivariate calibration models should also be verified before concentration prediction and is addressed in a process called validation (Kramer, 1998b; Daszykowski and Walczak, 2006). If separate validation standards are not available, the training set can be used as the validation set in a method called cross-validation (Kramer, 1998b). One severe disadvantage to the current PCR analysis of *in vivo* FSCV data is that there is no independent method to calculate the “true” concentration of the species being measured. The reference concentration values of *in vivo* training sets are determined empirically by dividing the measured peak current by an *in vitro* calibration factor so any validation procedure may not be of much use.

The goal of this work was to improve the PCR prediction of neuromodulator concentrations detected by FSCV *in vivo*. PCR prediction of *in vivo* FSCV data was previously limited to 90 seconds because the presence of electrode drift caused Q to cross the Q_α tolerance level (Heien et al., 2005). One way to circumvent this problem

would be to break up a long continuous measurement into smaller increments, perform PCR with residual analysis on each increment, and concatenate the results into one concentration trace for each analyte. However, this approach has not been evaluated. In addition, other diagnostic tools are applied here to characterize the overall multivariate calibration model. As suggested in the literature (Weisberg, 1983), these diagnostics should be simple, graphical, and give specific guidance of how to improve the calibration methodology. We describe the first interpretation of a residual color plot, qualitatively evaluate an estimation of pure analyte cyclic voltammograms determined from the PCR calibration relationship, and incorporate Cook's distance to successfully identify and remove standards classified as outliers in the training set.

Theory

PCR and K generation

Throughout the manuscript, uppercase bold letters represent matrices, lowercase bold letters represent vectors, and normal notation represent scalar values. PCR prediction of unknown neuromodulator concentrations (\mathbf{C}_{unk}) can be described according to

$$\mathbf{C}_{\text{unk}} = \mathbf{F}\mathbf{V}_c^T\mathbf{A}_{\text{unk}} \quad (\text{eq 4.1})$$

where \mathbf{A}_{unk} contains the unknown cyclic voltammograms to be predicted, \mathbf{V}_c contains the relevant PCs of rank r (the superscript T represents the matrix transpose), and \mathbf{F} contains the regression coefficients that relate unknown concentrations of each analyte to the scores of the relevant PCs (Kramer, 1998b). The regression coefficients in \mathbf{F} are calculated using the training set according to

$$\mathbf{F} = \mathbf{C}_{\text{TS}}\mathbf{A}_{\text{projTS}}^T[\mathbf{A}_{\text{projTS}}\mathbf{A}_{\text{projTS}}^T]^{-1} \quad (\text{eq 4.2})$$

where \mathbf{C}_{TS} are the training set reference concentration values and $\mathbf{A}_{\text{projTS}}$ are the relevant PC scores of the training set cyclic voltammograms (Kramer, 1998b). Here we define

\mathbf{C}_{TS} as being size $j \times m$, where j is the number of analytes and m is the number of training set samples. The training set voltammetric matrix (\mathbf{A}_{TS}) is size $w \times m$, where w is the number potential steps in the cyclic voltammetric waveform.

Ignoring error, the relevant currents of any unknown data set can be predicted if pure analyte cyclic voltammograms are known according to

$$\mathbf{A}_{\text{unk}} = \mathbf{K}\mathbf{C}_{\text{unk}} \quad (\text{eq 4.3})$$

where \mathbf{K} is a matrix containing cyclic voltammograms of each analyte j in units of current per concentration change. Substituting equation 1 into equation 2 shows that \mathbf{K} (as defined here) is the inverse of the quantity \mathbf{FV}_c^T calculated during the PCR procedure. However, since the quantity \mathbf{FV}_c^T is not square, \mathbf{K} can be calculated by taking the pseudoinverse of \mathbf{FV}_c^T (Hendler and Shrager, 1994). We have previously used the calculation of \mathbf{K} to compare the specific current contributions of dopamine, pH change, and electrode drift after an intravenous infusion of cocaine in a freely moving rat (Hermans et al., 2008).

Each column of \mathbf{K} , \mathbf{k}_j , can be thought of as a cyclic voltammetric representation of the regression vector for each analyte in the relevant multivariate calibration space of the training set. Stated another way, each \mathbf{k}_j vector can be thought of as the PCR interpretation of a pure analyte cyclic voltammogram based on the training set cyclic voltammograms, reference concentration values, and the relevant PCs of the multivariate model. Therefore, the shape of each \mathbf{k}_j vector could possibly be used as an overall qualitative measure to assess the validity of multivariate PCR calibration models.

Leverage

Several statistics exist for the evaluation and optimization of multivariate calibration models (ASTM International, 2000). Leverage (h_i) is a measure of uniqueness and describes how far away the i^{th} sample is away from the other $m - 1$ training set samples in the calibration space. While there are multiple ways to calculate

h_i , if singular value decomposition is used to decompose the $n \times m$ training set voltammetric matrix (Hendler and Shrager, 1994; Keithley et al., 2009; Keithley et al., 2010a), then each h_i value is easily calculated as the i^{th} diagonal element of the following multiplication

$$h_i = \text{diag}(\mathbf{V}_n \mathbf{V}_n^T) \quad (\text{eq 4.4})$$

where \mathbf{V}_n is the $m \times n$ subset that spans the relevant row information of the training set voltammetric matrix. h_i is a scalar that takes on values between 0 and 1, with samples of higher leverage having greater potential to influence the calculation of the regression vector. A good rule of thumb in for eliminating high leverage samples is to delete those that have h_i values higher than $2n/m$ or $3n/m$ (Marbach and Heise, 1990; ASTM International, 2000).

While conservative, eliminating samples based on leverage is not always ideal. First, multiple outliers make the identification of truly high leverage outliers difficult (Zhang et al., 2003). It is also possible that a sample with high leverage may have an extreme composition relative to other samples in the training set, which may occur at either the low or high end of a calibration. These regions are usually of great interest to the user during the analysis. Leverage does not take into account accuracy so samples could be eliminated based on the *possibility* of harm, rather than the actual error.

Practically, *in vivo* FSCV training sets can be inherently high leverage. *In vivo* FSCV training samples are generated by stimulating the freely-moving rat to elicit neuromodulator release of varying amplitudes. Stimulations are given to encompass a wide range of responses, but do not always evenly span the calibration space. In addition, only five cyclic voltammograms per analyte are traditionally incorporated into a training set (Keithley et al., 2009; Keithley et al., 2010b; Keithley et al., 2010a). Therefore, excluding samples with $h_i > 3n/m$ is not ideal in practice.

Studentized residual

Another figure of merit that can be used to evaluate multivariate calibrations is termed studentized residual and has the notation t_i . If e_i is the difference between the estimated and reference concentration values, t_i can be calculated as

$$t_i = \frac{e_i}{SEC \sqrt{1-h_i}} \quad (\text{eq 4.5})$$

where SEC is the standard error of the calibration (ASTM International, 2000). Pure concentration prediction error cannot be used to evaluate fit because of h_i . Samples with high leverage tend to determine the overall multivariate calibration model, which would tilt the regression vector towards them, and would as such have a lower overall prediction error (ASTM International, 2000; Stevens, 2002). Because studentized residuals should be normally distributed with common variance, a statistical test can be used to determine if the i^{th} sample is a potential outlier (Marbach and Heise, 1990; ASTM International, 2000). However, a significant value of t_i may also sometimes be indicative of an imprecise estimate of the reference concentration. Deletion of this sample may cause an underestimation of the PRESS statistic that is sometimes used for rank estimation (Marbach and Heise, 1990).

Cook's distance

Cook's distance (Cook, 1977b) (D_i) combines h_i and t_i and is a measure of the effect of the i^{th} sample on the overall multivariate calibration. In PCR, D_i is calculated as (without mean centering of the training set voltammetric matrix)

$$D_i = \frac{t_i^2}{n} \frac{h_i}{1-h_i} \quad (\text{eq 4.6})$$

where n is the number of retained PCs (Marbach and Heise, 1990). D_i is a measure of the distance that the regression vector moves within the calibration space if the i^{th} sample is removed from the training set (Cook, 1977b; Gunst and Mason, 1980; Marbach and Heise, 1990). D_i takes into account the overall extent to which a sample

can be considered an outlier (t_i) and the sensitivity of the regression vector to outliers at each data point $[h_i/(1-h_i)]$ (Cook, 1977b). Large values of D_i indicate that the i^{th} sample is highly influential in the calculation of the regression coefficients and deletion of the i^{th} sample would cause a dramatic difference in their values (Cook, 1977b; Cook and Weisberg, 1980; Gunst and Mason, 1980; Naes, 1989).

Calculated D_i values can be compared to the F -distribution to determine the extent to which the removal of the i^{th} sample changes the calculation of the regression coefficients greater than a user-defined tolerance. In PCR, the tabulated F -value used is $F_{1-\gamma}(r, m - n - 1)$ where γ is the significance level (Naes, 1989). However, in this case γ is a descriptive significance level and does not take the familiar p -value interpretation (Cook, 1977a; Obenchain, 1977; Gunst and Mason, 1980). Specifically, a D_i value that equals $F_{1-\gamma}(r, m - n - 1)$ means that deletion of the i^{th} sample moves the regression vector to the distance away corresponding to the edge of a γ confidence ellipsoid around the original regression vector. D_i is *not* distributed as F and, therefore, D_i is not a true test statistic. Instead, D_i is an indicator of how close the regression vectors are with and without the i^{th} sample (for further review see (Cook, 1977a; Obenchain, 1977; Gunst and Mason, 1980)).

D_i values that are greater than the tabulated $F_{1-\gamma}(n, m - n - 1)$ mean that deletion of the i^{th} sample causes the regression vector to move farther than a tolerable amount in the relevant multivariate calibration space. Therefore the i^{th} sample is said to be very influential in calculating the regression vector (Cook and Weisberg, 1980). Such samples should be removed from the training set because of their adverse influence on the overall regression model (Marbach and Heise, 1990). Cook's distance has been used successively with multivariate calibration to remove outliers in training sets and should serve as excellent assessment of the prediction model (Naes, 1989; Marbach and Heise, 1990; Walczak and Massart, 1995; Hawkins and Yin, 2002). D_i is more

powerful than either h_i or t_i alone because D_i simultaneously reflects error of prediction and uniqueness of spectral information (Walczak and Massart, 1995). Unfortunately, because h_i is used in the calculation of D_i , D_i suffers from the disadvantage that multiple outliers may not be detected (Lawrence, 1995).

Experimental

Electrochemical and animal experimentation

All FSCV data was collected with cylindrical, T-650 type (Thornel, Amoco Corporation, Greenville, SC) carbon-fiber microelectrodes. The preparation of the carbon-fiber microelectrodes is described elsewhere (Kawagoe et al., 1993; Hermans et al., 2008). All voltages are reported versus a Ag/AgCl reference electrode. The voltammetric waveform used was a triangular excursion at 400 V/s from -0.4 V to 1.3 V to -0.4 V. All data was acquired and collected as described previously (Michael et al., 1999). All animal experimentation was conducted on male Sprague Dawley Rats (Charles River Laboratory, Willmington, MA) weighing approximately 300 g in accordance with the University of North Carolina Institutional Animal Care and Use Committee. Surgical protocols and freely-moving experimental procedures used to generate the data analyzed here were carried out as described elsewhere (Heien et al., 2005; Day et al., 2007; Owesson-White et al., 2008).

Data analysis

All data analysis was carried out using locally written software in the MATLAB (Mathworks, Natick, MA) and LabVIEW (National Instruments, Austin, TX) programming environments. All voltammetric data was filtered at 2 kHz. PCR was performed as described previously, using singular value decomposition to decompose the training set voltammetric matrix (Hendler and Shrager, 1994; Keithley et al., 2009; Keithley et al., 2010b; Keithley et al., 2010a). Rank was estimated using Malinowski's F -test

(Malinowski, 1988, 1990; Keithley et al., 2010b). Score plots and analyte regression vectors were calculated from theory (Jackson, 1991a; Kramer, 1998b; Jolliffe, 2002).

Data was taken from experiments performed using analog background subtraction (Hermans et al., 2008) in the nucleus accumbens to determine the effect of electrode drift on predicted neuromodulator concentrations. The output was initially zero, with only analyte electrochemistry and electrode drift being detected. The data was collected continuously, but was broken up into eleven separate consecutive 60 second files.

Neuromodulator concentrations were predicted both with and without electrode drift in the training set. If electrode drift was to be accounted for, electrode drift training set cyclic voltammograms were collected at various times before and after the measurement. Because the unit for quantitation of electrode drift was arbitrary, reference values were taken to be the negative value of the measured current at -0.3 V on the forward sweep. This convention was used so electrode drift was predicted as to increase positively over time. Digital background subtraction (Howell et al., 1986) was not performed when the data was analyzed in this way.

When electrode drift was not accounted for, a training set was created using only dopamine and pH change cyclic voltammograms. Training sets including and excluding electrode drift contained the same dopamine and pH change cyclic voltammograms to maintain consistency in neuromodulator prediction. Each of the eleven 60 second data files were digitally background subtracted using an average of five cyclic voltammograms collected at the beginning of the data file and neuromodulator levels were predicted using PCR. The resulting traces were concatenated together to create analyte predictions over eleven minutes, where the last concentration value of the previous file was taken as the baseline value for the next file being predicted.

In vivo FSCV training sets

The training sets used in this work were taken from a library of 119 *in vivo* training sets measured in freely moving rats (Keithley et al., 2010b). The cyclic voltammograms were taken from stimulated neuromodulator release measured in the dorsal and ventral striatum but the location in the brain where the training sets were generated was irrelevant for the analyses. Unless noted, training sets were used without modification.

Each training set consisted of five dopamine and five pH change cyclic voltammograms. The reference concentration values reported in the library were determined by dividing peak current by a calibration factor determined using flow injection analysis (Kristensen et al., 1986b) after the experiment was performed (Owesson-White et al., 2008). The oxidation potential of dopamine (approximately 0.6 V on the positive sweep) and the C-peak of pH change (approximately -0.2 V on the positive sweep) (Takmakov et al., 2010a) were chosen for determining library reference concentrations of the training set, by convention. In this work, the QH-peak (approximately 0.3 V on the positive sweep) was also used for pH change quantitation to compare to the values calculated with the C-peak from the library.

Results and Discussion

Proper accounting of electrode drift and failure of the residual analysis procedure

Figure 4.1 compares *in vivo* dopamine and pH prediction using training sets that either include or exclude background drift for a continuous eleven minute measurement. When background drift was included in the training set, PCR predicted a minimal change in either dopamine (Figure 4.1A) or pH change levels (Figure 4.1B), while the electrode continually drifted as time progressed (Figure 4.1C). The Q-plot was below the Q_α threshold throughout the entire trace, verifying that the training set accounted for all significant variance in the measured data (Figure 4.1D).

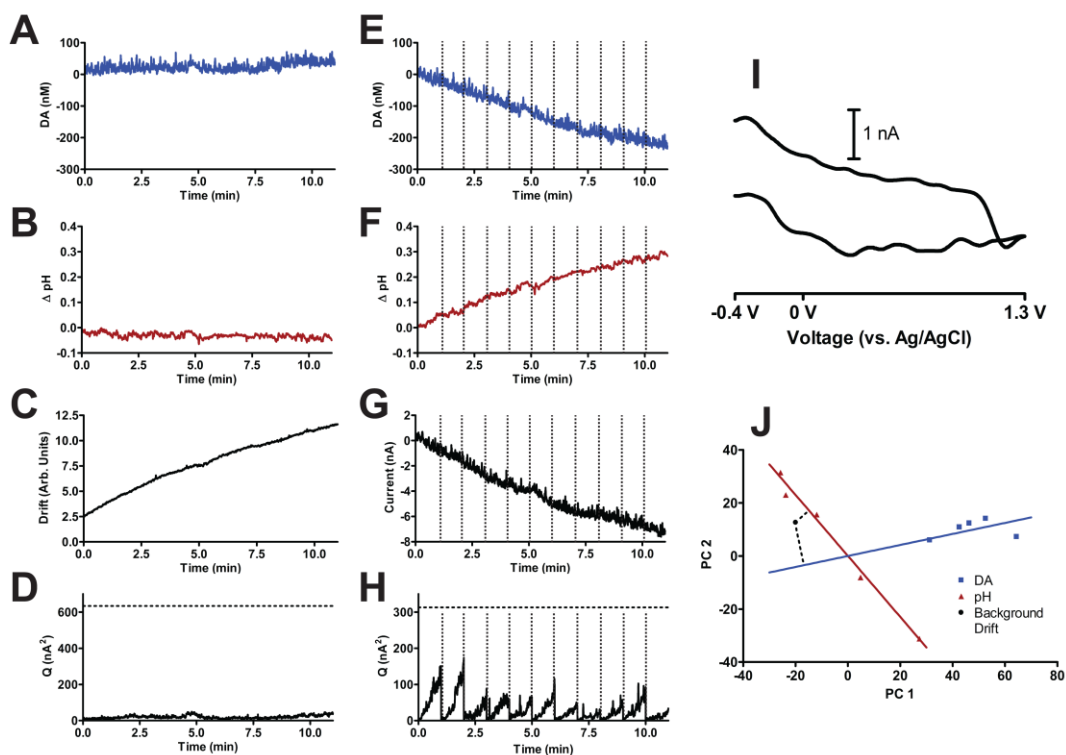


Figure 4.1. Neuromodulator prediction by PCR with and without electrode drift in the training set. The carbon-fiber microelectrode was located in the nucleus accumbens of a freely moving rat. A) Dopamine concentration predicted with background drift in the training set. B) pH change predicted with background drift in the training set. C) Background change predicted by PCR. D) Q-plot for the data predicted in A) through C). The horizontal dashed line represents Q_{α} . E) Concatenated dopamine concentrations predicted without background drift in the training set. F) Concatenated pH changes predicted without background drift in the training set. G) Concatenated digital background subtracted current versus time traces at the oxidation potential of dopamine. H) Concatenated Q-plots for the data predicted in E) and F). The horizontal dashed line represents Q_{α} . The vertical dotted lines in E) through H) represent the start of a new 60 s data file. I) Digital background-subtracted cyclic voltammogram taken at 60 s. J) Score plots and regression vectors for the training set without background drift. Blue squares represent the dopamine cyclic voltammograms and red triangles represent pH change cyclic voltammograms. The black circle represents the background drift cyclic voltammogram in I) and its projections onto the dopamine regression vector (blue) and pH regression vector (red) are plotted.

Neuromodulator levels were also predicted without electrode drift by separately analyzing the data in 60 s increments. Digital background subtraction was performed at the beginning of each increment and the resulting predicted concentration values were concatenated to generate continuous concentration traces. The last concentration value of the previous file was taken as the baseline for the next file, assuming that the concentration at the end of the previous file was the same as that in the beginning of the next file. PCR predicted an approximate 200 nM decrease in dopamine (Figure 4.1E) and a 0.3 basic pH shift (Figure 4.1F). Figure 4.1G shows the current versus time trace at the oxidation potential of dopamine decreased approximately 8 nA over the course of eleven minutes and likely contributed to both the predicted decrease in dopamine and the basic pH shift.

Interestingly, the Q-plot was below the Q_{α} threshold for each increment, although values increased as time progressed during the duration of each 60 second file as shown in Figure 4.1H. It was previously shown that the limiting duration of analysis of *in vivo* FSCV by PCR was determined by the magnitude of electrode drift. The limit was indicated when the Q-plot crossed the Q_{α} threshold (Heien et al., 2005). Here, incorrect concentrations were predicted even though the Q-plot was below the Q_{α} threshold throughout the entire trace. These drastic predicted changes in basal dopamine and pH levels were unrealistic because the animal was neither performing a behavioral task, nor was under the effect of any pharmacological agents (including anesthesia), and the carbon-fiber microelectrode is known to cause minimal damage *in vivo* (Jaquins-Gerstl and Michael, 2009). As further evidence, a digital background subtracted cyclic voltammogram at 60 s is shown in Figure 4.1I, which has a shape consistent with electrode drift, and not dopamine nor pH change (Hermans et al., 2008).

Figure 4.1J shows how electrode drift contributes to the erroneously predicted neuromodulator changes. The electrode drift cyclic voltammogram in Figure 4.1I has

projections onto the dopamine and pH change regression vectors which would make this artifact be interpreted as a combination of a decrease in dopamine and a basic pH change in this case. Background drift may not always be interpreted by PCR as a decrease in dopamine and/or a basic pH change because the magnitude and shape of background drift is known to vary and depends on the state of the carbon-fiber electrode surface (Hermans et al., 2008). A score plot, such as the one shown in Figure 4.1J, provided an excellent way to assess how electrode drift impacted neuromodulator levels predicted with PCR.

One possibility to account for electrode drift is to fit and subtract a baseline to the predicted neuromodulator concentration traces. Alternatively, in a multivariate sense, a cyclic voltammogram of electrode drift could be multiplied by a scaling factor determined by a baseline fit and subtracted from the entire measurement. The obvious flaw is that the determination of the baseline used to fit the data would be highly subjective. The change of electrode drift with time has been shown to be highly nonlinear (Hermans et al., 2008) so any baseline would be questionable at best and prone to bias. Therefore, electrode drift should be included in the PCR training set in the analysis of long continuous measurements. Rather than digitally background subtracting individual separate files and stitching the predicted concentrations together, an alternative analysis method would be to subtract background taken at the beginning of the first file from all other files of the continuous measurement, include electrode drift in the training set, and predict neuromodulator concentrations. This would yield a data structure similar to what has been analyzed previously (Hermans et al., 2008).

Transformation of the Q_α value

The residual error in the Q-plot at time t , Q_t , describes the amount of residual error contained in a specific cyclic voltammogram. Q_t is calculated by summing the squared residual current in the data not included in the retained PCs of the training set.

Q_α represents a tolerable noise level based on the discarded noise of the training set and is calculated independently of Q_t (Keithley et al., 2009; Keithley et al., 2010a). Because each Q_t value is calculated by summing the square residual current between the original data and the data described by the primary PCs at each point of the cyclic voltammogram, an approximate noise threshold in units of current can be calculated as

$$i_{TH} = \pm \sqrt{\frac{Q_\alpha}{w}} \quad (\text{eq 4.7})$$

where i_{TH} could be either positive or negative. The quantity i_{TH} represents a current value that $1-\alpha\%$ of currents due to random noise would be below based on the amount of random noise discarded during PC selection.

The value of i_{TH} can give a user an approximation of tolerable noise in units that have physical significance, rather than being an abstract transformation representing the sum of squared currents. The analysis of all 119 library training sets gave an average i_{TH} value of 0.41 ± 0.17 nA, but this value will vary based on the signal-to-noise ratio of the training set cyclic voltammograms (Keithley et al., 2010b). An uncharacteristically large value of i_{TH} would correspond to a large amount of information being discarded during factor selection and could alert the user that Q_α is too high to be of practical use.

Interpretation of residual color plots for the identification of deterministic error

A residual color plot (Keithley et al., 2009; Keithley et al., 2010a) provides extra information to the Q-plot for assessing training set augmentation; the specific peak potentials causing the error can quickly be identified. Figure 4.2A shows a representative color plot of stimulated neuromodulator release measured in the nucleus accumbens of a freely moving rat. At the time of the stimulation (as indicated by the red bar) dopamine was released, followed by a basic pH change that lasted for approximately seven seconds. There was also a transient increase in dopamine before the stimulation was given.

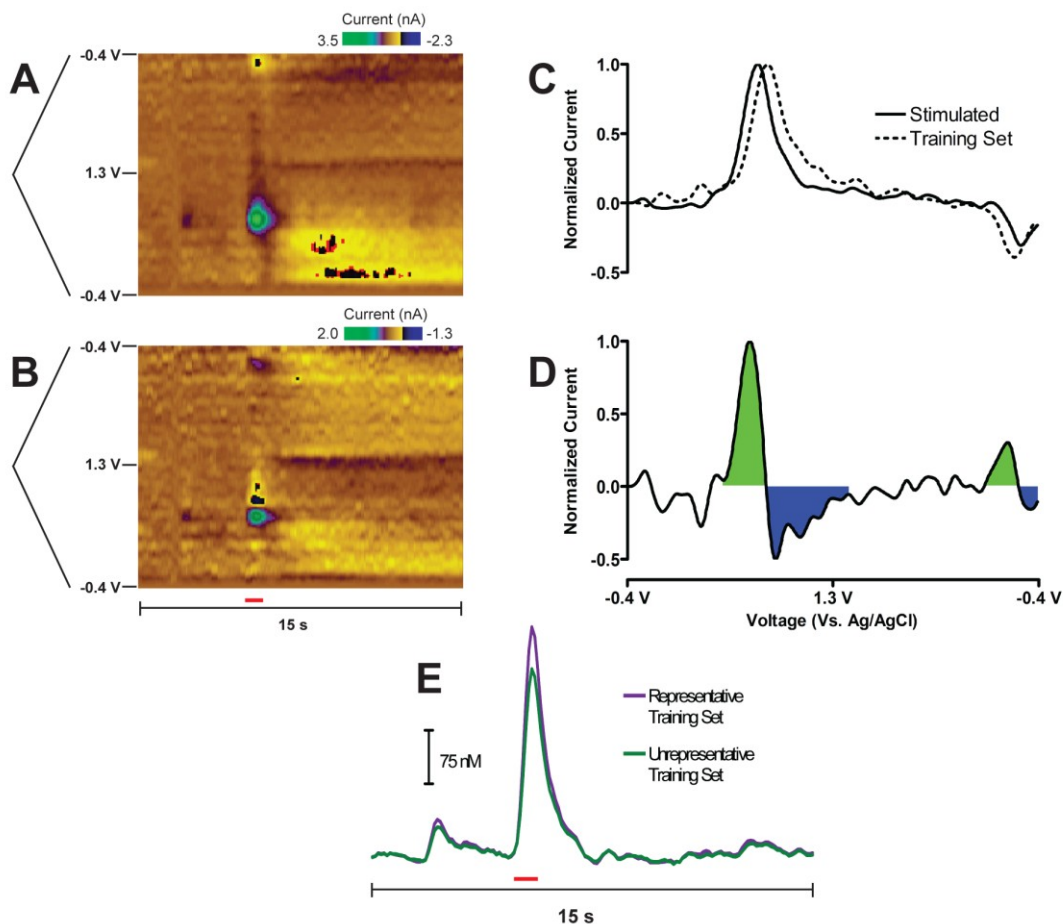


Figure 4.2. Interpretation of a residual color plot when an unrepresentative training set is used for concentration prediction. A) Color plot representation of stimulated dopamine release in the nucleus accumbens of a freely moving rat. The voltammetric sweep is plotted to the left of the color plot. B) Residual color plot after an unrepresentative training set was used for concentration prediction. A) and B) share the time axis below B), with the red bar indicating a stimulation given to the animal (60 Hz, 24 pulses, 125 μ A). C) Unfolded normalized dopamine cyclic voltammograms for the stimulated dopamine release in A) (solid line) and a dopamine cyclic voltammogram from the unrepresentative training set (dashed line). D) Unfolded cyclic voltammogram representing the subtraction of the improper training set dopamine cyclic voltammogram from the stimulated dopamine release shown in C). The green and blue shadings are shown to highlight differences at the oxidation and reduction peaks, with the color scheme mimicking that of the residual color plot shown in B). E) Concentration prediction comparison between the proper representative and improper unrepresentative training sets.

A training set was generated by exchanging representative dopamine cyclic voltammograms for those taken from a different animal to illustrate how the residual color plot can be used to improve the multivariate calibration and to show why training sets generated in one animal is risky for concentration prediction in another animal. Both the dopamine calibration factor and the pH change cyclic voltammograms remained consistent. After concentration prediction using the unrepresentative training set, the residual color plot was calculated and is shown in Figure 4.2B. There was considerable deterministic error that was only present during the prediction of dopamine events. Specifically, positive-negative current deflections at the oxidation and reduction peak positions were calculated.

The origin of the residual color plot can be explained by the unfolded cyclic voltammograms shown in Figure 4.2C. The unfolded cyclic voltammogram of dopamine taken at maximal release from Figure 4.2A is shown as the solid black trace in Figure 4.2C and one of the dopamine cyclic voltammograms of the unrepresentative training set used for the prediction is shown as the dashed trace in Figure 4.2C. There was a difference in peak separation (ΔE_p) of approximately 130 mV between dopamine from the measured stimulation and the dopamine cyclic voltammograms of the training set. Such shifts in ΔE_p can arise from differences in electron transfer kinetics or resistance differences between carbon-fiber microelectrodes (Wipf et al., 1988).

Subtracting training set dopamine from stimulated dopamine release gives the pattern shown in Figure 4.2D that arises from the differences in ΔE_p . This difference shows positive-negative current deflections at the oxidation and reduction peak potentials apparent in the color representation (Figure 4.2B). Ideally, the residual color plot should contain only pure noise. Deterministic error will arise if the training set is not representative of the unknown data set either because of differences in the shapes of analyte cyclic voltammograms or because of the presence of an interfering

species. Theoretically, these should cause the Q-plot to cross the Q_α threshold, but this does not always occur as shown in Figure 4.1H. To minimize the possibility of such errors, training sets should be collected within the same animal at the same location of the unknown measurement.

Differences in ΔE_p values occurred even though the exact same type of carbon-fiber microelectrodes was used for all experiments. The predicted dopamine concentration values differed by approximately 50 nM or 18% between the two training sets (Figure 4.2E), but the same general trend was measured. Therefore, slight variations in peak shapes may yield qualitative information on neuromodulator changes, but neuromodulator quantitation will likely be inaccurate. Therefore, the creation of a standard training set of *in vivo* cyclic voltammograms applicable to all experiments (Flagel et al., 2010) is risky. Moreover, if the residual analysis procedure was to be used, a standardized training assumes that the noise level of all electrodes in all animals performing all types of behavioral tasks is constant. It was previously hypothesized that the noise level of *in vivo* FSCV measurements was correlated to animal movement (Keithley et al., 2010b) so tasks that involve more motor movements would likely contain an overall larger noise level. Therefore, standard training sets may also invalidate the proper application of the residual analysis procedure.

*The use of **K** as a qualitative diagnostic tool*

Another possible source of deterministic error in the residual color plot is the calculation of improper regression vectors. If the calculated regression vectors were erroneous, the multivariate calibration space would be altered, causing errors during concentration prediction when analytes of interest are present. There is a need for a rapid, simple diagnostic criterion that can be used to verify that the PCR model correctly identified the characteristic voltammetric pattern associated with each neuromodulator of

interest. In a qualitative way, the \mathbf{k}_j vector provides this information as illustrated by the following two data sets.

Figures 4.3A and 4.3B shows an example of a proper training set consisting of five dopamine cyclic voltammograms and five pH change cyclic voltammograms. The cyclic voltammograms for each species had a consistent shape and spanned the calibration space well with an estimated rank of two. The calculated values of \mathbf{k}_j for dopamine (\mathbf{k}_{DA}) and pH change (\mathbf{k}_{pH}) are shown in Figures 4.3C and 4.3D respectively. These cyclic voltammetric representations are consistent with those of the training set and the known cyclic voltammograms of these two neuromodulators (Heien et al., 2004b; Takmakov et al., 2010a). The sensitivity at the peak potentials of dopamine and pH change were also consistent with values reported in the literature (Heien et al., 2003b; Heien et al., 2004b; Takmakov et al., 2010a).

Figures 4.3E and 4.3F show an example of an improper training set with an estimated rank of three (the rank of *in vivo* FSCV training sets varies with signal-to-noise ratio and is not a diagnostic criterion for an invalid training set (Keithley et al., 2010b)). The dopamine cyclic voltammograms showed a consistent shape that spanned a wide concentration range. However the 0.14 basic pH change cyclic voltammogram was inconsistent with the rest of the pH change cyclic voltammograms. The pH change cyclic voltammogram normally has three peaks known as the C-peak at approximately -0.2 V on the oxidative sweep, the QH-peak at approximately 0.3 V on the oxidative sweep, and the Q-peak at approximately -0.3 V on the reductive sweep (Takmakov et al., 2010a). Using the other pH change cyclic voltammograms for comparison, the peak current of the C-peak for the 0.14 basic pH change was much too large for reasons that are not understood. Since the C-peak was used for quantitation, the 0.14 basic pH change reference value was also likely incorrect.

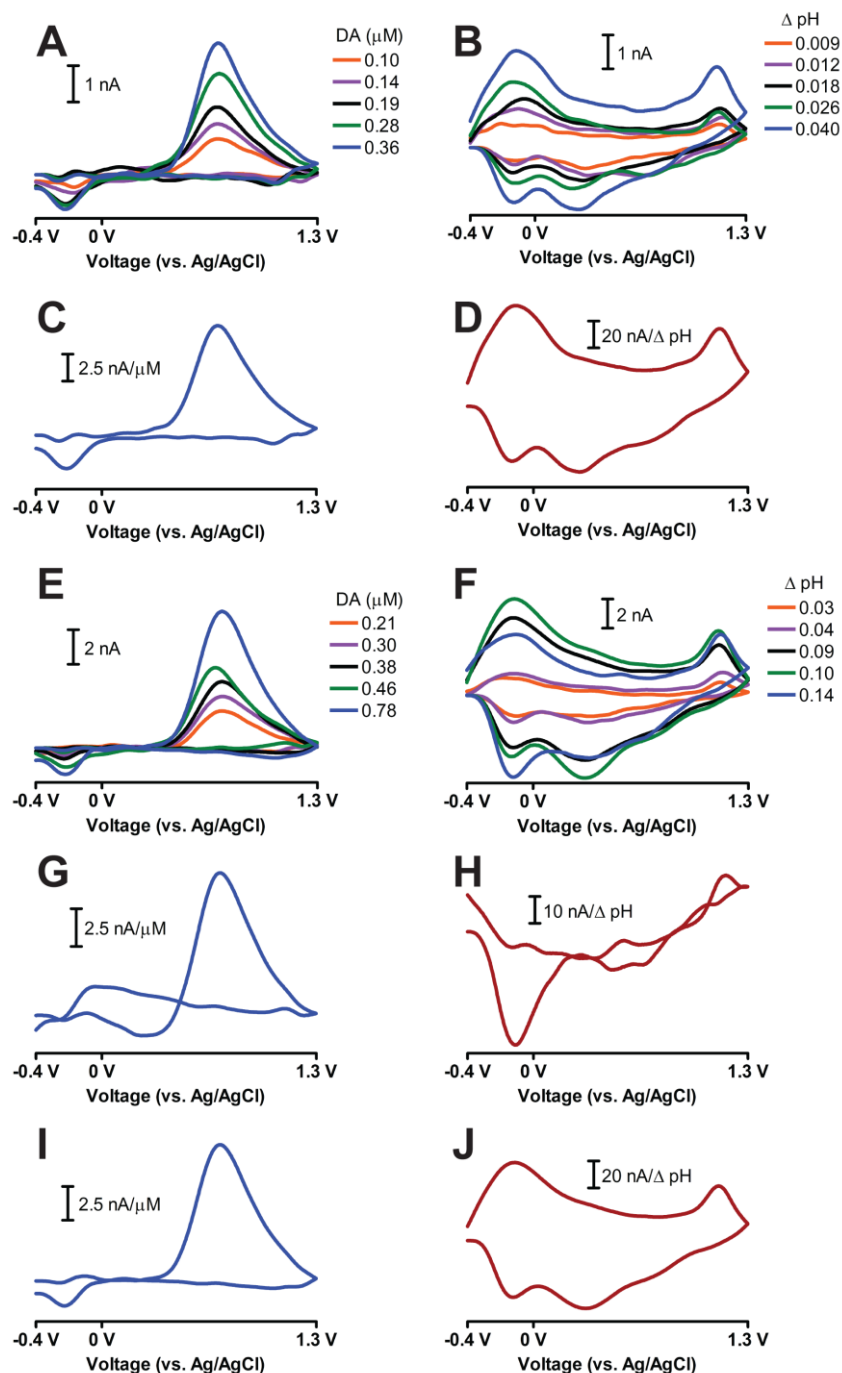


Figure 4.3. K representations of a proper and an improper training set. A) Dopamine cyclic voltammograms of the proper training set. B) pH change cyclic voltammograms of the proper training set. C) k_{DA} for the proper training set shown in A) and B). D) k_{pH} for the proper training set shown in A) and B). E) Dopamine cyclic voltammograms of the improper training set. F) pH change cyclic voltammograms of the improper training set. G) k_{DA} for the improper training set shown in E) and F). H) k_{pH} for the improper training set shown in E) and F). I) and J) show the recalculated k_{DA} and k_{pH} vectors, respectively, for the improper training set shown in E) and F) if the QH-peak is used for pH change quantitation rather than the C-peak.

Figures 4.3G and 4.3H show the calculated \mathbf{k}_{DA} and \mathbf{k}_{pH} vectors for the poor training set. Even though the dopamine cyclic voltammograms of the poor training set were of good quality, the shape of \mathbf{k}_{DA} was distorted. Moreover, the shape of \mathbf{k}_{pH} was even worse with only the C-peak was apparent. The broad shape of the pH change cyclic voltammogram was incorporated into \mathbf{k}_{DA} rather than \mathbf{k}_{pH} , as well as most of the QH- and Q-peaks. In fact, the sensitivity of dopamine at the reduction potential was a positive value. PCR would generate concentration information for the species with cyclic voltammograms shown in Figures 4.3G and 4.3H, rather than those of the desired neuromodulators. If the training set shown in Figures 4.3E and 4.3F was used for prediction, the resulting dopamine concentrations would likely represent a blend of dopamine and pH change information and the predicted pH changes would be difficult to interpret. Moreover, there would be considerable deterministic error associated during the prediction of neuromodulator changes, which could be visualized with the residual color plot, similar to the one shown in Figure 4.2B.

Since \mathbf{K} is calculated from the inverse of \mathbf{FV}_c^T , there are three reasons that would cause \mathbf{k}_j vectors to deviate from ideal behavior. First, the number of relevant PCs chosen during factor selection could be incorrect. This was unlikely because factor selection has been previously evaluated for *in vivo* FSCV training sets (Keithley et al., 2010b). Second, the reference concentration values could be incorrect leading to erroneous relationships between the projections onto the regression vectors and predicted concentrations. To illustrate this point, the QH-peak was used instead of the C-peak to determine the amplitude of the basic pH shifts from the improper training set in Figure 4.3F. \mathbf{k}_{DA} and \mathbf{k}_{pH} were recalculated and are shown in Figures 4.3I and 4.3J. These values were consistent with the known cyclic voltammograms (Heien et al., 2004b). This result showed that the reference pH changes determined using the QH-

peak were more appropriate, given the shapes of the pH change cyclic voltammograms of the improper training set.

PCR assumes that the amplitude of the entire cyclic voltammogram linearly increases with concentration so the choice of which of the C-, QH-, or Q-peaks is used for quantitation should be irrelevant because their relative ratios should remain constant. However, the amplitude of the C-peak has been shown to vary depending on the extracellular environment meaning that the C-peak is more susceptible to voltammetric inconsistencies and overall error (Takmakov et al., 2010a). In that work it was suggested that a current versus time trace taken at the C-peak was unsuitable for quantitation of pH changes *in vitro* or *in vivo*. The results here provide clear evidence that extends this conclusion to multivariate analysis of *in vivo* FSCV data. Instead, the QH- or Q-peak should be used to determine the value of the reference pH changes for *in vivo* FSCV training sets.

A third possibility for improper k_{DA} or k_{pH} values is that inconsistent cyclic voltammograms could be included in the training set that drastically alter the multivariate calibration space. Such samples could unduly influence the position of the regression vector and thus \mathbf{K} . While the \mathbf{K} approach can be used as a simple, rapid, qualitative graphical diagnostic tool of overall model prediction, another criterion should be included to identify any cyclic voltammograms of the training set that act as outliers, unduly influencing the position of the regression vectors and the relevant calibration space.

Identifying and removing training set outliers using Cook's distance

If there is a significant change in a calibration model upon the deletion of one sample, the sample is likely an outlier and should not be included in the training set. Mathematically, if D_i is larger than a tabulated F -value, that sample should be considered for rejection. Originally, Cook suggested that a value of 0.1 be used for γ , but this selection was arbitrary (Cook, 1977b). Using a value of 0.1 for γ determined that

31 out of a library of 119 training sets contained at least one poor standard. Careful visual inspection of the questionable training sets determined that this was unreasonable (data not shown). A γ value of 0.1 led to the calculation of tolerable distance shifts that were too small for the high leverage FSCV data (*vide supra*). Instead, a γ value of 0.05 was used here that yielded satisfactory results, as shown below.

Figure 4.4 shows how Cook's distance can be used to improve the PCR analysis of *in vivo* FSCV data. Figures 4.4A and 4.4B show the dopamine and pH change cyclic voltammograms, respectively, for an improper training set. The estimated rank of this training set was two. The 0.25 μM dopamine and 0.062 basic pH change samples were clearly uncharacteristic of the other neuromodulator cyclic voltammograms. The 0.25 μM dopamine cyclic voltammogram had an extra peak at -0.2 V on the forward sweep and the 0.062 basic pH shift had a positive current deflection at 0.4 V on the forward sweep.

k_{DA} and k_{pH} for this improper training set are shown in Figures 4.4C and 4.4D, respectively. The inclusion of the questionable standards negatively affected the interpretation of pure analyte voltammograms by the PCR model, especially for pH change. Figure 4.4E shows the score plot for the improper training set from Figures 4.4A and 4.4B. Visually, the 0.25 μM dopamine and the 0.062 basic pH shift samples resemble possible outliers in the relevant calibration space. h_i of the questionable dopamine and pH change standards were calculated to be 0.61 and 0.60 respectively, higher than all the other samples, indicating that these two samples had moderate potential to influence the multivariate calibration. Indeed, the position of the regression vectors appear tilted towards these outliers and away from the other analyte standards.

The calculated D_i values for these questionable dopamine and pH standards were 5.49 and 5.01, respectively, which were significantly higher than the tabulated F -value of 4.74. The significant D_i values indicate that these two samples were outliers

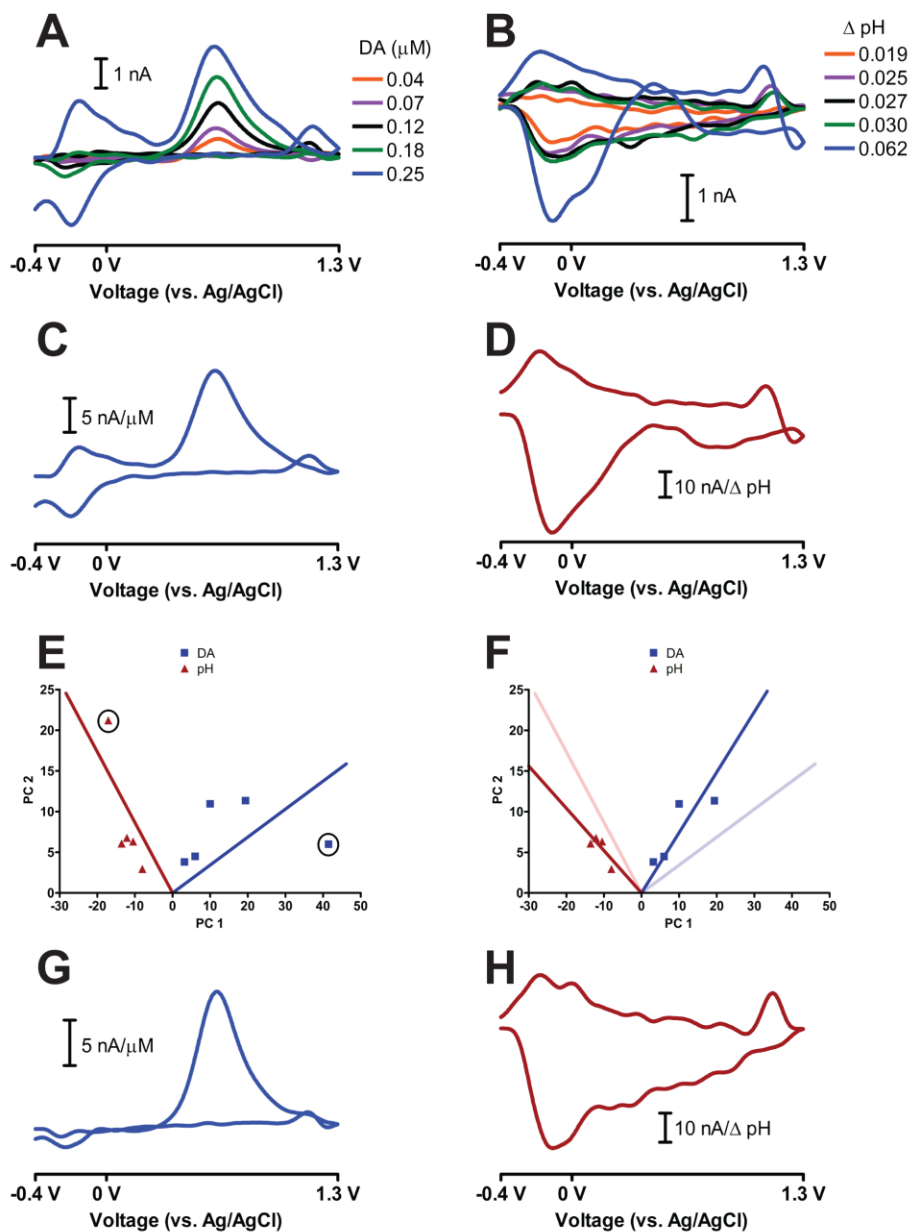


Figure 4.4. The use of Cook's distance to improve PCR calibration. A) and B) show the dopamine and pH change cyclic voltammograms (respectively) of an improper training set. C) and D) show k_{DA} and k_{pH} , respectively, for the improper training set shown in A) and B). E) Score plot showing both the dopamine (blue squares) and pH change (red triangles) cyclic voltammograms of the training set in A) and B). The solid lines represent the calculated regression vectors for both dopamine (blue) and pH change (red). The circled points represent the 0.25 μM dopamine and 0.062 basic pH change standards. F) Score plot as in E) with the 0.25 μM dopamine and 0.062 basic pH change standards removed. The regression vectors without these standards were recalculated and are plotted. The original regression vectors in E) are also shown as faded solid lines. G) and H) show the recalculated k_{DA} and k_{pH} vectors, respectively, after the removal of the 0.25 μM dopamine and 0.062 basic pH change standards.

and should not have been included in the calibration model because of their overall adverse impact on the regression vectors. The regression vectors were recalculated with the outliers removed from this training set and are plotted in Figure 4.4F. There was a dramatic shift in the position of the regression vectors for each neuromodulator. Without the outliers, the regression vectors more accurately spanned the remaining training set samples for both dopamine and pH change.

k_{DA} and k_{pH} were also recalculated without the outliers and are shown in Figures 4.4G and 4.4H, respectfully. k_{DA} and k_{pH} differed in shape from the proper training set shown in Figure 4.3, but were consistent with the remaining neuromodulator cyclic voltammograms of this training set. The shape of a pH change cyclic voltammogram depends on both the extracellular environment and carbon surface chemistry (Takmakov et al., 2010a) and has been published with varying C-/QH-/Q-peak ratios (Roitman et al., 2004; Heien et al., 2005; Stuber et al., 2005; Hermans et al., 2008).

D_i was also used to evaluate the improper training set shown in Figures 4.3E and 4.3F. h_i was calculated to be 0.86 for the questionable pH change cyclic voltammogram labeled as a 0.14 basic pH shift. Such a large h_i indicates that this sample had a large potential to influence the calculation of the regression vectors. Calibrating with the pH change cyclic voltammograms with the C-peak gave a D_i value of 6.65 and calibrating with the QH-peak gave a D_i value of 11.42. Since both of these values were larger than the tabulated F -value of 4.76, this standard was considered an outlier no matter how the reference pH change value was determined.

Cook's distance may also likely improve model selection. Recently it was shown that Malinowski's F -test improved factor selection for *in vivo* FSCV training sets (Keithley et al., 2010b). This approach estimates rank by identifying PCs that contain statistically more variance than PCs that span noise. While the ideal rank of a training set containing only dopamine and pH is two, many training sets had an estimated rank

higher than two. One reason for a large estimated rank is that inconsistencies were present in the cyclic voltammograms that were significantly larger than the noise. For these training sets Malinowski's F -test could retain more PCs to span inconsistencies in outlier cyclic voltammograms rather than only the relevant calibration space.

Cook's distance was used to test this hypothesis. Of the 119 training sets analyzed, 15 were identified to contain outliers based on Cook's distance. Interestingly, Malinowski's F -test estimated the rank to be larger than two for 13 of the 15 training sets. Upon removal of the identified outliers, the estimated rank decreased for 10 of those 13 training sets. This result shows that the estimated rank increased for some training sets only to span samples that would adversely impact the overall prediction of the multivariate calibration model. Therefore, Cook's distance can be used to improve both the prediction ability and selection of the relevant factor space of multivariate *in vivo* FSCV calibration models.

Conclusions

This work presents several vital improvements in the multivariate prediction of neuromodulators detected with FSCV using PCR with residual analysis. The presence of electrode drift introduced significant error in the prediction of dopamine and pH change for multi-minute recordings, even if the continuous data set was analyzed in smaller segments. The residual color plot was shown to be effective in specifically describing how training sets can be augmented to be more representative of the unknown data to be predicted. An approach based on the pseudoinverse of the PCR calibration matrix allowed for a simple, straightforward, rapid graphical way to qualitatively assess the validity of the multivariate prediction model. Using this approach, it was determined that the C-peak of the pH cyclic voltammogram should not be used to determine the reference pH change values of *in vivo* FSCV training sets.

Finally, the incorporation of Cook's distance successfully demonstrated how outliers could be removed from the training set before unknown concentrations are predicted. Overall, these methods prove to be crucial to provide more precise, accurate, and robust concentration prediction of *in vivo* FSCV data using PCR with residual analysis.

References

- ASTM International (2000) Standard Practices for Infrared Multivariate Quantitative Analysis, Doc. E 1655-00 in ASTM Annual Book of Standards, vol. 03.06. Standard Practices for Infrared Multivariate Quantitative Analysis, Doc E 1655-00 in ASTM Annual Book of Standards, Vol 0306.
- Cook RD (1977a) Letters to the Editor. *Technometrics* 19:349-350.
- Cook RD (1977b) Detection of Influential Observation in Linear-Regression. *Technometrics* 19:15-18.
- Cook RD, Weisberg S (1980) Characterizations of an Empirical Influence Function for Detecting Influential Cases in Regression. *Technometrics* 22:495-508.
- Daszykowski M, Walczak B (2006) Use and abuse of chemometrics in chromatography. *TrAC, Trends Anal Chem* 25:1081-1096.
- Day JJ, Roitman MF, Wightman RM, Carelli RM (2007) Associative learning mediates dynamic shifts in dopamine signaling in the nucleus accumbens. *Nat Neurosci* 10:1020-1028.
- Flagel SB, Clark JJ, Robinson TE, Mayo L, Czuj A, Willuhn I, Akers CA, Clinton SM, Phillips PEM, Akil H (2010) A selective role for dopamine in stimulus-reward learning. *Nature* 469:53-57.
- Gunst RF, Mason RL (1980) Regression analysis and its application : a data-oriented approach. New York: M. Dekker.
- Hawkins DM, Yin X (2002) A faster algorithm for ridge regression of reduced rank data. *Comput Stat Data An* 40:253-262.
- Heien M, Khan AS, Ariansen JL, Cheer JF, Phillips PEM, Wassum KM, Wightman RM (2005) Real-time measurement of dopamine fluctuations after cocaine in the brain of behaving rats. *Proc Natl Acad Sci U S A* 102:10023-10028.
- Heien ML, Johnson MA, Wightman RM (2004) Resolving neurotransmitters detected by fast-scan cyclic voltammetry. *Anal Chem* 76:5697-5704.
- Heien ML, Phillips PE, Stuber GD, Seipel AT, Wightman RM (2003) Overoxidation of carbon-fiber microelectrodes enhances dopamine adsorption and increases sensitivity. *Analyst* 128:1413-1419.
- Hendler RW, Shrager RI (1994) Deconvolutions Based on Singular-Value Decomposition and the Pseudoinverse - a Guide for Beginners. *J Biochem Bioph Meth* 28:1-33.
- Hermans A, Keithley RB, Kita JM, Sombers LA, Wightman RM (2008) Dopamine detection with fast-scan cyclic voltammetry used with analog background subtraction. *Anal Chem* 80:4040-4048.

- Howell JO, Kuhr WG, Ensman RE, Wightman RM (1986) Background Subtraction for Rapid Scan Voltammetry. *J Electroanal Chem* 209:77-90.
- Jackson JE (1991) *A User's Guide to Principal Components*. New York: Wiley.
- Jackson JE, Mudholkar GS (1979) Control Procedures for Residuals Associated with Principal Component Analysis. *Technometrics* 21:341-349.
- Jaquins-Gerstl A, Michael AC (2009) Comparison of the brain penetration injury associated with microdialysis and voltammetry. *J Neurosci Meth* 183:127-135.
- Jolliffe IT (2002) *Principal Component Analysis*. New York: Springer-Verlag.
- Kawagoe KT, Zimmerman JB, Wightman RM (1993) Principles of voltammetry and microelectrode surface states. *J Neurosci Meth* 48:225-240.
- Keithley RB, Wightman RM, Heien ML (2009) Multivariate concentration determination using principal component regression with residual analysis. *TrAC Trends Anal Chem* 28:1127-1136.
- Keithley RB, Wightman RM, Heien ML (2010a) Erratum to Multivariate concentration determination using principal component regression with residual analysis. *TrAC Trends Anal Chem* 29:110-110.
- Keithley RB, Carelli RM, Wightman RM (2010b) Rank Estimation and the Multivariate Analysis of in Vivo Fast-Scan Cyclic Voltammetric Data. *Anal Chem* 82:5541-5551.
- Kramer R (1998) *Chemometric Techniques for Quantitative Analysis*. New York, NY: Marcel Dekker, Inc.
- Kristensen EW, Wilson RL, Wightman RM (1986) Dispersion in flow injection analysis measured with microvoltammetric electrodes. *Anal Chem* 58:986-988.
- Lawrence AJ (1995) Deletion Influence and Masking in Regression. *J Ro Stat Soc B Met* 57:181-189.
- Malinowski ER (1988) Statistical F-tests for abstract factor analysis and target testing. *J Chemom* 3:49-60.
- Malinowski ER (1990) Erratum to Statistical F-tests for abstract factor analysis and target testing. *J Chemom* 4:102.
- Marbach R, Heise HM (1990) Calibration Modeling by Partial Least-Squares and Principal Component Regression and Its Optimization Using an Improved Leverage Correction for Prediction Testing. *Chemometr Intell Lab* 9:45-63.
- Michael DJ, Joseph JD, Kilpatrick MR, Travis ER, Wightman RM (1999) Improving Data Acquisition for Fast-Scan Cyclic Voltammetry. *Anal Chem* 71:3941-3947.
- Naes T (1989) Leverage and Influence Measures for Principal Component Regression. *Chemometr Intell Lab* 5:155-168.

- Obenchain RL (1977) Letters to the Editor. *Technometrics* 19:348-349.
- Owesson-White CA, Cheer JF, Beyene M, Carelli RM, Wightman RM (2008) Dynamic changes in accumbens dopamine correlate with learning during intracranial self-stimulation. *Proc Natl Acad Sci U S A* 105:11957-11962.
- Phillips PEM, Wightman RM (2003) Critical guidelines for validation of the selectivity of in-vivo chemical microsensors. *TrAC Trends Anal Chem* 22:509-514.
- Robinson DL, Wightman RM (2007) Rapid Dopamine Release in Freely Moving Rats. In: *Electrochemical Methods for Neuroscience* (Michael AC, Borland LM, eds), pp 17-34. Boca Raton, FL, USA: CRC Press.
- Roitman MF, Stuber GD, Phillips PEM, Wightman RM, Carelli RM (2004) Dopamine operates as a subsecond modulator of food seeking. *J Neurosci* 24:1265-1271.
- Stevens J (2002) *Applied multivariate statistics for the social sciences*. Mahwah, N.J.: Lawrence Erlbaum Associates.
- Stuber GD, Roitman MF, Phillips PEM, Carelli RM, Wightman RM (2005) Rapid dopamine signaling in the nucleus accumbens during contingent and noncontingent cocaine administration. *Neuropsychopharmacol* 30:853-863.
- Takmakov P, Zachek MK, Keithley RB, Bucher ES, McCarty GS, Wightman RM (2010) Characterization of Local pH Changes in Brain Using Fast-Scan Cyclic Voltammetry with Carbon Microelectrodes. *Anal Chem* 82:9892-9900.
- Walczak B, Massart DL (1995) Robust principal components regression as a detection tool for outliers. *Chemometr Intell Lab* 27:41-54.
- Weisberg S (1983) Discussion: Some Principles for Regression Diagnostics and Influence Analysis. *Technometrics* 25:240-244.
- Wightman RM, Heien ML, Wassum KM, Sombers LA, Aragona BJ, Khan AS, Ariansen JL, Cheer JF, Phillips PE, Carelli RM (2007) Dopamine release is heterogeneous within microenvironments of the rat nucleus accumbens. *Eur J Neurosci* 26:2046-2054.
- Wipf DO, Kristensen EW, Deakin MR, Wightman RM (1988) Fast-Scan Cyclic Voltammetry as a Method to Measure Rapid, Heterogeneous Electron-Transfer Kinetics. *Anal Chem* 60:306-310.
- Zhang MH, Xu QS, Massart DL (2003) Robust principal components regression based on principal sensitivity vectors. *Chemometr Intell Lab* 67:175-185.

CHAPTER V

HIGHER SENSITIVITY DOPAMINE MEASUREMENTS WITH FASTER-SCAN CYCLIC VOLTAMMETRY

Abstract

Fast-scan cyclic voltammetry with carbon-fiber microelectrodes has been successfully used to detect catecholamine release *in vivo*. Generally, waveforms with anodic voltage limits of 1.0 V or 1.3 V (vs. Ag/AgCl) are used for detection. The 1.0 V excursion provides good temporal resolution, but suffers from a lack of sensitivity. The 1.3 V excursion increases sensitivity, but also increases response time which can blur the detection of neurochemical events. Here, the scan rate was increased to improve the sensitivity of the 1.0 V excursion while maintaining the rapid temporal response. However, increasing scan rate increases both the desired faradaic current response and the already large charging current associated with the voltage sweep. Analog background subtraction was used to prevent the analog-to-digital converter from saturating from the high currents generated with increasing scan rate by neutralizing some of the charging current. In addition, because the gain of the current-to-voltage converter was held constant, quantization noise did not increase. *In vitro* results with the 1.0 V waveform showed approximately four-fold increase in signal to noise ratio with maintenance of the desired faster response time by increasing scan rate up to 2400 V/s. *In vivo*, stable stimulated release was detected with an approximate four-fold increase in faradaic response. In an attempt to create an ultra-sensitive waveform, the scan rate of the 1.3 V waveform was also increased, but the signal was unstable with time *in vitro*.

and in vivo. Adapting the 1.3 V triangular wave into a novel sawhorse design prevented signal decay and increased the faradaic response. The use of the 1.3 V sawhorse waveform decreased the detection limit of dopamine with FSCV to 0.96 ± 0.08 nM in vitro and showed improved performance in vivo. Furthermore, the higher currents obtained with this waveform did not alter the firing rates of adjacent neurons. Electron microscopy showed the effects of faster scan rates of all waveforms on the carbon-fiber surface. The unstable loss in sensitivity with the 1.3 V cyclic excursion at faster scan rates was accompanied by a lack of electrochemical etching. This result suggests the lack of electrochemical etching decreases dopamine adsorption and dopamine sensitivity is in a quasi-steady state with carbon-fiber microelectrodes scanned to potentials above 1.0 V.

Introduction

Fast-scan cyclic voltammetry (FSCV) with carbon-fiber microelectrodes is a useful technique for the in vivo detection of various electroactive species including catecholamines. FSCV offers many advantages including sub-second time resolution, high spatial resolution, moderate selectivity, and excellent sensitivity (Robinson and Wightman, 2007). These advantages have allowed users to probe neurochemical signaling dynamics in single cells, adrenal slices, brain slices, and in the intact brains of anesthetized and freely moving rats (Phillips et al., 2003; Rice and Cragg, 2004; Heien et al., 2005; Cheer et al., 2007; Clark et al., 2009; Fulks et al., 2010; Ge et al., 2010; Petrovic et al., 2010).

Several approaches have been used to improve the signal-to-noise ratios in the detection of neuromodulators with FSCV including improving electrode fabrication (Rice and Nicholson, 1989; Strand and Venton, 2008), signal processing (Wiedemann et al., 1991; Cahill et al., 1996; Heien et al., 2005; Keithley et al., 2010), instrumentation

(Howell et al., 1986; Michael et al., 1999), and the incorporation of novel electrode coatings (Kawagoe and Wightman, 1994; Swamy and Venton, 2007). Electrochemical pretreatment also enhances sensitivity towards catecholamines through the creation of adsorption sites (Gonon et al., 1980; Gonon et al., 1981; Hafizi et al., 1990; Heien et al., 2003). Traditional experiments employed FSCV waveforms that had an anodic potential limit of 1.0 V (vs. Ag/AgCl), which provided for good temporal resolution (Heien et al., 2003). These waveforms suffered from a lack of sensitivity so waveforms with an anodic limit of 1.3 V are frequently used to provide increased sensitivity in vivo (Day et al., 2007; Roitman et al., 2008; Gan et al., 2010). However, the increase in catecholamine adsorption sites associated with higher anodic limits that improve sensitivity increases the response time of the carbon-fiber microelectrode (Heien et al., 2003).

Constant potential amperometry is a useful electrochemical technique for the detection of neuromodulators in vivo that offers far superior temporal resolution compared to FSCV, typically around 50 kHz (Wightman et al., 1991; Petrovic et al., 2010). However, any approaches that could be used to increase the signal-to-noise ratio in constant potential amperometry (coatings, surface modifications, increasing electrode area) can also be applied to improve FSCV measurements. Though FSCV measurements cannot be performed with the temporal resolution of constant potential amperometry, the ability to customize scan rate provides an additional parameter to increase the signal-to-noise ratio and is one reason submicromolar concentrations of neuromodulator can be detected with microelectrodes using FSCV. Microelectrodes offer several advantages including reduced ohmic loss and cell time constant which allows scan rates to be increased without appreciable signal distortions (Michael and Wightman, 1996). Scan rates in the range of 10^5 to 10^6 V/s have been used with disc microelectrodes to probe reaction mechanisms and study electron transfer of short lived species (Montenegro and Pletcher, 1986; Amatore et al., 1987; Andrieux et al., 1988b, a;

Wipf and Wightman, 1988). However, at these high scan rates, classical cyclic voltammetry theory is no longer valid (Amatore and Lefrou, 1990) and signal distortions even with microelectrodes can occur (Wipf et al., 1988).

Basic cyclic voltammetry theory predicts that peak current for diffusion-mediated electron transfer varies with the square root of scan rate while peak current for species that adsorb to the electrode surface scales proportionally with scan rate (Bard, 2001). Catecholamines such as dopamine strongly adsorb to the electrode surface (Baur et al., 1988; Bath et al., 2000; Heien et al., 2003) so increasing scan rate proportionally increases their faradaic response. For this reason, increasing the scan rate above the traditional (Heien et al., 2003) 300-400 V/s range is advantageous in the detection of neuromodulators and has been used previously (Pihel et al., 1994; Jackson et al., 1995; Hsueh et al., 1997; Bath et al., 2000; Troyer and Wightman, 2002; Hashemi et al., 2009).

Unfortunately, charging current also increases proportionally with scan rate (Michael and Wightman, 1996). Charging current overwhelms the faradaic signal at the small concentrations of neurotransmitters typically measured, but can be digitally subtracted over short time scales such that only the signal of interest is viewed (Howell et al., 1986). However, the large charging current is still measured at the working electrode and provides numerous disadvantages. First, if the charging current is too large, it can saturate the current-to-voltage converter because of its finite power supply and/or the analog-to-digital converter (ADC) because of its limited voltage range. Also, large charging currents force lower gains to be used which increase quantization error and digitization noise (Cahill et al., 1996; Hermans et al., 2008). Dynamically changing the gain requires either the reconfiguration of the current-to-voltage converter or the use of a potentiostat with an adjustable gain, both of which are impractical for experiments in behaving animals.

Recently, analog background subtraction (ABS) was developed in our lab to remove charging current in real time before digitization (Hermans et al., 2008). In this approach, charging current is recorded and played back at the summing point of the current-to-voltage converter thereby nulling the output in a procedure similar to that of some noise-cancelling headphones. This approach was successfully used to decrease quantization noise and enabled continuous FSCV measurements for up to 30 minutes.

Here, dopamine sensitivity was increased by scanning faster than 400 V/s, but ABS was used to decrease the larger charging currents associated with scanning faster, thereby circumventing the aforementioned disadvantages. One goal was to create a more sensitive 1.0 V excursion while maintaining rapid response time. Another aim was to develop an ultra-sensitive 1.3 V sweep to detect even smaller dopamine signaling events.

Experimental

Chemicals

All chemicals were purchased from Sigma-Aldrich (St. Louis, MO) and were used as received. Solutions were prepared in doubly distilled deionized water. In vitro experiments were conducted in PBS buffer (10 mM NaH₂PO₄, 140 mM NaCl, 3 mM KCl, adjusted to pH 7.4 with concentrated NaOH). Dopamine stock solutions were prepared in 0.1 N perchloric acid and were diluted with PBS buffer on the day of use. Both the PBS buffer and dopamine solutions were N₂ saturated to prevent oxidative degradation of dopamine over the course of the experiment.

Electrode fabrication

Carbon-fiber microelectrodes were fabricated as previously described (Cahill et al., 1996). Briefly, T-650 carbon-fibers (Thornel, Amoco Corporation, Greenville, SC) were aspirated into glass capillaries (A-M Systems, Carlsborg, WA) under vacuum. The

filled capillaries were then pulled with a micropipette puller (Narashige, Tokyo, Japan). The carbon-fibers were cut to a length of 50-75 μm with a scalpel and the aid of a light microscope (Thermo Fisher Scientific, Waltham, MA). Except for etching experiments, electrodes were backfilled with an electrolyte solution (4 M CH_3COOK and 150 mM KCl) and a stainless steel wire was inserted to make electrical contact. A multibarrel carbon-fiber microelectrode capable of performing iontophoresis was used for the combined electrochemistry/electrophysiology experiment, whose construction is described elsewhere (Herr et al., 2008; Herr et al., 2010). All electrodes were soaked in isopropanol purified with Norit A activated carbon for at least 20 minutes before use to remove any surface impurities (Bath et al., 2000).

Data acquisition

All data was acquired using locally constructed hardware (Carolina Chemistry Electronics Facility) and software in the LabVIEW programming environment (National Instruments, Austin, TX) as described previously (Michael et al., 1999; Hermans et al., 2008). The voltammetric waveform was generated and the data was acquired using a PCI-6052E DAC/ADC card (16 bit, National Instruments). A PCI 6711 card was used for synchronization and flow injection analysis control. A PCI 6040E card was used for electrophysiology recordings. Typically, voltammetric waveforms are also low-pass filtered at 2 kHz to remove digitization noise (Heien et al., 2003; Takmakov et al., 2010b). However, this filter is unsuitable for the use of faster scan rates and was removed. For combined electrochemistry and electrophysiology experiments, a locally constructed headstage was used that incorporated a solid-state relay that switched between a current-to-voltage converter capable of performing ABS for voltammetric scans and a voltage follower for unit recordings. Unit recordings were amplified ($\times 1000$), band-pass filtered (300 Hz – 3 kHz, Krohn Hite, Brockton, MA), and then digitized (Neurosurgery WorkStation, Plexon Inc., Dallas, TX).

Electrochemical experiments

Several voltage excursions at varying scan rates were used in this work. First, a triangular cyclic sweep from -0.4 V to 1.0 V back to -0.4 V (henceforth referred to as the “1.0 V waveform”) was used at scan rates varying from 400 V/s to 2400 V/s. Second, a triangular cyclic sweep from -0.4 V to 1.3 V back to -0.4 V (henceforth referred to as the “1.3 V cyclic waveform”) was used at scan rates of 400 V/s and 2400 V/s. Finally, a voltage excursion was constructed in piecemeal fashion by ramping from -0.4 V to 1.3 V at 2400 V/s, holding at 1.3 V for 0.55 ms, and ramping back to -0.4 V at 2400 V/s. The resulting waveform shape resembled a sawhorse pattern (henceforth referred to as the “1.3 V sawhorse waveform”, discussed *vide infra*).

The number of points in the voltammetric excursions was kept constant to maintain the same sampling rate. The 1.0 V waveform at 400 V/s (7 ms duration) was acquired with 1000 points giving a sampling rate of 143 kHz. Increasing the scan rate to 800 V/s, 1200 V/s, 1600 V/s, 2000 V/s, and 2400 V/s reduced the number of points in the voltammetric sweep to 500, 333, 250, 200, and 168, respectively. The 1.3 V cyclic excursion at 400 V/s (8.5 ms duration) was acquired with 1000 points giving a sampling rate of 118 kHz. To maintain the same sampling rate, the 1.3 V cyclic excursion at 2400 V/s was acquired with 168 points and the 1.3 V sawhorse waveform contained 230 points. All waveforms used a holding voltage of -0.4 V between voltammetric sweeps.

All experiments began with either the 1.0 V waveform or the 1.3 V cyclic waveform at 400 V/s. Electrodes were cycled with the corresponding waveform for 15 minutes at 60 Hz and 10 Hz for 15 minutes before use. Afterwards, all experiments were conducted with a waveform application frequency of 10 Hz except the combined electrochemistry and electrophysiology experiment which used an application frequency of 5 Hz for sufficient unit recording. A Ag/AgCl reference electrode was used for all

electrochemical experiments. All experiments were performed in a grounded Faraday cage to reduce noise.

Data analysis

All analyses were conducted using locally written LabVIEW software (National Instruments, Austin, TX), Microsoft Excel (Redmond, WA), and MATLAB (Mathworks, Natick, MA). Cell firing was analyzed using Offline Sorter (Plexon). Statistical tests were performed using GraphPad Prism (GraphPad Software Inc., San Diego, CA). Specific statistical tests are listed in the text. All values and traces are reported as averages \pm standard error of the mean. For quantitation of peak currents, the data was denoised using only a nearest-neighbor smoothing algorithm as was done previously for faster scan rate experiments (Bath et al., 2000). The effect of the time constant of the current-to-voltage converter was evaluated by convolution as described elsewhere (Wipf et al., 1988).

Quantization noise was calculated as follows. First, an electrode was cycled with the 1.0 V waveform at 400 V/s. Next, an average of three digital background-subtracted cyclic voltammograms without the presence of analyte was calculated without filtering or smoothing. The standard deviation of the resulting cyclic voltammogram was taken as a noise level. Finally, the scan rate was increased in 400 V/s increments up to 2400 V/s and the procedure was repeated.

Signal-to-noise ratios were calculated by analyzing peak current versus time traces. A low frequency polynomial was used to fit a baseline to remove drift and signal to noise ratios were determined by dividing the maximal response by the standard deviation of 1 s of noise. For the calculation of temporal responses, the data was denoised solely with a 4th order Bessel low-pass filter. The frequency of the filter in Hz was chosen by multiplying the scan rate by five (ex: 400 V/s filtered at 2 kHz, 800 V/s

filtered at 4 kHz, etc.). Response time was quantified to be the amount of time necessary for the peak current to rise from 0% to 90% of its maximum value.

Flow injection analysis

All in vitro experiments were conducted using a flow injection analysis system to expose carbon-fiber microelectrodes to a bolus of analyte (Kristensen et al., 1986). The electrodes were placed at the output of a six-port rotary valve attached to a pneumatic actuator, controlled by a 12 V DC solenoid (Rheodyne, Rohnert Park, CA). Buffer was pumped into the system at a flow rate of 0.5 mL/min (New Era Pump Systems, Inc., Wantagh, NY).

Etching studies

Scanning electron microscopy was used to study the effect of the applied waveform on the carbon-fiber microelectrode (Takmakov et al., 2010b). Carbon-fiber microelectrodes were imaged before and after electrochemical etching. Microelectrodes were rinsed with copious quantity of DI water to remove residual salt. A total of 6.48×10^6 cycles of a selected waveform was applied to a carbon-fiber microelectrode as done previously (Takmakov et al., 2010b) in PBS buffer, pH 7.4. Electrical connection with the carbon-fiber microelectrode was made using a stainless steel wire and a silver-based paint (GC Electronics, Rockford, IL); backfill solution was not used to prevent evaporation in the instrument. Because the duration of each voltammetric excursion differed, each waveform was applied at a different frequency such that all waveforms had 6.5 ms of holding time between sweeps. Images were collected using FEI Quanta 200 FEG environmental scanning electron microscope (FEI Company, Hillsboro, OR) in low-vacuum mode with electron beam energy of 13 kEV and at magnifications of 1.5 k, 3 k and 10 k. Diameters were estimated using ImageJ (Rasband, 1997-2009). A one-way ANOVA with Bonferroni's post-test was used to determine significant differences between groups.

In vivo experiments in anesthetized rats

Male Sprague-Dawley rats (~ 350 g, Charles River, Wilmington, MA) were anesthetized with urethane (1.5 g/kg i.p., made in a 50% w/w solution of saline). Rats were mounted in a stereotaxic frame (Narashige, Tokyo, Japan) and holes were drilled for the carbon-fiber microelectrode in the striatum (+1.3 A/P, +2.3 M/L, -4.0 to -7.5 D/V, relative to bregma), a stimulating electrode in the ventral tegmental area (-5.2 A/P, +1.0 M/L, -7.0 to -9.0 D/V), and a reference placed contralateral to the carbon-fiber microelectrode. The working and stimulating electrodes were adjusted for maximal dopamine release. A bipolar stimulating electrode was used (Plastics One, Roanoke, VA). Biphasic stimulations (300 μ A, 60 Hz, 40 pulses) were delivered using optically isolated constant current stimulators (Digitimer Ltd., Letchworth, UK).

Use of ABS for faster scan rate experiments

Figure 5.1 shows how ABS was used for faster scan rate experiments. First, charging current was recorded at 400 V/s in the absence of analyte, digitized, and fed into the summing point of the current to voltage converter as a voltage signal as described previously (Hermans et al., 2008). Because the recorded charging current at 400 V/s was recorded as an inverted voltage, the addition of this signal at the summing point of the current-to-voltage converter will initially yield a zeroed output. Next, the scan rate was increased which results in a larger charging current at the working electrode, but because some of the current can be neutralized, the output voltage will not saturate the ADC. The resulting output was then digitized and digitally background-subtracted (Howell et al., 1986) to generate analyte cyclic voltammograms and color plots (Michael et al., 1998).

Combined electrochemistry and electrophysiology

A combined iontophoresis, ABS, and electrophysiology experiment was performed to study the effect of the increased charging current on local neuronal firing of

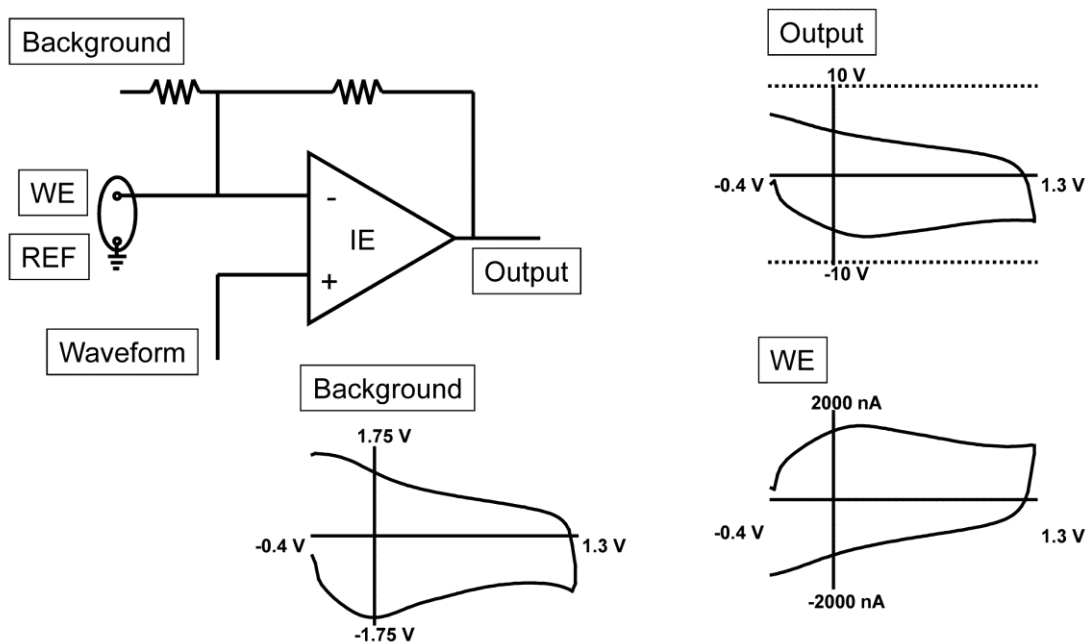


Figure 5.1. ABS utilization for faster-scan cyclic voltammetry. When the working electrode (WE) is scanned faster, a larger charging current is generated. A digitized version of background charging current measured at 400 V/s is fed into the summing point of the current-to-voltage converter, neutralizing some of the measured charging current, preventing the analog to digital converter from reaching saturation (dotted lines).

medium spiny neurons in anesthetized animals. The procedure was adapted from previous work (Cheer et al., 2005; Herr et al., 2008; Owesson-White et al., 2009; Herr et al., 2010). To maintain consistency, the experiments were performed in anesthetized animals with the same coordinates previously mentioned for the reference, stimulating and working electrodes (*vide supra*). The Ag/AgCl electrode served as the reference for both the electrochemical and electrophysiological experiments, as well as the return for the iontophoresis current.

First, the dorsal-ventral position of the working and stimulating electrodes was optimized to ensure the experiments were performed in an area displaying stimulated dopamine release. Next, a 200 mM L-glutamate solution was locally iontophoresed using a constant current source (15 nA – 35 nA, Neurophore, Harvard Apparatus, Holliston, MA) into the extracellular environment at the carbon-fiber microelectrode tip to evoke firing of medium spiny neurons in the anesthetized animal (White et al., 1995; Hu and White, 1997). Units were then recorded for 10 minutes to ensure a stable baseline.

The waveform application frequency was 5 Hz for these experiments. The duration of the voltammetric scans was 20 ms, which included the voltammetric sweep time and amplifier settling time. The remaining 180 ms was used for unit recording. Cell firing was recorded for 60 s with the 1.3 V waveform at 400 V/s. Next, the 1.3 V sawhorse waveform at 2400 V/s was applied using ABS to prevent saturation and cell firing was again recorded for 60 s. Finally, the 1.3 V waveform at 400 V/s was reapplied and cell firing was measured for another 60 s. The procedure was repeated for multiple locations within an animal, but locations were at least 300 μm apart.

Results and Discussion

Scanning faster with the 1.0 V waveform

The scan rate of the 1.0 V waveform was increased to improve sensitivity while maintaining temporal resolution. Figure 5.2 shows the effect of increasing scan rate with the 1.0 V waveform. Figure 5.2A shows a color plot representation of a 1 μ M dopamine injection in vitro at 400 V/s. Increasing the scan rate to 2400 V/s increased the faradaic response (Figure 5.2B), but there was a 190 mV shift in peak potential. This peak shift at high scan rates has been reported before (Hsueh et al., 1997; Bath et al., 2000) and was likely due to a combination of slow kinetics of dopamine oxidation (Deakin et al., 1986; Deakin and Wightman, 1986), an increased cell time constant, and ohmic drop (Wipf et al., 1989; Wightman and Wipf, 1990), both of which are larger for cylindrical microelectrodes (Robinson et al., 1982) compared to disc microelectrodes (Wightman and Wipf, 1989). The capacitance of the glass coated portion of the carbon-fiber microelectrode present with longer electrode tapers may also play a role (Wipf et al., 1989). The time constant of the current-to-voltage converter was approximately 2.4 μ s which negligibly distorts the measured response (Wipf et al., 1988). Convolution with the system transform of a low-pass filter with such a time constant further supported this theory (data not shown) (Wipf et al., 1988). While undesirable, this peak shift did not interfere with dopamine identification but 2400 V/s was chosen as the maximal scan rate to prevent oxidation from occurring past the 1.0 V switching potential.

Figure 5.2C shows normalized peak current versus time traces for a 1 μ M dopamine injection in vitro at various scan rates. The rapid response time of the 1.0 V waveform was not significantly different between 400, 800, 1200, 1600, 2000, and 2400 V/s ($N = 5$, $P = 0.5113$, repeated measures ANOVA). Previous work has shown that a major noise source of FSCV measurements is due to the finite step size of data quantization (Hermans et al., 2008). Since gain of the current-to-voltage converter remains unchanged while increasing scan rate in this work, the noise level should remain constant as long as the application of faster scan rates does not affect the

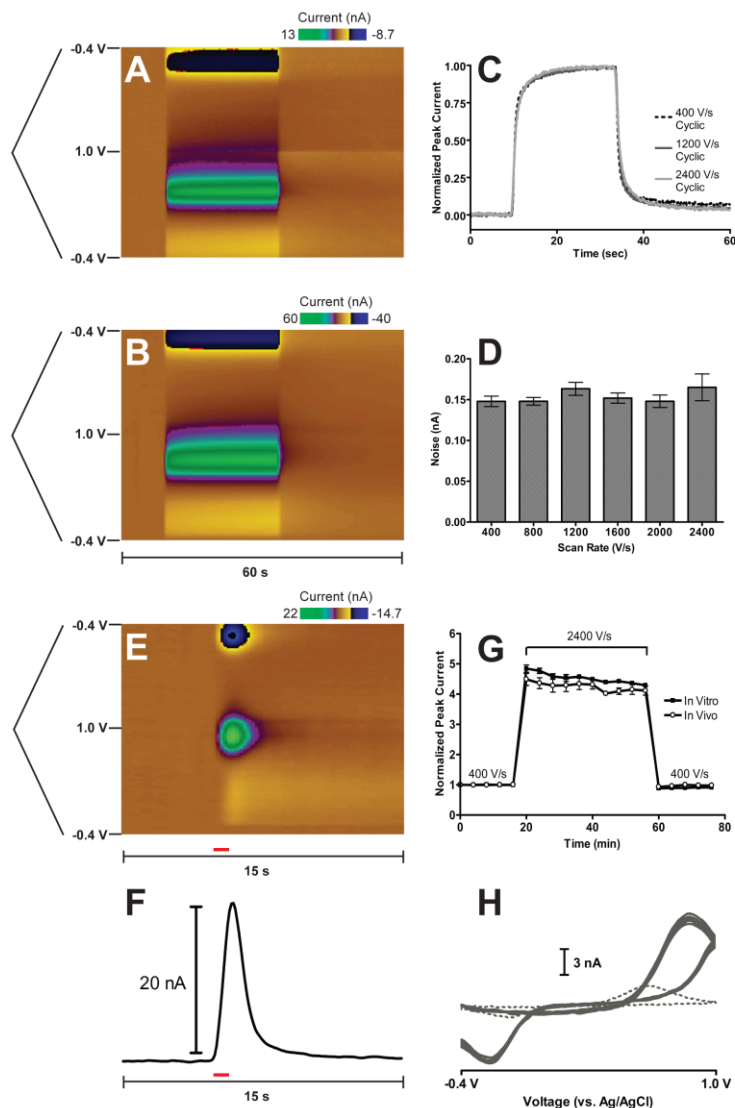


Figure 5.2. Performance characteristics of the 1.0 V waveform upon increasing scan rate. A) Color plot representation of a 1 μM dopamine injection at 400 V/s. B) Color plot representation of a 1 μM dopamine injection at 2400 V/s. A) and B) share the same time axis. C) Temporal response for in vitro injections of 1 μM dopamine at 400 V/s (black dashed line), 1200 V/s (dark grey solid line), and 2400 V/s (light grey solid line) for a representative electrode. D) Quantization electrode noise as a function of scan rate ($N = 5$). E) Color plot representation of stimulated dopamine release with the 1.0 V waveform at 2400 V/s in an anesthetized rat. The red bar indicates the duration of the stimulation. A), B), and E) have the voltammetric sweep plotted to the left of the color plot. F) Current versus time trace at the oxidation potential of dopamine from the color plot shown in E). G) Baseline normalized dopamine peak current as a function of time for the 1.0 V waveform at 400 V/s, 2400 V/s, and back to 400 V/s in vitro (filled squares) and in vivo (open circles). In vitro peak currents were measured from 1 μM dopamine injections ($N = 5$) and in vivo responses were measured from stimulated dopamine release ($N = 5$) in anesthetized rats. Both responses were measured every four minutes. H) Ten consecutive cyclic voltammograms of stimulated dopamine measured in vivo at 2400 V/s (solid lines) from a representative animal. The dotted line represents the cyclic voltammogram of dopamine at 400 V/s for comparison.

carbon-fiber microelectrode. Figure 5.2D shows that quantization noise was independent of scan rate ($N = 5$, $P = 0.5707$, repeated measures ANOVA). However, electrode drift increased as the scan rate was increased.

Figures 5.2E and 5.2F show the in vivo response seen with the 1.0 V waveform at 2400 V/s. Figure 5.2E shows a representative color plot of stimulated dopamine release. Figure 5.2F shows the current versus time trace from Figure 5.2E taken at the oxidation potential of dopamine. The measured dopamine current increased throughout the duration of the stimulation and uptake caused the current response to decrease after the stimulation ended as dopamine was removed from the extracellular space.

Increasing scan rate from 400 V/s to 2400 V/s with the 1.0 V waveform initially gave a 4.8 ± 0.1 fold increase in peak current in vitro that stabilized to a 4.4 ± 0.1 fold increase after approximately 20 minutes (Figure 5.2G, filled squares, $N = 5$). Dopamine is known to strongly adsorb to the carbon-fiber microelectrode using this waveform because of the negative holding potential and electrostatic effects (Bath et al., 2000; Heien et al., 2003; Takmakov et al., 2010b); therefore, peak current should scale proportionally with scan rate. Since the amount of dopamine that is oxidized should remain constant, integral charge should also remain constant. However, the broadening shift of the oxidation peak (Figure 5.2B) would cause peak current to be smaller than theory predicts to maintain the same overall peak area.

ABS was originally used to increase signal to noise ratios of electrochemical measurements by decreasing quantization noise (Hermans et al., 2008). At the highest digital gain tested, the overall noise level decreased approximately 60%, which would result in a net gain in signal to noise ratio of 2.5. Unfortunately, ABS cannot be used in this manner for faster scan rate experiments because substantial current is digitized. Here, ABS was used to increase the signal to noise ratio for 1 μ M dopamine

approximately 4-fold in vitro from 333 ± 48 at 400 V/s to 1321 ± 187 at 2400 V/s, higher than just decreasing quantization noise alone. However, this value is slightly less than expected for the 4.4-fold increase in signal. The addition of the background signal necessary for current subtraction with faster scan rate experiments likely introduces noise into the system. Also, the lack of a ramp filter likely introduces greater noise at higher scan rates (Michael et al., 1999). Assuming a limit of detection of three times the standard deviation of the noise (3σ), these signal to noise ratios correspond to limits of detection 9.7 ± 1.3 nM at 400 V/s to 2.5 ± 0.3 nM at 2400 V/s.

In vivo, a stable 4.1 ± 0.1 fold increase in oxidative peak current of stimulated dopamine release was detected (Figure 5.2G, open circles, N = 5). Figure 5.2H shows ten consecutive cyclic voltammograms measured in vivo at 2400 V/s (solid traces), compared to the response seen at 400 V/s (grey dotted trace) with the 1.0 V waveform. The relative standard deviations of stimulated dopamine release oxidative peak currents at 400 V/s and 2400 V/s were $2.9 \pm 0.4\%$ and $4.3 \pm 1.0\%$, respectively and were not significantly different (N = 5, P = 0.1958, paired t-test). This result showed that dopamine release in vivo remained stable with higher scan rates with the 1.0 V waveform.

Scanning faster with the 1.3 V cyclic waveform

The scan rate of the 1.3 V cyclic waveform was increased to create an ultra-sensitive voltage sweep. Figure 5.3 shows the effect of increasing scan rate with the 1.3 V cyclic waveform. Unlike the 1.0 V waveform, the 1.3 V cyclic waveform showed an unstable increase in peak current both in vitro and in vivo, as shown in Figure 5.3A. Figure 5.3B shows consecutive in vivo cyclic voltammograms of stimulated dopamine release measured at 2400 V/s with the 1.3 V cyclic waveform every four minutes (grey solid lines). There was again a larger than expected peak shift compared to the cyclic voltammogram measured at 400 V/s (grey dashed line).

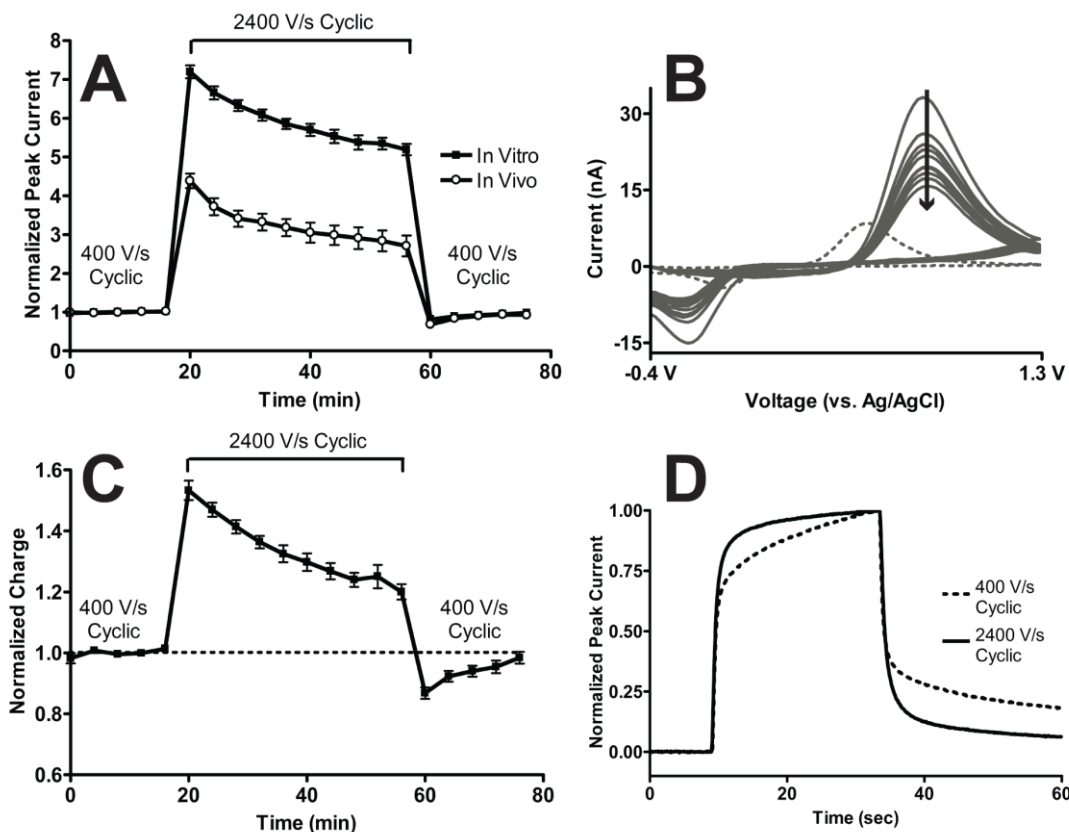


Figure 5.3. Performance characteristics of the 1.3 V cyclic waveform upon increasing scan rate. A) Baseline normalized dopamine peak current as a function of time for the 1.3 V cyclic waveform at 400 V/s, 2400 V/s, and back to 400 V/s in vitro (filled squares) and in vivo (open circles). In vitro peak currents were measured from 1 μ M dopamine injections (N = 5 electrodes) and in vivo responses were measured from stimulated dopamine release in anesthetized rats (N = 5 rats). Both responses were measured every four minutes. B) Ten consecutive cyclic voltammograms of stimulated dopamine measured in vivo at 2400 V/s (solid lines) from a representative animal. The arrow indicates time progression. The dotted line represents the cyclic voltammogram of dopamine at 400 V/s for comparison. C) Baseline normalized charge for the in vitro data shown in A). D) Temporal response for in vitro injections of 1 μ M dopamine at 400 V/s (black dashed line) and 2400 V/s (black solid line).

Figure 5.3A showed that increasing scan rate 6-fold increased the peak current 7.2 ± 0.1 fold in vitro. To investigate this phenomenon, in vitro cyclic voltammograms were integrated to calculate charge as a function of time for the in vitro data shown in Figure 5.3A with the results plotted in Figure 5.3C. Ideally, charge should stay constant as scan rate is increased as long as the number of moles of dopamine electrolyzed does not change. Upon switching from 400 V/s to 2400 V/s with the 1.3 V cyclic waveform, there was an initial $53 \pm 3\%$ ($N = 5$) increase in charge that quickly decayed over time. When switching back to 400 V/s, there was significantly less charge than there had been during the 400 V/s baseline period, but integral charge returned to baseline after approximately 20 minutes.

According to theory, only an increase in electrode area and/or adsorbed species would result in a higher than expected peak current for adsorption-mediated electron transfer (Bard, 2001). While the 1.3 V cyclic waveform is known to oxidatively etch carbon-fiber surfaces, it is unlikely that electrode area changed in such an erratic manner so quickly because the oxidative etch is mild compared to other voltammetric excursions which are known to fracture carbon surfaces (Takmakov et al., 2010b). Instead, this result suggests that the amount of dopamine adsorbed on the carbon-fiber microelectrode surface increased upon increasing scan rate. In other words, surface chemistry rather than surface structure likely changes, as hypothesized previously (Hafizi et al., 1990).

The duration of the 1.3 V cyclic waveform at 400 V/s is 8.5 ms, compared to 1.4 ms at 2400 V/s, so some of the increased charge could be due to an increased holding time. However, the duration of both waveforms are similar, compared to the application frequency of the voltammetric sweeps so this is unlikely. Taking into account that dopamine can still adsorb during the voltage sweep before its oxidation (Bath et al., 2000), the holding time at 2400 V/s is equivalent to an application frequency of 9.4 Hz at

400 V/s with the 1.3 V cyclic waveform. Charge did not significantly change with this longer holding time at 400 V/s ($N = 3$, $P = 0.9015$, paired t-test) so the increase in charge seen at 2400 V/s with the 1.3 V cyclic waveform was due to a drastic increase in adsorption site availability.

While the exact potential necessary to oxidatively etch the carbon-fiber surface for enhanced sensitivity is unknown, each 1.3 V cyclic sweep at 400 V/s spends approximately 1.5 ms above 1.0 V as shown in Figure 5.4A. Increasing scan rate to 2400 V/s decreases this time by 6 to approximately 250 μs (Figure 5.4B). We previously hypothesized that adsorption sites are consumed with a Kolbe-like electrolysis that occurs at potentials above 1.0 V (Takmakov et al., 2010b). Decreasing the amount of time at potentials above 1.0 V would also prevent adsorption site degradation, thereby increasing the number of available sites for dopamine adsorption which could explain the increase in measured charge. If an oxidative etching mechanism constantly renews and maintains adsorption sites necessary for dopamine sensitivity, scanning faster would decrease the amount of time spent at potentials necessary for this process to occur. As time progresses, sensitivity could decrease as adsorption sites foul, possibly due to irreversible adsorption of impurities or oxidative byproducts (Takmakov et al., 2010b).

Supporting this hypothesis, Hafizi et al. described decreasing sensitivity with time as the anodic voltage limit of the applied waveform was switched from 1.4 V to 1.0 V (Hafizi et al., 1990). Specifically, they describe a “semi-reversible change in the electrode surface”, which likely also explains the return to baseline behavior seen in Figure 5.3C after switching back to 400 V/s from 2400 V/s. The authors go on to state that continual application of the 1.4 V waveform was necessary for maintenance of enhanced sensitivity with time. While increasing scan rate decreases the time necessary to oxidatively etch the carbon-fiber microelectrode, it is also possible that the

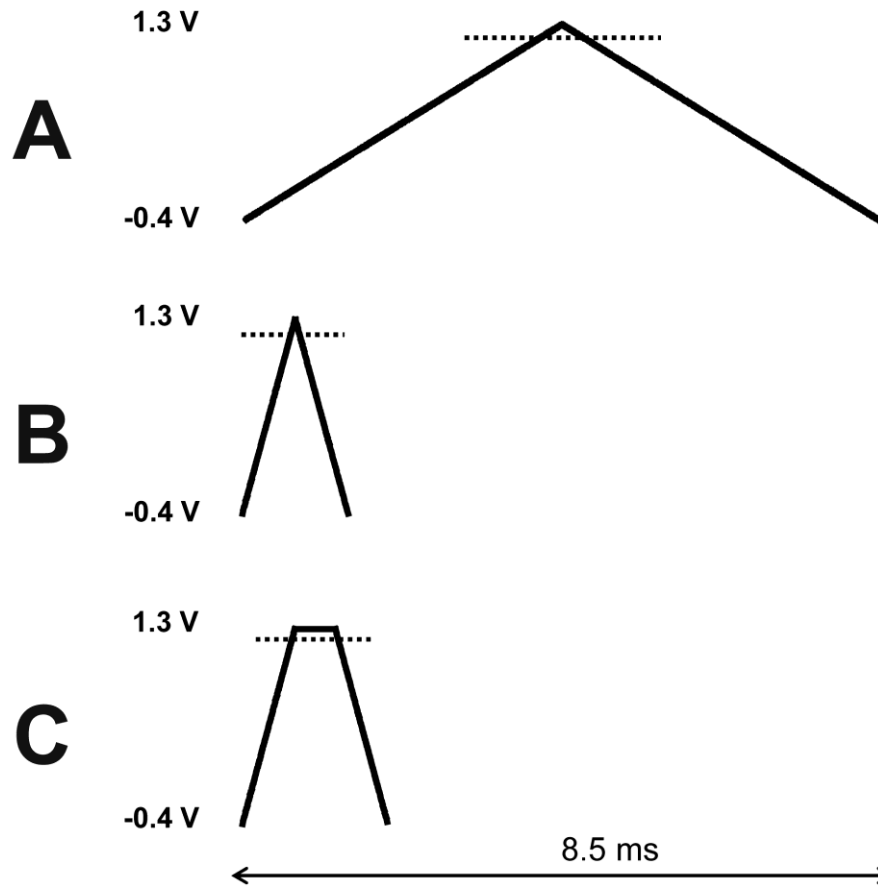


Figure 5.4. 1.3 V excursions versus time. The 400 V/s cyclic ramp (A), the 2400 V/s cyclic ramp (B), and the 2400 V/s sawhorse waveform (C). The horizontal dotted line represents 1.0 V.

combination of ohmic loss and an increased cell time constant exacerbates this effect by also decreasing the applied voltage necessary for the process to occur.

Interestingly, switching from 400 V/s to 2400 V/s also decreased the response time of the 1.3 V cyclic waveform by $60 \pm 5\%$ ($N = 5$) as shown in Figure 5.3D. This decreased response time occurred even though more material was adsorbed on the carbon-fiber microelectrode surface (Figure 5.3C). If the amount of time spent at potentials above 1.0 V becomes insufficient for surface activation, the temporal response of the 1.3 V cyclic waveform at 2400 V/s may become similar to that seen with the 1.0 V waveform. Taken together, these data show how scanning to anodic potentials higher than 1.0 V on carbon-fiber microelectrodes creates a quasi-steady state electrochemical surface and the behavior of adsorption dependent electron transfer can be extremely sensitive to even minor changes in electrochemical experimental parameters.

Modification of the 1.3 V cyclic waveform for maintaining increased sensitivity

The 1.3 V cyclic waveform was adapted in an effort to correct the unstable loss in sensitivity over time. To increase the sensitivity, the scan rate was increased from 400 V/s to 2400 V/s. An anodic holding time was added at the switching potential between the anodic and cathodic voltage sweeps to create a 1.3 V sawhorse-shaped waveform as shown in Figure 5.4C. For a stable response, the ideal holding time between scans was 0.55 ms for a total waveform length of 1.97 ms. If the anodic holding time was less than 0.55 ms, the performance mimicked the response seen in Figure 5.3A. If the anodic holding time was greater than 0.55 ms, the opposite trend was seen with an unstable increase in dopamine sensitivity (data not shown).

Figure 5.5 shows the in vitro performance of the 1.3 V sawhorse waveform. Switching from the 1.3 V cyclic waveform at 400 V/s to the 1.3 V sawhorse waveform at 2400 V/s corrected the instability measured with the 1.3 V cyclic waveform at 2400 V/s (Figure 5.5A, $N = 5$). The application of the 1.3 V sawhorse waveform at 2400 V/s also

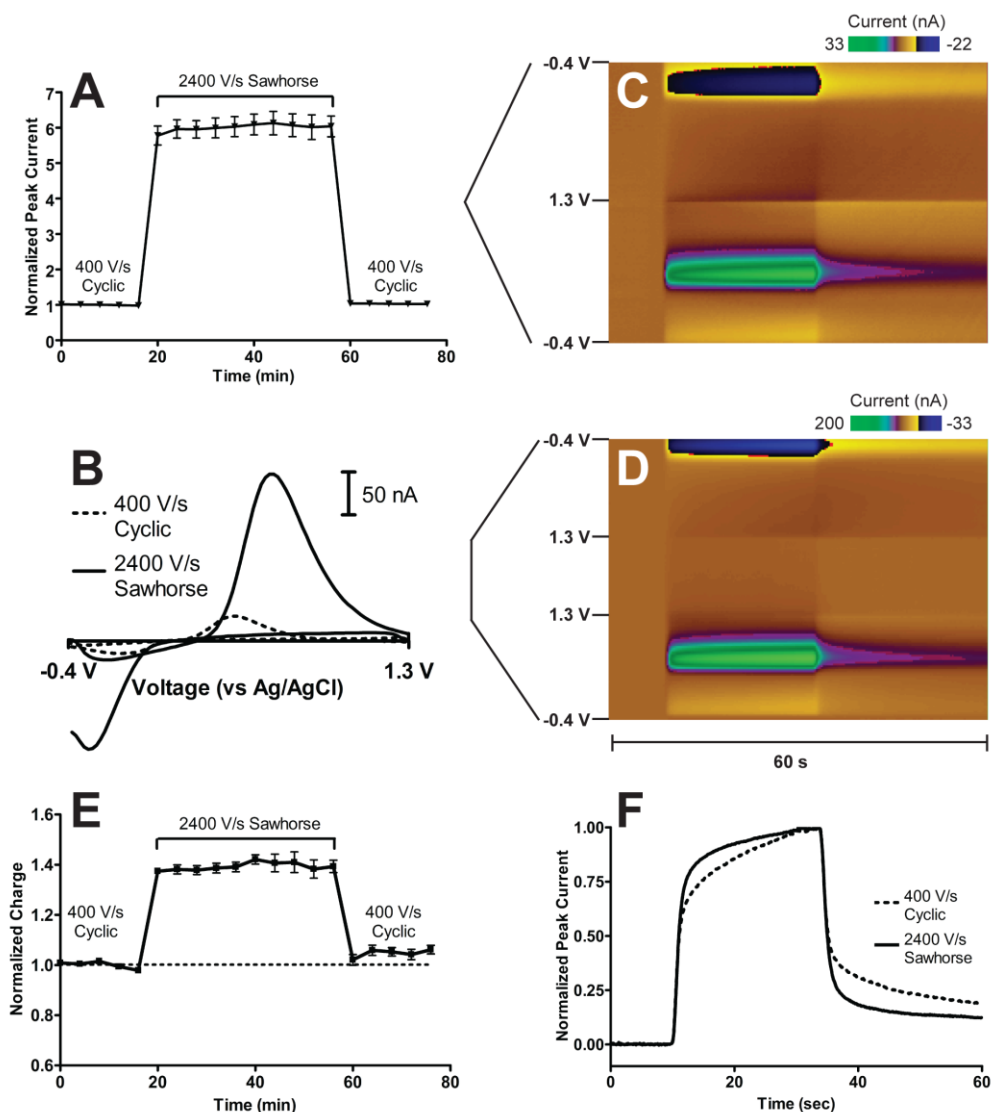


Figure 5.5. In vitro performance of the 1.3 V sawhorse waveform. A) Baseline normalized dopamine peak current as a function of time for the 1.3 V cyclic waveform at 400 V/s, the 1.3 V sawhorse waveform at 2400 V/s, and back to the 1.3 V cyclic waveform at 400 V/s in vitro. In vitro peak currents were measured from 1 μ M dopamine injections measured every four minutes (N = 5). B) Representative cyclic voltammograms for the 1.3 V cyclic waveform at 400 V/s (black dashed trace) and the 1.3 V sawhorse waveform at 2400 V/s (black solid trace). C) Color plot representation of a 1 μ M dopamine injection with the 1.3 V cyclic waveform at 400 V/s. D) Color plot representation of a 1 μ M dopamine injection with the 1.3 V sawhorse waveform at 2400 V/s. Both C) and D) have the voltammetric sweep plotted to the left of the color plot. E) Baseline normalized charge for the in vitro data shown in A). F) Temporal response for in vitro injections of 1 μ M dopamine at 400 V/s with the 1.3 V cyclic waveform (black dashed line) and at 2400 V/s with the 1.3 V sawhorse waveform (black solid line).

significantly increased voltammetric noise by $7.9 \pm 1.8\%$, which remained elevated even after switching back to the 1.3 V cyclic waveform at 400 V/s ($N = 5$, $P = 0.0015$, repeated measures ANOVA). In all, the signal to noise ratio for 1 μM dopamine increased from 602 ± 73 to 3322 ± 311 when switching from the 1.3 V cyclic waveform at 400 V/s to the 1.3 V sawhorse waveform at 2400 V/s, respectively. Assuming a limit of detection of 3σ , these signal to noise ratios correspond to a lowering of the limits of detection from 5.3 ± 0.7 nM to 0.96 ± 0.08 nM when switching from the 1.3 V cyclic waveform at 400 V/s to the 1.3 V sawhorse waveform at 2400 V/s, respectively.

A representative cyclic voltammogram for 1 μM dopamine with the 1.3 V sawhorse waveform at 2400 V/s is shown in Figure 5.5B (solid trace) with the response towards dopamine at 400 V/s with the 1.3 V cyclic waveform with the same electrode is also shown (dashed trace) for comparison. The increase in faradaic response is also shown in color plot representation in Figures 5.5C and 5.5D. Integrating peak charge showed that upon switching to the 1.3 V sawhorse waveform at 2400 V/s, charge initially increased $39 \pm 2\%$. However, unlike the 1.3 V cyclic waveform at 2400 V/s, the 1.3 V sawhorse waveform at 2400 V/s showed a stable level of integral charge throughout the period of waveform application. Again, it is unlikely that electrode area would show such a rapid, dramatic increase during the 1.3 V sawhorse waveform at 2400 V/s, only to return to baseline when switching back to the 1.3 V cyclic waveform at 400 V/s. Instead, it is much more likely that the application of the 1.3 V sawhorse waveform at 2400 V/s increased the amount of material adsorbed to the carbon-fiber microelectrode surface. The response time of the 1.3 V sawhorse waveform at 2400 V/s decreased by $26 \pm 6\%$ ($N = 5$) as shown in Figure 5.5F, despite having more material adsorbed. This implies that the 1.3 V sawhorse waveform at 2400 V/s, the 1.3 V cyclic waveforms at 400 V/s and 2400 V/s, and the 1.0 V waveform at all scan rates had distinct surface chemistries that adsorbed dopamine differently.

The performance of the 1.3 V sawhorse waveform at 2400 V/s in vivo is shown in Figure 5.6. Representative color plot representations show that the application of the 1.3 V sawhorse waveform at 2400 V/s increased the measured faradaic response without generally altering stimulated dopamine release (Figures 5.6A and 5.6B). Overall, there was a stable 4.3 ± 0.3 increase in peak current of stimulated dopamine release (N = 8 locations in seven rats), similar to that seen with the 1.0 V waveform at 2400 V/s (Figure 5.2E). One animal showed over a 40% decrease in peak current after switching to the 1.3 V sawhorse waveform at 2400 V/s and these data were discarded. The average relative standard deviation of stimulated dopamine release peak currents significantly increased from 2.5 ± 0.3 % with the 1.3 V cyclic waveform at 400 V/s to 5.6 ± 1.0 % with the 1.3 V sawhorse waveform at 2400 V/s (N = 8, P = 0.0468, paired t-test) but was still small overall and was well within the known stability of stimulated dopamine release over time (Ewing et al., 1983a). Integrating peak current showed that, except for the stimulated release events immediately following the switches in waveforms, charge remained constant throughout the course of the in vivo experiment (Figure 5.6D). It is possible that biomolecules foul and/or deactivate the surface (Park et al., 2005), which would lower both the increase in peak current and the increase in charge from that detected in vitro.

Effect of increased charging current on neuronal firing

With the exception of chronoamperometry with larger electrodes (Hefti and Felix, 1983), previous work has shown that currents associated with electrochemical measurements performed with microelectrodes are too small to impact neuronal firing (Ewing et al., 1983b; Armstrong-James and Millar, 1984; Stamford et al., 1993; Johnson et al., 2008). However, the charging currents generated at the working electrode by scanning faster are dramatically larger (typically between 2.5 μ A to 3.5 μ A for the 1.3 V sawhorse waveform at 2400 V/s). Therefore, it is possible that the carbon-fiber

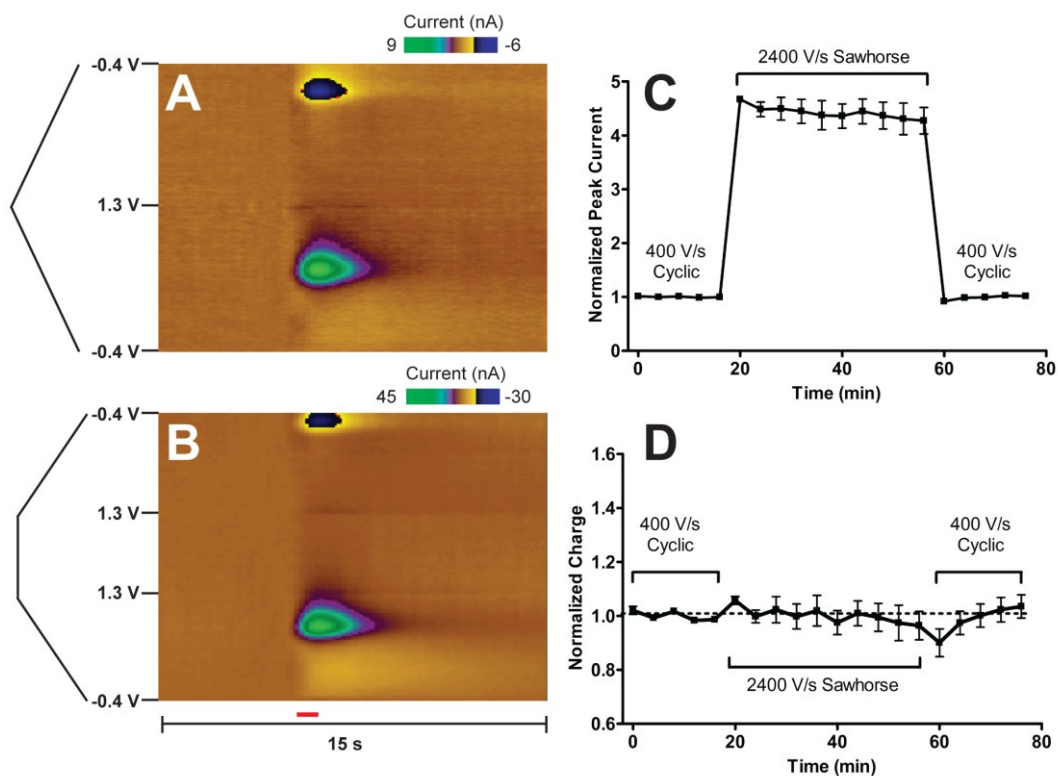


Figure 5.6. In vivo performance of the 1.3 V sawhorse waveform in vivo in anesthetized rats. A) Color plot representation of stimulated dopamine release with the 1.3 V cyclic waveform at 400 V/s. B) Color plot representation of stimulated dopamine release with the 1.3 V sawhorse waveform at 2400 V/s. Both A) and B) have the voltammetric sweep plotted to the left of the color plot and the time axis plotted below B). The red bar indicates the duration of the stimulus. C) Baseline normalized dopamine peak current as a function of time for the 1.3 V cyclic waveform at 400 V/s, the 1.3 V sawhorse waveform at 2400 V/s, and back to the 1.3 V cyclic waveform at 400 V/s in vivo (N = 8 locations in seven rats). D) Baseline normalized charge for the in vivo data shown in C).

microelectrode could act as a local stimulating electrode, altering neuronal firing and stimulated release.

A combined electrochemistry and electrophysiology experiment (Cheer et al., 2005; Owesson-White et al., 2009) was performed to examine if such an effect exists in vivo. This approach used a device capable of switching the carbon-fiber microelectrode between two amplifiers: a current-to-voltage converter capable of performing ABS for a faster scan rate voltammetric experiment and a voltage follower that was used to measure unit recordings. To maintain consistency, the combined electrochemistry and electrophysiology experiment was performed in anesthetized rats. The firing rate of medium spiny neurons in anesthetized animals is generally low so glutamate was locally delivered in vivo to evoke cell firing (White et al., 1995; Hu and White, 1997). A multibarrel iontophoresis probe (Herr et al., 2008; Herr et al., 2010) was used to deliver glutamate to the same local area in which the charging current was generated and the electrophysiological recordings were made. The 1.3 V sawhorse waveform at 2400 V/s generated the largest background current of any waveform used. Therefore, if the charging current generated with this waveform does not impact neuronal firing, the charging currents of all other waveforms would not affect cell firing.

Figure 5.7 shows the effect of increased charging current on glutamate-evoked cell firing (N = 21 cells in 4 rats). The multibarrel iontophoresis probe was successfully able to evoke cell firing of striatal medium spiny neurons in the anesthetized animal while simultaneously measuring their firing pattern, as well as performing a voltammetric measurement. Switching the applied waveform from the 1.3 V cyclic waveform at 400 V/s to the 1.3 V sawhorse waveform at 2400 V/s and back to the 1.3 V cyclic waveform at 400 V/s did not significantly affect the average glutamate-evoked firing rate of medium spiny neurons in vivo ($P = 0.7713$, repeated measures ANOVA). Since the 1.3 V sawhorse waveform at 2400 V/s had the largest charging current of any of the voltage

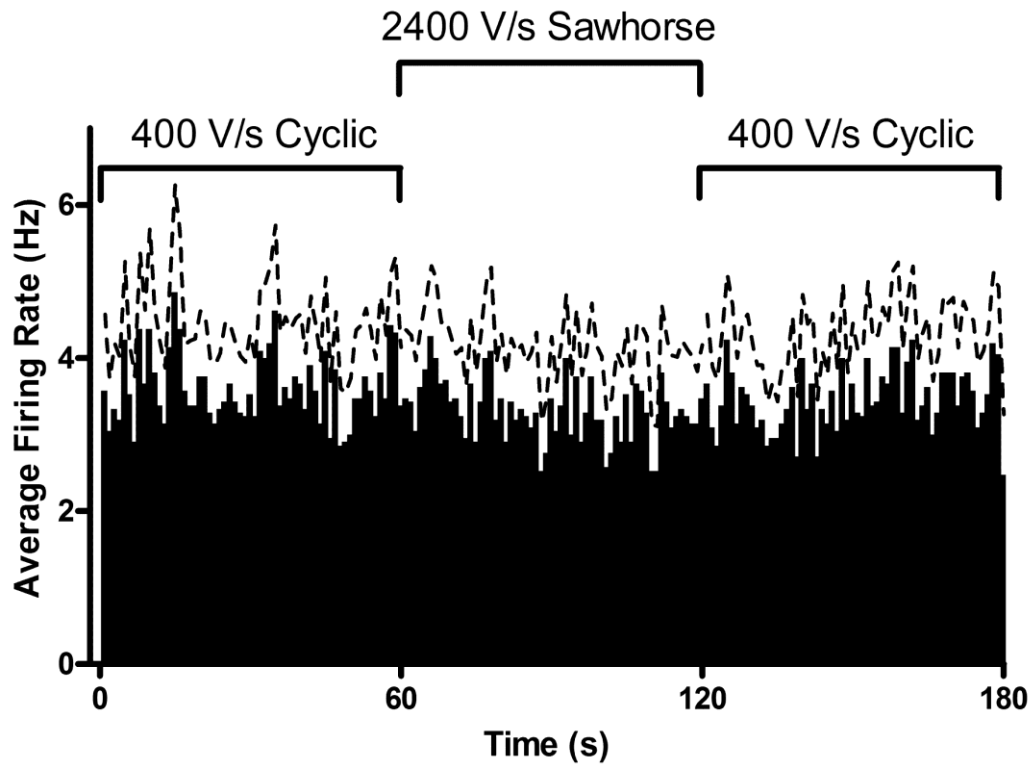


Figure 5.7. The effect of waveform application on firing rate activity. Average glutamate-evoked firing rate of medium spiny neurons as a function of time for the 1.3 V cyclic waveform at 400 V/s, the 1.3 V sawhorse waveform at 2400 V/s, and back to the 1.3 V cyclic waveform at 400 V/s (N = 21 cells in 4 rats). The dashed line represents standard error of the mean.

excursions studied, scanning faster with all other waveforms also should not affect the local cellular environment, as long as the overall charging current is less than approximately the 3.5 μA studied here.

Surface integrity of carbon-fiber microelectrodes after waveform application

The in vitro data presented here suggest that each voltage excursion uniquely affects the carbon-fiber microelectrode surface. Recently, we have demonstrated the use of environmental scanning electron microscopy (ESEM) as a way to monitor etching that occurs upon waveform application (Takmakov et al., 2010b). Unlike traditional scanning electron microscopy, the samples to be imaged do not need to be coated with a conductor in ESEM. This difference allows one to image, perform electrochemistry, and reimage the same carbon-fiber microelectrode.

Figure 5.8 shows the effect of each waveform on the etching of carbon-fiber microelectrodes. Figure 5.8A shows representative images of carbon-fiber microelectrodes after the application of each waveform. Figure 5.8B shows that the waveform applied significantly affects the etching rate of the carbon-fiber microelectrode ($N = 5$ each, $P < 0.0001$, one-way ANOVA). Figure 5.8A-I shows a representative carbon-fiber microelectrode before any waveform application. As shown previously (Takmakov et al., 2010b, application of the 1.0 V waveform at 400 V/s did not significantly etch the carbon-fiber microelectrode (Figure 5.8A-II). Increasing the scan rate to 2400 V/s with the 1.0 V waveform also did not significantly etch the microelectrode (Figure 5.8A-III). No difference in etching rates suggests that the increased current density with scanning faster at the carbon-fiber microelectrode does not alter its surface structure. This result also confirms earlier observations from Figure 5.2 regarding the stable increase in signal, maintenance of time response, and similar voltammetric noise levels when increasing scan rate of the 1.0 V waveform.

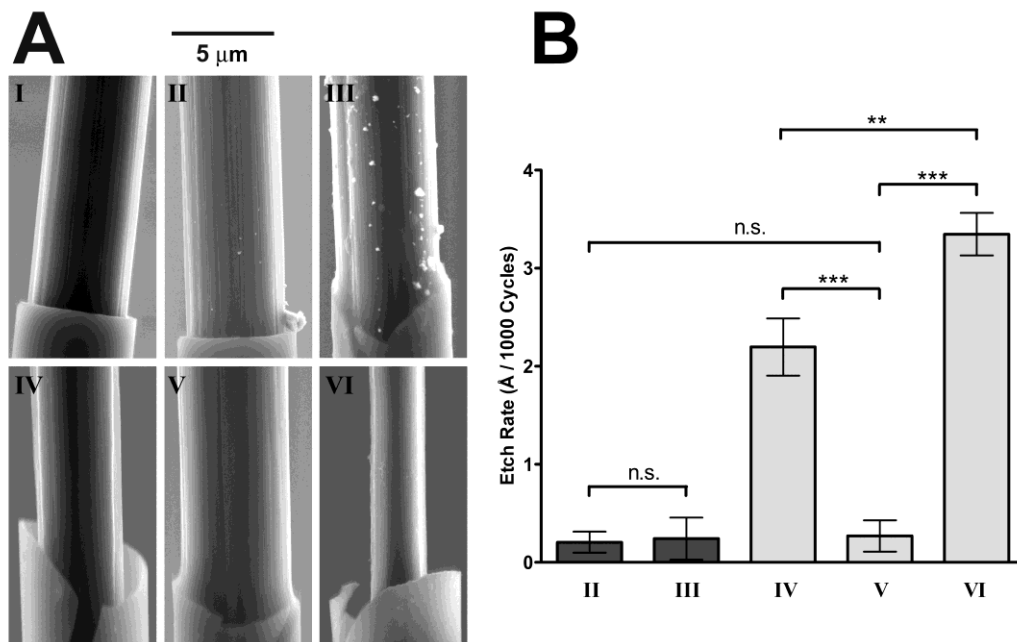


Figure 5.8. Carbon fiber microelectrode etching as a function of the applied waveform. A) Representative ESEM images of an electrode (I) before waveform application, (II) after the 1.0 V waveform at 400 V/s, (III) after the 1.0 V waveform at 2400 V/s, (IV) after the 1.3 V cyclic waveform at 400 V/s, (V) after the 1.3 V cyclic waveform at 2400 V/s, and (VI) after the 1.3 V sawhorse waveform at 2400 V/s. B) Etch rates for each waveform application described in A) (N = 5 electrodes each). Only selected comparisons are shown for clarity (n.s. – no significant difference, ** - P < 0.01, *** - P < 0.001).

The 1.3 V cyclic waveform at 400 V/s etched the surface as shown before (Takmakov et al., 2010b) (Figure 5.8A-IV), but increasing the scan rate of this waveform to 2400 V/s significantly decreased the etch rate (Figure 5.8A-V) to a value comparable to that of the 1.0 V excursions. This comparable etch rate probably contributes to the decreased time response and loss in sensitivity with the 1.3 V cyclic waveform at 2400 V/s. The decreased etch rate accompanying the diminishing dopamine sensitivity with the 1.3 V cyclic waveform at 2400 V/s confirms the hypothesis that the 1.3 V anodic potential limit creates a carbon surface that is in a quasi-steady state and is etching-dependent.

The 1.3 V sawhorse waveform at 2400 V/s had the largest etch rate of any waveform evaluated (Figure 5.8A-VI), etching significantly more than the 1.3 V cyclic waveform at 400 V/s and 2400 V/s. The 1.3 V sawhorse waveform at 2400 V/s increased the etching done by the 1.3 V cyclic waveform at 2400 V/s and, at the same time, corrected the unstable loss in measured signal. It is interesting that more etching was needed than the 1.3 V cyclic waveform at 400 V/s to maintain sensitivity over time. An increased etching rate, yet faster time response suggests that the adsorption sites created with the 1.3 V sawhorse waveform at 2400 V/s differ from those present with the 1.3 V cyclic excursions. The increase in electrode noise measured with the 1.3 V sawhorse waveform at 2400 V/s, that is still present upon switching back to the 1.3 V cyclic waveform at 400 V/s, was likely due to either a more reactive electrode etching process, sub-micron electrode resurfacing not visible with the ESEM, or a deterioration of the electrode-glass seal as more of the carbon-fiber microelectrode is etched. Taken together, the in vitro responses and etching data shows that while the 1.3 V sawhorse waveform at 2400 V/s maintains sensitivity over time, it does not maintain the same surface structure and chemistry.

Conclusions

This work demonstrates the use of faster than the traditional scan rates for enhanced in vivo sensitivity towards dopamine without increasing quantization error. Signal to noise ratios increased approximately 4-fold upon increasing scan rate from 400 V/s to 2400 V/s with the 1.0 V waveform. The temporal response and stability of measured dopamine release was unaffected by increasing scan rate with this waveform. However, increasing the scan rate from 400 V/s to 2400 V/s led to an unstable decrease in sensitivity in vitro and in vivo with the 1.3 V cyclic waveform. The creation of a novel sawhorse waveform corrected this loss in sensitivity, but did not maintain the same surface chemistry as the 1.3 V cyclic waveform at 400 V/s.

A prime advantage in focusing on increasing sensitivity is that other methods of noise reduction referenced in the introduction can be combined with this approach for even higher signal to noise ratios. Another significant improvement will likely come from the incorporation of a tunable low-pass filter on the applied waveform to remove digitization steps (Michael et al., 1999; Heien et al., 2003). Likewise, a filter should be placed on the background signal to remove noise from this additional input to the system, but care must be taken such that the subtraction process is time locked appropriately. If more current could be subtracted, ABS can also be used in the way it was originally designed, lowering quantization noise and improving the overall signal to noise ratio 2.5-fold further. Increasing the number of points in the applied waveform will also allow for better signal averaging in the current versus time dimension (Wiedemann et al., 1991).

This initial characterization necessitates several future experiments. Localized pH changes are also routinely measured in vivo (Heien et al., 2005; Takmakov et al., 2010a). The origin of pH change cyclic voltammograms is highly dependent on the state of the carbon surface (Runnels et al., 1999; Takmakov et al., 2010a). Studying the

effect of any distortions in the shape of the pH change cyclic voltammograms could give extra insight into any changes that occur to specific functional groups on the carbon surface upon the application of either the 1.3 V cyclic waveform at 2400 V/s or the 1.3 V sawhorse waveform. Also, this work could be extended to measurements in freely-moving rats performing behavioral tasks. Finally, norepinephrine and serotonin are present in low levels so their detection would be facilitated by improved sensitivity (Hashemi et al., 2009; Park et al., 2009).

References

- Amatore C, Lefrou C (1990) Is cyclic voltammetry above a few hundred kilovolts per second still cyclic voltammetry? *J Electroanal Chem* 296:335-358.
- Amatore CA, Jutand A, Pflüger F (1987) Nanosecond time resolved cyclic voltammetry: Direct observation of electrogenerated intermediates with bimolecular diffusion controlled decay using scan rates in the megavolt per second range. *J Electroanal Chem* 218:361-365.
- Andrieux CP, Hapiot P, Saveant JM (1988a) Fast potential step techniques at ultramicroelectrodes: application to the kinetic characterization of electrochemically generated short-lived species. *J Phys Chem* 92:5992-5995.
- Andrieux CP, Hapiot P, Saveant JM (1988b) Fast chemical steps coupled with outer-sphere electron transfers: application of fast scan voltammetry at ultramicroelectrodes to the cleavage of aromatic halide anion radicals in the microsecond lifetime range. *J Phys Chem* 92:5987-5992.
- Armstrong-James M, Millar J (1984) High-Speed Cyclic Voltammetry and Unit Recording with Carbon Fibre Microelectrodes. In: *Measurement of neurotransmitter release in vivo* (Marsden CA, ed), pp 209-224. Chichester [West Sussex] ;New York: Wiley.
- Bard AJ, Faulkner, L.R. (2001) *Electrochemical Methods: Fundamentals and Applications*, 2nd Edition. New York: John Wiley & Sons, Inc.
- Bath BD, Michael DJ, Trafton BJ, Joseph JD, Runnels PL, Wightman RM (2000) Subsecond adsorption and desorption of dopamine at carbon-fiber microelectrodes. *Anal Chem* 72:5994-6002.
- Baur JE, Kristensen EW, May LJ, Wiedemann DJ, Wightman RM (1988) Fast-Scan Voltammetry of Biogenic-Amines. *Anal Chem* 60:1268-1272.
- Cahill PS, Walker QD, Finnegan JM, Mickelson GE, Travis ER, Wightman RM (1996) Microelectrodes for the measurement of catecholamines in biological systems. *Anal Chem* 68:3180-3186.
- Cheer JF, Heien MLAV, Garris PA, Carelli RM, Wightman RM (2005) Simultaneous dopamine and single-unit recordings reveal accumbens GABAergic responses: Implications for intracranial self-stimulation. *Proc Natl Acad Sci U S A* 102:19150-19155.
- Cheer JF, Aragona BJ, Heien MLAV, Seipel AT, Carelli RM, Wightman RM (2007) Coordinated accumbal dopamine release and neural activity drive goal-directed behavior. *Neuron* 54:237-244.
- Clark JJ, Sandberg SG, Wanat MJ, Gan JO, Horne EA, Hart AS, Akers CA, Parker JG, Willuhn I, Martinez V, Evans SB, Stella N, Phillips PEM (2009) Chronic microsensors for longitudinal, subsecond dopamine detection in behaving animals. *Nat Meth* 7:126-129.

- Day JJ, Roitman MF, Wightman RM, Carelli RM (2007) Associative learning mediates dynamic shifts in dopamine signaling in the nucleus accumbens. *Nat Neurosci* 10:1020-1028.
- Deakin MR, Wightman RM (1986) The Kinetics of Some Substituted Catechol/Ortho-Quinone Couples at a Carbon Paste Electrode. *J Electroanal Chem* 206:167-177.
- Deakin MR, Kovach PM, Stutts KJ, Wightman RM (1986) Heterogeneous Mechanisms of the Oxidation of Catechols and Ascorbic-Acid at Carbon Electrodes. *Anal Chem* 58:1474-1480.
- Ewing AG, Bigelow JC, Wightman RM (1983a) Direct in vivo Monitoring of Dopamine Released from Two Striatal Compartments in the Rat. *Science* 221:169-171.
- Ewing AG, Alloway KD, Curtis SD, Dayton MA, Wightman RM, Rebec GV (1983b) Simultaneous electrochemical and unit recording measurements: Characterization of the effects of d-amphetamine and ascorbic acid on neostriatal neurons. *Brain Res* 261:101-108.
- Fulks JL, O'Bryhim BE, Wenzel SK, Fowler SC, Vorontsova E, Pinkston JW, Ortiz AN, Johnson MA (2010) Dopamine Release and Uptake Impairments and Behavioral Alterations Observed in Mice that Model Fragile X Mental Retardation Syndrome. *ACS Chem Neurosci* 1:679-690.
- Gan JO, Walton ME, Phillips PEM (2010) Dissociable cost and benefit encoding of future rewards by mesolimbic dopamine. *Nat Neurosci* 13:25-27.
- Ge S, Koseoglu S, Haynes C (2010) Bioanalytical tools for single-cell study of exocytosis. *Anal Bioanal Chem* 397:3281-3304.
- Gonon F, Buda M, Cespuglio R, Jouvet M, Pujol J-F (1980) In vivo electrochemical detection of catechols in the neostriatum of anaesthetized rats: dopamine or DOPAC? *Nature* 286:902-904.
- Gonon FG, Fombarlet CM, Buda MJ, Pujol JF (1981) Electrochemical treatment of pyrolytic carbon fiber electrodes. *Anal Chem* 53:1386-1389.
- Hafizi S, Kruk ZL, Stamford JA (1990) Fast cyclic voltammetry: improved sensitivity to dopamine with extended oxidation scan limits. *J Neurosci Meth* 33:41-49.
- Hashemi P, Dankoski EC, Petrovic J, Keithley RB, Wightman RM (2009) Voltammetric Detection of 5-Hydroxytryptamine Release in the Rat Brain. *Anal Chem* 81:9462-9471.
- Hefti F, Felix D (1983) Chronoamperometry in vivo: does it interfere with spontaneous neuronal activity in the brain? *J Neurosci Meth* 7:151-156.
- Heien M, Khan AS, Ariansen JL, Cheer JF, Phillips PEM, Wassum KM, Wightman RM (2005) Real-time measurement of dopamine fluctuations after cocaine in the brain of behaving rats. *Proc Natl Acad Sci U S A* 102:10023-10028.

- Heien ML, Phillips PE, Stuber GD, Seipel AT, Wightman RM (2003) Overoxidation of carbon-fiber microelectrodes enhances dopamine adsorption and increases sensitivity. *Analyst* 128:1413-1419.
- Hermans A, Keithley RB, Kita JM, Sombers LA, Wightman RM (2008) Dopamine detection with fast-scan cyclic voltammetry used with analog background subtraction. *Anal Chem* 80:4040-4048.
- Herr NR, Kile BM, Carelli RM, Wightman RM (2008) Electroosmotic Flow and Its Contribution to Iontophoretic Delivery. *Anal Chem* 80:8635-8641.
- Herr NR, Belle AM, Daniel KB, Carelli RM, Wightman RM (2010) Probing Presynaptic Regulation of Extracellular Dopamine with Iontophoresis. *ACS Chem Neurosci* 1:627-638.
- Howell JO, Kuhr WG, Ensman RE, Wightman RM (1986) Background Subtraction for Rapid Scan Voltammetry. *J Electroanal Chem* 209:77-90.
- Hsueh C, Bravo R, Jaramillo AJ, Brajter-Toth A (1997) Surface and kinetic enhancement of selectivity and sensitivity in analysis with fast scan voltammetry at scan rates above 1000 V/s. *Anal Chim Acta* 349:67-76.
- Hu X-T, White FJ (1997) Dopamine enhances glutamate-induced excitation of rat striatal neurons by cooperative activation of D1 and D2 class receptors. *Neurosci Lett* 224:61-65.
- Jackson BP, Dietz SM, Wightman RM (1995) Fast-Scan Cyclic Voltammetry of 5-Hydroxytryptamine. *Anal Chem* 67:1115-1120.
- Johnson MD, Franklin RK, Gibson MD, Brown RB, Kipke DR (2008) Implantable microelectrode arrays for simultaneous electrophysiological and neurochemical recordings. *J Neurosci Meth* 174:62-70.
- Kawagoe KT, Wightman RM (1994) Characterization of Amperometry for in-Vivo Measurement of Dopamine Dynamics in the Rat-Brain. *Talanta* 41:865-874.
- Keithley RB, Carelli RM, Wightman RM (2010) Rank Estimation and the Multivariate Analysis of in Vivo Fast-Scan Cyclic Voltammetric Data. *Anal Chem* 82:5541-5551.
- Kristensen EW, Wilson RL, Wightman RM (1986) Dispersion in flow injection analysis measured with microvoltammetric electrodes. *Analytical Chemistry* 58:986-988.
- Michael AC, Wightman RM (1996) Microelectrodes. In: *Laboratory techniques in electroanalytical chemistry* (Kissinger PT, Heineman WR, eds), pp 367-402. New York: Marcel Dekker, Inc.
- Michael D, Travis ER, Wightman RM (1998) Color images for fast-scan CV. *Anal Chem* 70:586a-592a.

- Michael DJ, Joseph JD, Kilpatrick MR, Travis ER, Wightman RM (1999) Improving Data Acquisition for Fast-Scan Cyclic Voltammetry. *Anal Chem* 71:3941-3947.
- Montenegro MI, Pletcher D (1986) The determination of the kinetics of electron transfer using fast sweep cyclic voltammetry at microdisc electrodes. *J Electroanal Chem* 200:371-374.
- Owesson-White CA, Ariansen J, Stuber GD, Cleaveland NA, Cheer JF, Wightman RM, Carelli RM (2009) Neural encoding of cocaine-seeking behavior is coincident with phasic dopamine release in the accumbens core and shell. *Eur J Neurosci* 30:1117-1127.
- Park J, Kile BM, Wightman RM (2009) In vivo voltammetric monitoring of norepinephrine release in the rat ventral bed nucleus of the stria terminalis and anteroventral thalamic nucleus. *Eur J Neurosci* 30:2121-2133.
- Park J, Show Y, Quaiserova V, Galligan JJ, Fink GD, Swain GM (2005) Diamond microelectrodes for use in biological environments. *J Electroanal Chem* 583:56-68.
- Petrovic J, Walsh PL, Thornley KT, Miller CE, Wightman RM (2010) Real-Time Monitoring of Chemical Transmission in Slices of the Murine Adrenal Gland. *Endocrinology* 151:1773-1783.
- Phillips PE, Robinson DL, Stuber GD, Carelli RM, Wightman RM (2003) Real-time measurements of phasic changes in extracellular dopamine concentration in freely moving rats by fast-scan cyclic voltammetry. *Methods in Molecular Medicine* 79:443-464.
- Pihel K, Schroeder TJ, Wightman RM (1994) Rapid and Selective Cyclic Voltammetric Measurements of Epinephrine and Norepinephrine as a Method to Measure Secretion from Single Bovine Adrenal-Medullary Cells. *Anal Chem* 66:4532-4537.
- Rasband WS (1997-2009) ImageJ. In: Bethesda, Maryland, USA, <http://rsb.info.nih.gov/ij/>; U.S. National Institutes of Health.
- Rice ME, Nicholson C (1989) Measurement of nanomolar dopamine diffusion using low-noise perfluorinated ionomer-coated carbon fiber microelectrodes and high-speed cyclic voltammetry. *Anal Chem* 61:1805-1810.
- Rice ME, Cragg SJ (2004) Nicotine amplifies reward-related dopamine signals in striatum. *Nat Neurosci* 7:583-584.
- Robinson DL, Wightman RM (2007) Rapid Dopamine Release in Freely Moving Rats. In: *Electrochemical Methods for Neuroscience* (Michael AC, Borland LM, eds), pp 17-34. Boca Raton, FL, USA: CRC Press.
- Robinson RS, Mccurdy CW, Mccreery RL (1982) Microsecond Spectroelectrochemistry by External Reflection from Cylindrical Microelectrodes. *Anal Chem* 54:2356-2361.

- Roitman MF, Wheeler RA, Wightman RM, Carelli RM (2008) Real-time chemical responses in the nucleus accumbens differentiate rewarding and aversive stimuli. *Nat Neurosci* 11:1376-1377.
- Runnels PL, Joseph JD, Logman MJ, Wightman RM (1999) Effect of pH and Surface Functionalities on the Cyclic Voltammetric Responses of Carbon-Fiber Microelectrodes. *Anal Chem* 71:2782-2789.
- Stamford JA, Palij P, Davidson C, Jorm CM, Millar J (1993) Simultaneous "real-time" electrochemical and electrophysiological recording in brain slices with a single carbon-fibre microelectrode. *J Neurosci Meth* 50:279-290.
- Strand AM, Venton BJ (2008) Flame etching enhances the sensitivity of carbon-fiber microelectrodes. *Anal Chem* 80:3708-3715.
- Swamy BEK, Venton BJ (2007) Carbon nanotube-modified microelectrodes for simultaneous detection of dopamine and serotonin in vivo. *Analyst* 132:876-884.
- Takmakov P, Zachek MK, Keithley RB, Bucher ES, McCarty GS, Wightman RM (2010a) Characterization of Local pH Changes in Brain Using Fast-Scan Cyclic Voltammetry with Carbon Microelectrodes. *Anal Chem* 82:9892-9900.
- Takmakov P, Zachek MK, Keithley RB, Walsh PL, Donley C, McCarty GS, Wightman RM (2010b) Carbon Microelectrodes with a Renewable Surface. *Anal Chem* 82:2020-2028.
- Troyer KP, Wightman RM (2002) Temporal separation of vesicle release from vesicle fusion during exocytosis. *J Biol Chem* 277:29101-29107.
- White SR, Harris GC, Imel KM, Wheaton MJ (1995) Inhibitory effects of dopamine and methylenedioxymethamphetamine (MDMA) on glutamate-evoked firing of nucleus accumbens and caudate/putamen cells are enhanced following cocaine self-administration. *Brain Res* 681:167-176.
- Wiedemann DJ, Kawagoe KT, Kennedy RT, Ciolkowski EL, Wightman RM (1991) Strategies for Low Detection Limit Measurements with Cyclic Voltammetry. *Anal Chem* 63:2965-2970.
- Wightman RM, Wipf DO (1989) Voltammetry at Ultramicroelectrodes. In: *Electroanalytical Chemistry: A Series of Advances* (Bard AJ, ed), pp 221-374. New York, NY: Marcel Dekker.
- Wightman RM, Wipf DO (1990) High-Speed Cyclic Voltammetry. *Accounts Chem Res* 23:64-70.
- Wightman RM, Jankowski JA, Kennedy RT, Kawagoe KT, Schroeder TJ, Leszczyszyn DJ, Near JA, Diliberto EJ, Viveros OH (1991) Temporally resolved catecholamine spikes correspond to single vesicle release from individual chromaffin cells. *Proc Natl Acad Sci U S A* 88:10754-10758.

Wipf DO, Wightman RM (1988) Submicrosecond measurements with cyclic voltammetry. Anal Chem 60:2460-2464.

Wipf DO, Michael AC, Wightman RM (1989) Microdisk electrodes: Part II. Fast-scan cyclic voltammetry with very small electrodes. J Electroanal Chem 269:15-25.

Wipf DO, Kristensen EW, Deakin MR, Wightman RM (1988) Fast-Scan Cyclic Voltammetry as a Method to Measure Rapid, Heterogeneous Electron-Transfer Kinetics. Anal Chem 60:306-310.